Dissertation zur Erlangung des Doktorgrades

der Fakultät für Chemie und Pharmazie

der Ludwig-Maximilians-Universität München

Mechanoregulation of Notch signaling activity in endothelial cells and its influence on angiogenic sprouting

Maibritt Vanessa Kretschmer

aus Hamburg, Deutschland

2022

Erklärung

Diese Dissertation wurde im Sinne von § 7 der Promotionsordnung vom 28. November 2011 von Herrn Prof. Dr. Stefan Zahler betreut.

Eidesstattliche Versicherung

Diese Dissertation wurde eigenständig und ohne unerlaubte Hilfe erarbeitet.

München, den 12.07.2022

M. Kretschmer

Maibritt Kretschmer

Dissertation eingereicht am	17.05.2022
1. Gutachter:	Prof. Dr. Stefan Zahler
2. Gutachterin:	Prof. Dr. Angelika M. Vollmar
Mündliche Prüfung am	27.06.2022

Research is seeing what everybody else has seen,

and thinking what nobody else has thought

- Albert Szent-Györgyi

Contents

Abbreviations

2D	Two-dimensional
3D	Three-dimensional
ADAM	A disintegrin and metalloproteinase
ADAMTS	A disintegrin and metalloproteinase with thrombospondin motifs
AFM	Atomic force microscopy
ANOVA	Analysis of variance
BSA	Bovine serum albumin
$CaCl_2$	Calcium chloride
CO_2	Carbon dioxide
Co-A	Co-activator
Co-R	Co-repressor
CSL	CBF1, Suppressor of Hairless, Lag-1
DAPT	γ-secretase inhibitor (N-[N-(3, 5-difluorophenacetyl)-l-alanyl]-s-phenylglycinet-butyl ester)
Dll4	Delta-like ligand 4
DMEM	Dulbecco's modified eagle medium
DMSO	Dimethyl sulfoxide
ECGM	Endothelial cell growth medium
ECM	Extracellular matrix
ECs	Endothelial cells
EDTA	Ethylenediaminetetraacetic acid
e.g.	For example
EGTA	Ethylene glycol tetraacetic acid
FCS	Fetal calf serum
Fig.	Figure
FRAP	Fluorescence recovery after photobleaching
H_2O	Water

HD	Heterodimerization domain
HES	Hairy-enhancer of split
HUVEC	Human umbilical vein endothelial cell
HyD	Hybrid detector
IgG	Immunoglobulin G
Jag1	Jagged ligand 1
KCl	Potassium chloride
KH_2PO_4	Potassium hydrogen phosphate
MAML	Mastermind-like protein
MCEC	Mouse cardiac endothelial cell
$MgCl_2$	Magnesium chloride
MMP	Matrix metalloprotease
NaCl	Sodium chloride
Na_2EDTA	Ethylenediamine tetraacetic acid disodium salt
Na_2HPO_4	Disodium phosphate
NaOH	Sodium hydroxide
NECD	Notch extracellular domain
NEXT	Notch extracellular truncation
NICD	Notch intracellular domain
Notch1	Notch1 receptor
NRR	Negative regulatory region
NTM	Notch transmembrane domain
PBS	Phosphate buffered saline
PDMS	Polydimethylsiloxane
PFA	Paraformaldehyde
PMT	Photomultiplier
RBPJ	Recombination signal binding protein for immunoglobulin kappa J region
rhDll4	Recombinant human Dll4
RLU	Relative luciferase unit

SEM	Standard error of the mean
TAZ	Transcriptional coactivator with PDZ-binding motif
T/E	Trypsin/EDTA
TEC	Trans-endocytosis
TP1	Terminal protein 1
UV	Ultraviolet radiation
VE-cadherin	Vascular endothelial cadherin
VEGF	Vascular endothelial growth factor
VEGFR2	VEGF receptor 2
YAP	Yes-associated protein

List of figures

List of tables

1 Summary

The Notch signaling pathway plays a critical role in many developmental and disease related processes. Furthermore, Notch regulates the differentiation of tip and stalk cells during angiogenesis. It is widely accepted that Notch has a mechanotransduction module that regulates cleavage of the receptor. However, the role of biomechanical properties of the cellular environment on this module and on Notch signaling in general is still poorly understood.

In the first part of this thesis, the influence of substrate stiffness on the Notch signaling pathway was investigated in endothelial cells. Using stiffness-tuned PDMS substrates it could be shown that Notch signaling pathway activity inversely correlates with the physiologically relevant substrate stiffness, with increased Notch activity on softer substrates. In this context, trans-endocytosis of the Notch extracellular domain, but not the overall endocytosis, is regulated by substrate stiffness. Furthermore, Notch related adhesion pathways were studied in connection with different substrate stiffnesses. It was observed that integrin cell-matrix connections are both stiffness-dependent and influenced by Notch. Cadherin-mediated cell-cell adhesion and Notch influence each other in that basal Notch signaling is cell-cell contact-dependent. Inhibition of the Notch signaling pathway however also results in a reduction of VE-cadherin levels.

In the second part of the project, 2D and 3D approaches were used to investigate the role of Notch and substrate stiffness in angiogenesis. It was shown that both overexpression of Dll4 and inhibition of the Notch signaling pathway drive sprouting, although Notch blocking led to excessive and ineffective sprout formation. By analyzing the cell positions of Dll4 overexpressing cells, it was further identified that Dll4 expression is not a selection factor for tip cell differentiation, but a consequence. In connection to the identified stiffness-dependent activation of the Notch signaling pathway, it was also shown that sprouting and sprout elongation is increased in matrices with low stiffness.

In sum, the present work demonstrates a mechanosensitivity of the Notch signaling pathway likely associated with the process of trans-endocytosis, suggesting a second mechanical aspect of the Notch signaling pathway besides the pulling force generated by the ligand presenting cell. Furthermore, a new insight into the influence of stiffness on the sprouting behavior of endothelial cells as well as the role of Dll4 overexpression in tip cell selection is provided.

2 Introduction

2.1 Mechanosensing of endothelial cells

Mechanosensing describes the ability of cells to sense and respond to the local microenvironment [1]. In this process, the composition and structure of the extracellular matrix (ECM) as well as changes in density and stiffness have an impact on cellular behavior [1-3]. Due to endothelial cells (ECs) being surrounded by a complex extracellular microenvironment, these cells have the ability to respond to cues from the surrounding matrix and to adapt their gene expression profiles accordingly [1, 4]. Signals and changes from the ECM allow for the adaption of different endothelial cell phenotypes that enable, among other things, interaction with other endothelial cells or signal transduction through pathway activation, which makes ECs also highly dependent on the local matrix [1, 5]. The cells interact with the components of the matrix through cell-matrix adhesion, i.e. integrins, and ECM receptors, implementing transmission of the cues of ECM proteins [4, 5]. Upon cell matrix interaction via integrin, the integrins form local clusters, recruiting intracellular molecules that affect the actin cytoskeleton and focal adhesion sites [4]. Consequently, especially migration, proliferation and cell-cell connections are influenced and regulated [1, 6]. Changes in the microenvironment are initiated either by contractile forces, or by the expression of degradation enzymes or cross-linking proteins by the endothelial and surrounding cells [7, 8]. Furthermore, matrix remodeling can be caused by the release of signaling molecules such as VEGF inducing deposition of the ECM proteins, which plays a major role during angiogenesis [4].

2.2 The Notch signaling pathway

The Notch signaling pathway plays a crucial role in most tissues, regulating cell fate decisions, cell cycle progression and apoptosis during tissue development and maintenance [9, 10]. This pathway acts in a highly context-dependent manner by enabling cell-cell communication in neighboring cells through juxtacrine signaling [10, 11]. Signaling is activated by the interaction of single-pass transmembrane Notch ligands and receptors [12, 13]. In mammals, five types of ligands, divided into the groups Delta-like (Dll1, Dll3, Dll4) and Serrate-like (Jag1, Jag2), and four types of receptors (Notch1-4) have been identified [11, 12]. The Notch pathway leads to the activation of Notch target genes, whereby the different ligands initiate specific target programs [10]. In endothelial biology, mainly the receptor Notch1 and its ligands Delta-like-4 and Jagged1 are involved [9, 14].

2.2.1 Notch processing and signal transduction

Before cells express the Notch1 receptor at the plasma membrane, the receptor must undergo a conformational change by post-translational cleavage [15, 16]. A furin-like protease proteolytically processes the extracellular domain at the S1 cleavage site, resulting in a Notch extracellular domain (NECD), a transmembrane domain (NTM) and an intracellular domain (NICD) non-covalently associated by the heterodimerization domain (HD) [16, 17]. Processing takes place in the *trans*-Golgi network [15]. Subsequently, the S1-cleaved Notch transits to the cell surface and accumulates at the plasma membrane [16, 18].

Interaction between a Notch ligand of one cell (signal sending cell) with a processed receptor of an adjacent cell (signal receiving cell) triggers a signaling cascade in the receiver cell [11, 13, 19]. Two control mechanisms ensure the correct signal transduction: a negative regulatory region (NRR) in the extracellular part of the receptor and the activation state of the receptor. The NRR prevents the signaling cascade from continuing in case of absent or insufficient activation. In addition, the ligand can acquire two different activities: in *cis* the ligand inhibits binding of a receptor of the same cell, in *trans* the ligand enables binding of the receptor of a neighboring cell [11, 19]. *Trans* interaction of receptor and ligand ensures separation of the receptor heterodimer by two further proteolytic cleavage events, resulting first in separation of the NECD, and subsequently in release of the NICD [10, 12, 20]. Proteolytic separation of

the extracellular portion of the receptor (S2 cleavage) is mediated by the metalloprotease ADAM close to the membrane, leaving the transmembrane and intracellular domain [16, 20]. The NECD is pulled into the ligand presenting cell along with the ligand during trans-endocytosis [20, 21]. The intracellular domain is dissociated at an intracellular cleavage site by γ-secretase (S3 cleavage) [16, 22]. The NICD is translocated to the nucleus of the receiver cell, where it associates with the transcriptional regulator RBPJ (also known as CBF1 or CSL), activating the Notch target genes such as Hairy-Enhancer of Split (HES) and HES-related proteins [9, 12, 21]. A schematic overview of the process is presented in Figure 2-1.

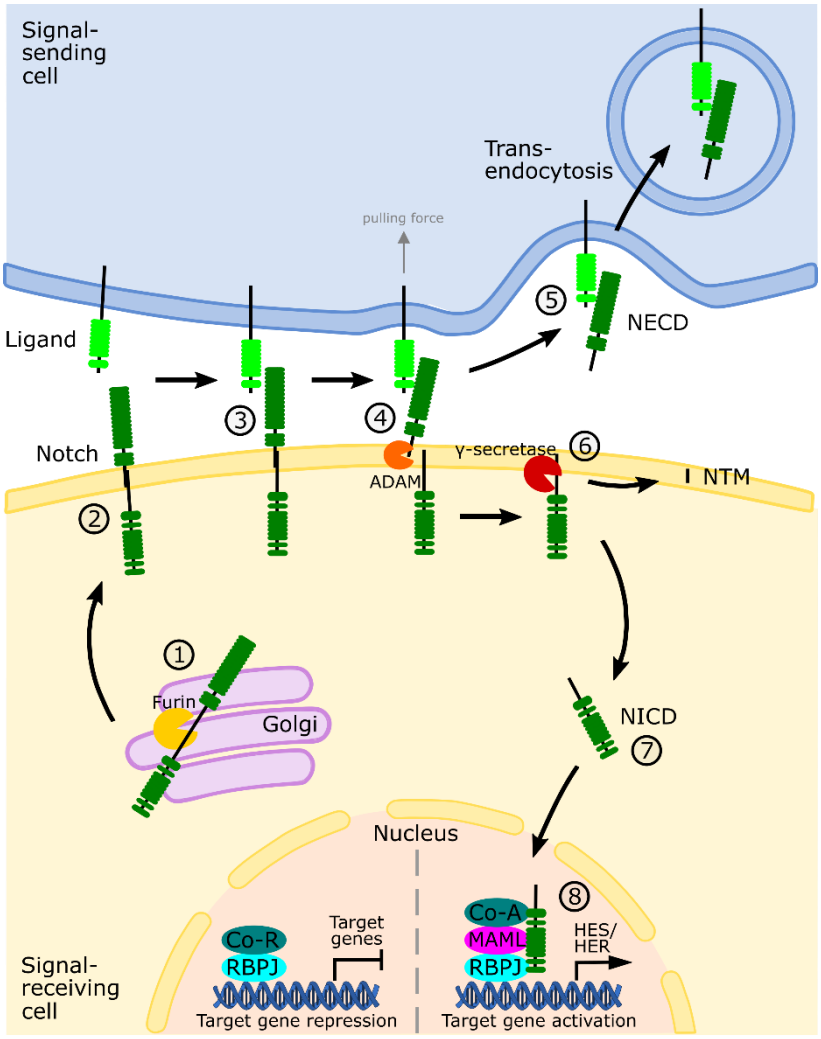

Figure 2-1: The Notch signaling pathway. (1) Furin-mediated Notch receptor processing in the *trans*-Golgi network (S1 cleavage); (2) Notch transit to the plasma membrane; (3) Receptor-ligand binding; (4) ADAM-mediated separation of the NECD from the receptor (S2 cleavage); (5) Endocytic uptake of the NECD bound to the ligand into the signal-sending cell (trans-endocytosis); (6) γ-secretase-mediated separation of the NICD from the transmembrane domain (S3 cleavage), leaving the NTM; (7) NICD translocation to the nucleus; (8) Complex formation of the receptor with a co-activator (CO-A), MAML and RBPJ to activate Notch target genes.

2.2.2 Mechanical forces during Notch signaling

During the Notch signaling pathway, mechanical forces are involved in the form of intercellular adhesion at receptor-ligand binding, and at trans-endocytosis during NECD uptake into ligand presenting cells [21, 23]. Receptor-ligand binding is mechanically linked to the intercellular adhesive strength and becomes stronger as the tension between receptor and ligand expressing cells increases [23-25]. With increased tension between two neighboring cells, receptor-ligand binding also increases [23]. The high force between the receptor and the ligand originates from the Notch receptor and is based on both the extracellular and intracellular domain [25]. For subsequent receptor activation by proteolytic cleavage, however, a mechanical pulling force is necessary [21, 26, 27]. After receptor-ligand binding in the process of trans-endocytosis into the ligand presenting cell, the ligand exerts a molecular strain on the extracellular portion of the receptor, thereby exposing the S2 ADAM cleavage site [21, 27]. The pulling force acts on the negative regulatory region of the receptor, making the NRR a mechanosensitive switch [24, 27]. The masked S2 cleavage site in the receptor serves as an autoinhibition, providing additional control over pathway activation [27].

2.3 Physiological and tumor angiogenesis

Angiogenesis describes the process of new vessel formation from existing vascular systems [1, 28]. The process is usually induced during tissue growth and repair, serving to supply all tissues and organs with oxygen and nutrients as well as removing metabolic products [29-31]. Uncontrolled and abnormal vascular growth triggers or facilitates numerous disease processes: inadequate growth or vascular occlusion results in ischemia and necrosis, excessive growth promotes diseases such as inflammatory disorders or cancer progression [29, 31]. Tumor angiogenesis is considered a crucial hallmark of cancer and also contributes significantly to tumor cell metastasis [29, 32].

2.3.1 Mechanism of angiogenesis

The process of angiogenesis can be divided into four steps: endothelial activation, tip/stalk cell selection, vessel elongation, and vessel stabilization [29, 33]. Angiogenesis is initiated by local hypoxia, which releases angiogenic factors, including biochemical and mechanical cues. Through these pro-angiogenic factors, ECs in the existing vessel structure are activated and become motile [31, 34]. Loosened cell-matrix connections, due to increased ECM elasticity, allow the breakout of an endothelial cell from the vessel and its migration in the direction of a VEGF gradient, released by the hypoxic tissue [8, 31, 35]. The determination of which of the cells break out of the vessel and form a new sprout is decided by the adaption of tip or stalk cell phenotypes of the ECs [36]. The selection of tip and stalk cells is initially regulated by biochemical signals transmitted by the surrounding tissue, with VEGF having the greatest influence by regulating Dll4-Notch signaling, which defines the tip and stalk cells, and by reorganizing the ECM structure, which enables the migration of tip cells [4, 8, 34]. By forming filopodia, the tip cells can mediate sprout formation and induce ECM degradation by expression of endopeptidases (matrix metalloproteinases, MMPs) [8, 28]. The tip cells are followed by proliferating stalk cells that collectively invade the hypoxic tissue, allowing vessel elongation and lumen formation [2, 3]. Cell proliferation is driven by increased matrix stiffness as the matrix exerts a mechanical stretch on the ECs that induces morphological changes [36]. Also, the stalk cell phenotype is enhanced by increased cell-matrix contacts due to the increased ECM stiffness [4]. During lumen formation, stalk cells additionally synthesize a

basement membrane around the newly formed vessel [37]. The final phase of angiogenesis is the maturation and stabilization of the newly formed vessels [38, 39]. External stabilization occurs by cell recruitment of mural cells and the basement membrane. Whereas vascular maturation includes vessel condensation and alignment via increased cell–cell adhesion, shear stress induces vessel shaping [34, 38, 39].

2.3.2 Mechanical aspects of angiogenesis

The initiation of angiogenesis by hypoxia, whereby angiogenic factors are released and subsequent cellular signaling pathways are thus activated by biochemical signals, is widely known and well-studied [40]. However, the influence of mechanical cues in angiogenesis is now receiving more attention [3, 33, 34]. Besides the shear force due to the blood flow, most of the mechanical forces on the endothelial cells are exerted by the ECM, caused by matrix structural changes that can locally alter the matrix stiffness and density [2, 8, 36]. Changes in the matrix result either from biochemical and mechanical signals from the surrounding tissue, influencing the endothelial cell behavior or from the ECs themselves, affecting the matrix assembly and thus creating defined conditions for the different stages of angiogenesis [2, 28]. In a stable and mature vessel, medium mechanical forces act between the endothelial cells lining the inner surface of the vessel and between the ECs and the surrounding tissue [3]. When a tip cell breaks out of a vessel wall, the mechanical forces between two neighboring cells and between matrix and tip cell decrease, allowing migration [2, 36]. In addition, the mechanical forces of the vessel-stabilizing cells and the surrounding tissue breaks open as the ECM is degraded [8, 35]. During vessel elongation, the cell-matrix junctions must be strengthened to allow proliferation of stalk cells, resulting in high mechanical forces [36]. At the end of angiogenesis, during vessel maturation, in the process of cell recruitment stabilizing cells and the surrounding tissue exert weak forces on the ECs, but between the endothelial cells in the newly formed vessel, the medium mechanical forces already occur, guaranteeing a stable vessel [41, 42]. Thus, coordinated stiffness gradients and local matrix stiffening in the respective steps of angiogenesis are essential for the formation of new blood vessels [3]. The local stiffness changes and the resulting mechanical forces acting during angiogenesis are shown in Figure 2.2.

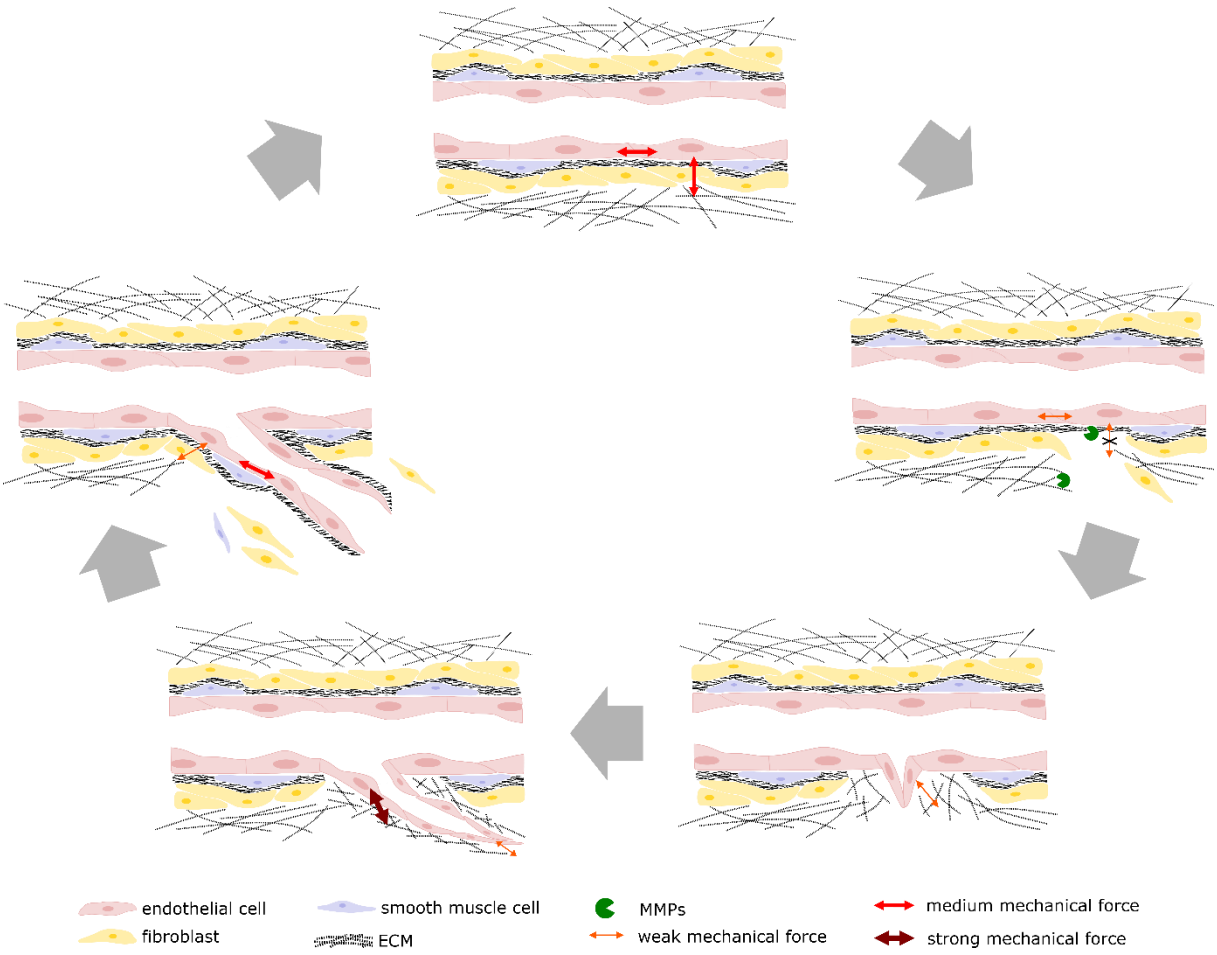

Figure 2-2: Mechanical forces during angiogenesis [33]. During the different steps of angiogenesis, mechanical forces act between the endothelial cells or between the ECs and the extracellular matrix. Weak, medium, and strong mechanical forces are indicated by force arrows.

2.3.3 Microenvironmental changes in tumor angiogenesis

The tumor microenvironment and tumor microvasculature are very different from those in healthy tissue [6]. Tumor vessels show a malformed structure with deviant branching patterns as well as tortuous and permeable vessels, originated by an elevated stiffness [6, 43]. In the tumor microenvironment stiffness can be changed separately from collagen density due to enhanced collagen deposition, inter alia through up-regulated VEGF levels, and collagen cross-linking proteins, secreted by tumor cells [6]. Since excessive matrix density reduces angiogenic sprouting, density-independent stiffening of the matrix allows blood vessels to form even in the tumor microenvironment. In addition, increased matrix stiffness leads to increased MMP activity, which enables tip cells to easily invade the surrounding tissue during the formation of new sprouts [6]. However, this makes for ineffective sprouting, as the pathologically high ECM stiffness affects cell-cell contacts, migration, and proliferation of capillary-forming endothelial cells and thus vessel integrity, causing the sprouts to either break off or become leaky [6, 43, 44]. Further studies show that the abnormal tumor microenvironment also leads to increased tumor aggressiveness and progression, metastatic potential as well as treatment resistance [45].

2.4 Notch signaling in angiogenesis

The Notch signaling pathway is instrumental in angiogenesis, regulating the selection of tip and stalk cells [46, 47]. Tip/stalk cell specification involves both Dll4-Notch1 signaling and Jagged1-Notch1 signaling [47]. Tip cells are characterized by increased Dll4 expression mediated by VEGF-VEGFR2 signaling [1, 47]. Stalk cells, on the other hand, exhibit increased Notch1 expression, which is caused by the high Dll4 level in the tip cells [1]. Activation of the Notch signaling pathway in stalk cells by Dll4 expression in tip cells, induces cell proliferation of stalk cells, resulting in extension of sprouts and lumen formation [1, 40]. Dll4-mediated Notch signaling further suppresses tip-like behavior in stalk cells and reduces VEGF receptor expression in tip cells, restricting tip cell selection [47, 48]. Thus, Dll4-Notch1 signaling supports vessel elongation [40, 47]. In contrast, the Notch ligand Jagged1 antagonizes Dll4-Notch1 signaling, promoting tip cell selection, and sprouting through Jagged1-Notch1 signaling [47, 49]. The expression of Dll4 and Notch1 varies in the endothelial cells, which also changes the tip and stalk cell specifications [50]. The heterogeneity of endothelial cells allows vessel branching. However, with high VEGF release, endothelial cells synchronize, leading to the maintenance of either a tip or stalk cell phenotype, allowing sprout formation and elongation to occur [50]. The process of Notch signaling during angiogenesis in connection with tip/stalk cell selection is shown schematically in Figure 2.3.

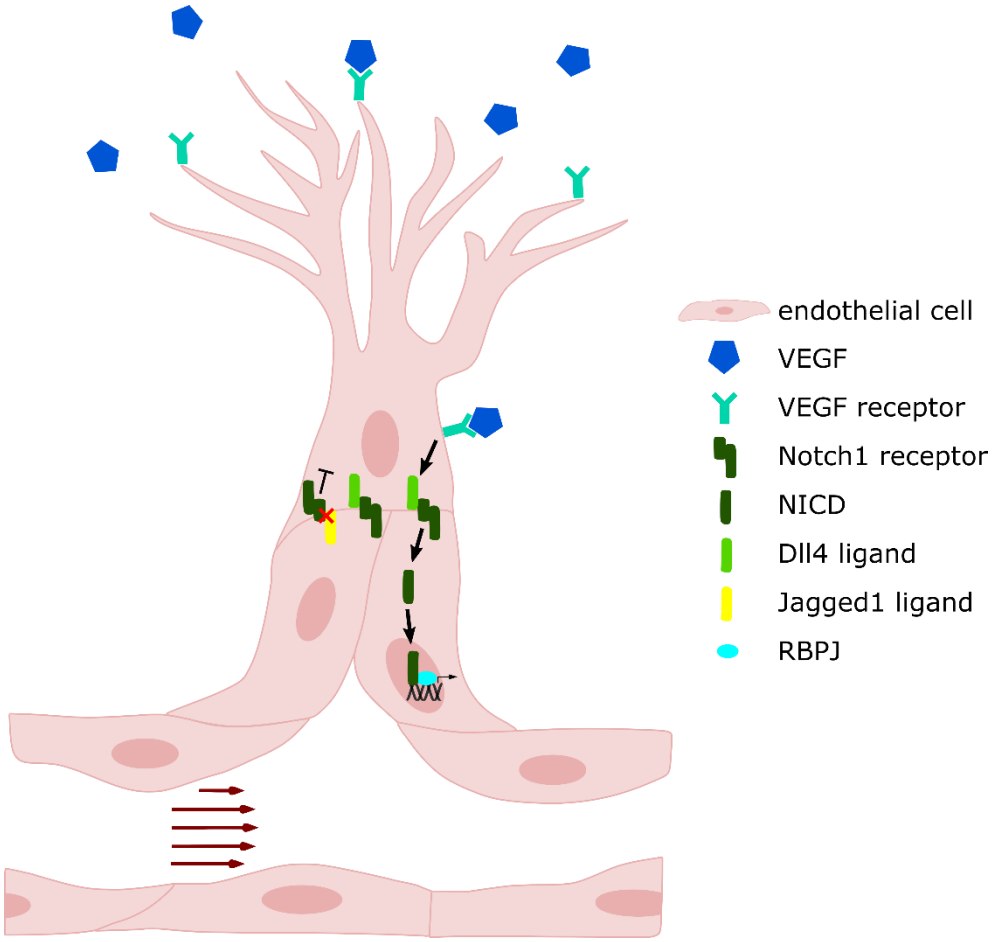

Figure 2-3: Notch signaling in tip/stalk cell selection. Upon VEGF/VEGFR2 signaling Dll4 expression increases in the cells braking out of a vascular network (tip cells), leading to Notch activation in the following stalk cells. The Notch signaling pathway terminates in activation of Notch target genes, supporting vessel elongation. Jagged1 antagonizes Dll4-Notch1 signaling. Jagged1-Notch1 signaling promotes tip cell selection and sprouting and restricts vessel elongation.

2.4.1 Notch signaling in tumor angiogenesis

Notch activity plays a major role in both tumor cells and the tumor vasculature [51, 52]. Depending on the tumor type, the signaling pathway acts either as an oncogene or as a tumor suppressor, whereas Notch-mediated promotion of tumor progression and especially tumor angiogenesis occurs more frequently in the different cancer types [52-54]. Oncogenic association of the Notch pathway involves Dll4/Notch1 signaling, as in normal angiogenesis [51]. The ligand Dll4 plays the major role, being strongly overexpressed in the tumor vasculature, induced by pro-angiogenic factors, especially VEGF [51, 52, 55]. Consequently, the Notch receptors as well as Notch target genes such as Hes1 are also upregulated [51]. Dll4 overexpression associated with activation of Notch receptors reduces branching and significantly increases the diameter of the tumor vessel [50]. Furthermore, activation of Notch signaling influences several cell fate decisions and contributes to elevated proliferation, decreased differentiation and dysregulated apoptosis [54]. However, especially in malignant tumors, activation of the signaling pathway is often impaired and mutated, leading to increasingly abnormal and uncontrolled tumor angiogenesis as well as altered endothelial phenotypes [6, 56]. Oncogenic involvement of the Notch signaling pathway in tumor angiogenesis and the resulting malformed vasculature not only facilitates tumor progression but also causes therapeutic resistance [45, 54].

2.5 Aim of the study

The Notch signaling pathway plays an important role in most tissues, enabling cell communication in a context-dependent manner, thereby regulating cell fate decisions, cell cycle progression and apoptosis. Thus, the Notch signaling pathway is also a key regulator of angiogenesis. The Notch-mediated selection of vascular endothelial cells into tip and stalk cells controls migration and proliferation, driving sprout formation, elongation, and branching. Angiogenesis is influenced by biochemical and mechanical signals, with the biochemical cues being well studied and the mechanical cues only recently gaining importance. Besides the shear force of the blood flow, most of the mechanical cues during angiogenesis are exerted by the ECM, caused by matrix structural changes that can locally alter the ECM stiffness and density. However, little is known about the mechanical impact via the matrix on the signaling pathways involved in angiogenesis, like the Notch signaling pathway.

The first part of the study therefore aims to investigate the influence of different physiological relevant substrate stiffnesses on the Notch signaling pathway and related other pathways in endothelial cells. Using different stiffness-tuned silicone substrates and Dll4 as a ligand, a mechanosensitivity of Notch is to be elucidated. Furthermore, this study considers the significance of cell-cell contacts on Notch activation and the mutual influence of Notch and adhesion proteins, as well as the crosstalk between Notch and YAP signaling, a well-known mechanosensitive pathway.

The second part of the study aims to investigate the Notch signaling pathway and substrate stiffness in angiogenesis. Using both a 2D tube formation and 3D spheroid sprouting angiogenesis model, the role of the Notch signaling pathway and Dll4-dependent tip cell coordination is to be investigated. Moreover, this study analyzes the influence of substrate stiffness of angiogenic sprouting behavior in endothelial spheroids.

3 Material and methods

3.1 Material

3.1.1 Technical equipment

Table 3-1: Technical equipment.

Device	Manufacturer
Bold Line incubation system	Okolab, Pozzouli, Italy
Compartment drier	Memmert, Schwabach, Germany
Digital UV Ozone Cleaner system	Novascan Technologies, Ames, IA, USA
Desiccator	Glaswerk Werthheim, Werthheim, Germany
HERACell 150i incubator	Thermo Scientific, Waltham, MA, USA
Lamina flow Heraeus, Herasafe	Thermo Scientific, Waltham, MA, USA
Leica DMi1 microscope + camera Leica MC120HD	Leica Microsystems, Wetzlar, Germany
Leica TCS SP8 confocal microscope	Leica Microsystems, Wetzlar, Germany
Megafuge 1.0 RS centrifuge	Thermo Scientific, Waltham, MA, USA
Modular Compact Rheometer MCR 100 + PP25 measuring plates	Physica, Stuttgart, Germany
Nanodrop® 1000 spectrophotometer	PEQLAB Biotechnologie GmbH, Erlangen, Germany
Orion II microplate luminometer	Titertek Berthold, Bad Wildbad, Germany
Plasma cleaner type 'ZEPTO'	Diener electronic, Berlin, Germany
SpectraFluor Plus™ plate reader	Tecan, Crailsheim, Germany
Vi-Cell™ XR cell counter	Beckman Coulter, Brea, CA, USA
Vibrax VXR basic lab shaker	IKA, Staufen, Germany
Water bath Haake W19	Thermo Scientific, Waltham, MA, USA

3.1.2 Consumables

Table 3-2: Consumables.

Product	Manufacturer
Cell culture flasks: 25 cm^2, 75 cm^2	Sarstedt, Nürnbrecht, Germany
Disposable pipettes: 5 ml, 10 ml, 25 ml	Sarstedt, Nürnbrecht, Germany
Falcon tubes: 15 ml, 50 ml	Sarstedt, Nürnbrecht, Germany
Microtiter plates: 6 well, 96 well	Sarstedt, Nürnbrecht, Germany
Petri dishes: 100 mm, 40 mm	Sarstedt, Nürnbrecht, Germany
Pipette tips: 10 µl, 100 µl, 1000 µl	Sarstedt, Nürnbrecht, Germany
SafeSeal tubes: 0.5 ml, 1.5 ml, 2 ml	Sarstedt, Nürnbrecht, Germany
µ-slide 2 well uncoated	ibidi, Martinsried, Germany
µ-slide 8 well ibiTreat, uncoated	ibidi, Martinsried, Germany
µ-slide angiogenesis ibiTreat	ibidi, Martinsried, Germany

3.1.3 Chemicals and reagents

Table 3-3: Chemicals and reagents.

Reagent	Company
Amaxa HUVEC Nucleofector Kit	Lonza, Basel, Switzerland
Amphotericin B	PAN Biotech, Aidenbach, Germany
Ampicillin	Sigma Aldrich, St. Louis, MO, USA
Bovine serum albumin (BSA)	Sigma Aldrich, St. Louis, MO, USA
Collagen G	Biochrom AG, Berlin, Germany
Crystal violet	Carl Roth, Karlsruhe, Germany
Dimethyl sulfoxide (DMSO)	Sigma Aldrich, St. Louis, MO, USA
Dual-Luciferase® Reporter Assay System	Promega, Mannheim, Germany
Dulbecco's Modified Eagle Medium (DMEM)	PAA Laboratories, Pasching, Austria

Reagent	Company
Endothelial Cell Growth Medium (ECGM) kit enhanced	Pelobiotech GmbH, Martinsried, Germany
Ethylenediaminetetraacetic acid (EDTA)	Sigma Aldrich, St. Louis, MO, USA
Ethylene glycol tetraacetic acid (EGTA)	Sigma Aldrich, St. Louis, MO, USA
Fetal calf serum (FCS)	Biochrom AG, Berlin, Germany
FluorSave™ Reagent	Merck Millipore, Darmstadt, Germany
FuGENE® Transfection Reagent	Promega, Mannheim, Germany
Hoechst 33342	Sigma Aldrich, St. Louis, MO, USA
Kanamycin	Sigma Aldrich, St. Louis, MO, USA
L-Glutamine	Sigma Aldrich, St. Louis, MO, USA
Methylcellulose	Sigma Aldrich, St. Louis, MO, USA
Paraformaldehyde (PFA)	Thermo Scientific, Waltham, MA, USA
Penicillin/Streptomycin 100x	PAN Biotech, Aidenbach, Germany
Recombinant human Dll4 His-tag protein	R&D Systems, Minneapolis, MN, USA
Recombinant human vascular endothelial growth factor (VEGF) 165	PeproTech, Rocky Hill, NJ, USA
Sodium chloride (NaCl)	Sigma Aldrich, St. Louis, MO, USA
Targefect-HUVEC™	Targeting Systems, El Cajon, CA, USA
Transferrin, Alexa Flour 488 conjugate	Life Technologies, Carlsbad, CA, USA
Trisodium citrate	Sigma Aldrich, St. Louis, MO, USA
Triton X-100	Sigma Aldrich, St. Louis, MO, USA
Trypsin	PAN Biotech, Aidenbach, Germany

3.1.4 Buffers and solutions

Table 3-4: Buffers and solutions.

Buffer / solution	Composition
Collagen G	1.25 ml collagen G (0.4 %) in 500 ml PBS
Methocel stock solution	1.2 % (v/w) methylcellulose (autoclaved) in ECGM
Phosphate buffered saline (PBS) pH 7.4	132.2 mM NaCl 10.4 mM Na_2HPO_4 3.2 mM KH_2PO_4 in H_2O
PBS + Ca^{2+}/Mg^{2+} (PBS^{+}) pH 7.4	137 mM NaCl 2.68 mM KCl 8.1 mM Na_2HPO_4 1.47 mM KH_2PO_4 0.25 mM $MgCl_2$ x 6 H_2O 0.5 mM $CaCl_2$ x 2 H_2O in H_2O
rhDll4	1 µg/ml rhDll4 in PBS + collagen G
Trypsin/EDTA (T/E)	Trypsin 0.05 % (w/v) Na_2EDTA x 2 H_2O 0.02 % (w/v) in PBS

3.1.5 Hydrogels and polymers

Table 3-5: Hydrogels and polymers.

Hydrogel / polymer	Manufacturer
Collagen I high concentration, rat tail	Corning, New York, NY, USA
Matrigel, growth factor reduced, phenol red free	Corning, New York, NY, USA
PhotoCol®-IRG	Advanced BioMatrix, Carlsbad, CA, USA
Polydimethylsiloxane (PDMS), Sylgard 184 silicone elastomer kit	Dow Corning, Midland, MI, USA

3.1.6 Antibodies

Table 3-6: Primary antibodies.

Name	Species	Catalogue	Manufacturer	Dilution
ADAMTS-1 (3C8F4)	mouse mAb IgG_1	Sc-47727	Santa Cruz Biotechnology, Dallas, TX, USA	1:200
Cleaved Notch1 (Val1744)	rabbit mAb IgG	4147	Cell Signaling Technology, Cambridge, UK	1:200
Integrin β1	rabbit IgG	4706	Cell Signaling Technology, Cambridge, UK	1:200
Integrin β1 (12G10)	mouse IgG_1	ab30394	Abcam, Cambridge, UK	1:200
VE-cadherin	rabbit IgG	2158	Cell Signaling Technology, Cambridge, UK	1:200
VE-cadherin, clone BV6	mouse IgG_{2a}	MABT134	Merck KGaA, Darmstadt, Germany	1:10 (blocking)
YAP (D8H1X) XP®	rabbit IgG	14074	Cell Signaling Technology, Cambridge, UK	1:200

Table 3-7: Secondary antibodies.

Name	Species	Catalogue	Manufacturer	Dilution
Alexa Fluor 488	goat anti-mouse IgG (H+L)	A-11001	Life Technologies, Carlsbad, CA, USA	1:400
Alexa Fluor 488	goat anti-rabbit IgG (H+L)	A-11008	Life Technologies, Carlsbad, CA, USA	1:400
Alexa Fluor 647	chicken anti-rabbit IgG (H+L)	A-21443	Life Technologies, Carlsbad, CA, USA	1:400

3.1.7 Compounds

The γ-secretase inhibitor DAPT was purchased from Sigma (St. Louis, MO, USA), handled according to the manufacturer's instructions, and used at a working concentration of 25 μM containing ≤0.25 % DMSO. DMSO controls were performed with the appropriate DMSO concentrations.

3.1.8 Software

Table 3-8: Software.

Software	Origin
GraphPad Prism 9	GraphPad Software, San Diego, CA, USA
ImageJ	National Institutes of Health, Behtesda, MD, USA
ImageJ plugin AnalyzeSkeleton	[57]
ImageJ plugin TrackMate	[58]
ImageJ plugin Trainable Weka Segmentation	[59]
ImageJ software tool Angiogenesis Analyzer	Gilles Carpentier, Faculte de Sciences et Technologie Universite Paris Est Creteil Val-de-Marne, Paris, France
ImageJ software tool Intensity Ratio Nuclei Cytoplasm	FAIR Data Informatics Lab, University of California, San Diego, CA, USA
LAS X Core Software	Leica Microsystems, Wetzlar, Germany
Microsoft Office Standard 2016	Microsoft, Redmond, WA, USA

3.2 Methods

3.2.1 Cell culture

3.2.1.1 Cell lines and culture media

All cells were cultivated under high humidity at 37 °C and a 5 % CO_2 atmosphere. ECGM cell culture medium was supplemented with the ECGM kit enhanced, 10 % FCS, 1 % penicillin / streptomycin and 1 % amphotericin B. DMEM cell culture medium was supplemented with 10 % FCS and 1 % L-Glutamine.

Human umbilical vein endothelial cells (HUVEC) were purchased from Promocell. Cells were cultivated in ECGM for a maximum of six passages. All experiments were performed in passage #6. Mouse cardiac endothelial wild type cells (MCEC-WT) were a kind gift from the laboratory of Prof. David Sprinzak (University of Tel Aviv, Israel). Dll4 overexpressing mouse cardiac endothelial cells (MCEC-Dll4-mCherry) were generated by Rose Mamistvalov (Prof. Sprinzak, University of Tel Aviv). Both MCEC cell lines were cultivated in DMEM medium and used in continuous passage. Before seeding, all surfaces were coated with collagen G for 30 min.

3.2.1.2 Passaging

Upon reaching confluence, the cells were detached from the cell culture flask by removing the growth medium, washing the cells twice with pre-warmed PBS, and incubation with trypsin / EDTA for 5 min at 37 °C. Tryptic digestion was stopped by addition of growth medium. Cells were centrifuged at 1000 rpm at room temperature for 5 min and resuspended in growth medium. For sub-cultivation, cells were split 1:2 - 1:20 and reseeded in 25 cm^2 or 75 cm^2 cell culture flasks (coated). For further experiments, cells were counted using a ViCell™ XR cell counter and seeded onto the appropriate substrates (coated) at the required cell concentrations.

3.2.1.3 Co-cultures

Co-cultures were seeded at 1:1, 1:5 and 1:10 ratios by determining cell concentrations. DMEM was used for the co-culture of both MCEC cell lines, whereas the co-cultures of HUVECs and MCECs were incubated in ECGM.

3.2.2 Polymers and hydrogels

3.2.2.1 PDMS preparation

PDMS base elastomer and curing agent were mixed in defined ratios. Air bubbles were removed by degassing in the desiccator for 15 – 20 min. Using cut pipette tips, specific volumes of PDMS were added to the cell culture dishes used: 1000 µl / 6 well, 450 µl / 2 well (ibidi), 90 µl / 8 well (ibidi). PDMS substrates were polymerized in compartment drier for 20 h at 60 °C. The following ratios of base elastomer and curing agent were used to prepare the indicated substrate stiffnesses.

Table 3-9: PDMS base elastomer to curing agent ratios.

Ratio of base elastomer to curing agent	Resulting stiffness
10:1	70 kPa
50:1	1.5 kPa
75:1	0.5 kPa

Before using the PDMS substrates, they were hydrophilized by plasma cleaning. The plasma process was performed at 0.3 mbar O_2 for 3 min. For cell seeding, the PDMS was coated as described above (3.2.1.1).

3.2.2.2 Rheological analyses

The stiffness of the PDMS substrates was verified using a Modular Compact Rheometer MCR 100. The substrates were prepared in 40 mm petri dishes and hydrophilized by plasma cleaning. The substrates were cut to the size of the PP25 measuring plates and measured in amplitude sweep mode with a constant frequency of 1 Hz at 37 °C. Deformations between 0.01 % and 10 % in ramp mode were applied. Each measurement consisted of 30 measurement

points, each with a duration of 15 sec. Three independent measurements per stiffness were averaged.

3.2.2.3 Hydrogel preparation

Two different hydrogels were used: collagen I (2 mg/ml) and PhotoCol® (4 mg/ml). All preparations were carried out on ice to avoid early polymerization.

For the collagen I gels, the collagen stock solution was diluted with 10 x PBS, 1 N NaOH and dH_2O according to the manufacturer's protocol to the final concentration of 2 mg/ml. For the PhotoCol® gels, the lyophilized methacrylated collagen initially was diluted with 20 mM acetic acid to a concentration of 4 mg/ml. In accordance with the manufacturer's instructions, the collagen solution was first mixed with neutralization solution and then with photoinitiator, depending on the volume of collagen.

Both collagen gels were used to embed the spheroids for the spheroid sprouting assay (see 3.2.8.2).

3.2.3 Cell-matrix adhesion assay

For the adhesion assay, cell culture plates were coated with collagen G and additionally incubated with heat denatured BSA for 30 min at room temperature. Cells were prepared in DMEM + 25 mM HEPES at a concentration of 500,000 cells/ml and incubated in suspension at 37 °C, 5 % CO_2 for 10 min. The blocking solution was removed and the cells were seeded into the cell culture plate. After 15 min, 45 min or 90 min incubation, the control was fixed directly with 4 % methanol free formaldehyde in PBS for 10 min. Cells from the remaining conditions were washed twice with PBS, fixed and stained with 0.5 % crystal violet in methanol for 15 min. Excess dye was removed by three washing steps with dH_2O. After drying, the cell-bound dye was redissolved in trisodium citrate solution in 50 % ethanol and the optical density was detected at 550 nm using a SpectraFluor Plus™ (Tecan).

3.2.4 Plasmids and transfections

The following plasmid constructs were used for transient transfections:

Table 3-10: Plasmid constructs.

Name	Insert	Backbone	Bac. Res.	Source
mCitrine-VE-cadherin-N-10	VE-cadherin	mCitrine-N1	Kanamycin	Addgene #56319
pcDNA3-hN1-citrine	hN1	pcDNA3	Ampicillin	Prof. Sprinzak Lab
pcDNA5-TO-hDll4-mCherry	hDll4	pcDNA5/TO	Ampicillin	Prof. Sprinzak Lab
Renilla	Luc control	n.a.	Ampicillin	Addgene #27163
TP1-Luc	TP1 reporter	n.a.	Ampicillin	Prof. Sprinzak Lab

Primary endothelial cells were transiently transfected with two different commercially available transfection systems: lipofection with the Targefect-HUVEC™ reagent (Targeting Systems) and nucleofection with the Amaxa® HUVEC Nucleofector® Kit (Lonza).
The lipofections were performed prior to the reporter gene assays. The day before transfection, 125,000 cells/ml were seeded into collagen G coated 6 well plates. A total amount of 1.1 µg plasmid DNA was added to the transfection complex and incubated on the cells for 2 h before replacing the complex with culture medium. All further experiments were performed 24 h after transfection. For nucleofections, $1x10^6$ cells each were transfected in suspension with 2.5 µg plasmid DNA. Cells were transferred into 6 well plates or 8 well µ-slides and the transfection solution was replaced by culture medium after 4 h incubation. All further experiments were performed 24 h after transfection.

MCECs were transiently transfected by lipofection with the FuGENE® HD reagent (Promega). One day prior to the transfection, 125,000 cells/ml were seeded into collagen G coated 6 well plates. For each well, 2 µg of plasmid DNA was mixed with the transfection reagent and incubated on the cells for 24 h before further experiments were performed.

3.2.5 Reporter gene assay

Notch-responsive luciferase reporter assays were performed 24 h subsequent to the co-transfection of endothelial cells with the CSL-binding plasmid TP1-Luc and Renilla. Firefly and Renilla vector levels were applied in a ratio 10:1. Using the Dual-Luciferase® Reporter Assay System by Promega and the Orion II microplate luminometer equipped with Simplicity analysis software, luciferase levels were determined. Firefly RLUs were normalized to the Renilla control.

3.2.6 Confocal imaging

Laser scanning confocal microscopy was performed with the Leica TCS SP8 microscope equipped with an HC PL APO CS2 63x/1.4 oil objective and photomultiplier (PMT) or HyD detectors, using the LAS X core software. In sequential scanning mode two frames were acquired for every channel with a scanning speed of 400 Hz and the pinhole size set to 1.0 airy units. Following excitation laser lines were applied: 405 nm, 488 nm, and 647 nm.

3.2.6.1 Immunofluorescence staining

For immunofluorescence stainings, cells were washed once with PBS^+ and fixed with 4 % methanol free formaldehyde in PBS for 10 min. Fixation was followed by a brief washing with PBS and cell permeabilization with 0.1 % Triton X-100 in PBS for 10 min. After another brief washing with PBS, nonspecific binding sites were blocked with 5 % BSA in PBS for 60 min at room temperature. Cells were then incubated with the primary antibody diluted in PBS with 1 % BSA overnight at 4 °C. Next, samples were washed 3 x 10 min with 1 % BSA in PBS, then incubated with the secondary antibody and Hoechst 33342 (1:100) for nuclear counter stain, again diluted in PBS with 1 % BSA for 1 h at room temperature. Cells were washed 2 x 10 min with 1 % BSA in PBS, once 10 min with PBS and sealed with FluorSave reagent mounting medium. All stainings were performed in coated 8 well or 2 well µ-slides.

3.2.6.2 Immunofluorescence staining of hydrogels

For immunostaining of spheroids embedded in collagen, hydrogels were washed with PBS^+ for 10 min followed by 30 min fixation with 4 % methanol free formaldehyde in PBS. After a 10 min washing step with PBS, spheroids were permeabilized with 0.1 % Triton X-100 in PBS for 30 min. Samples were washed again for 10 min with PBS. Nonspecific binding sites were blocked with 5 % BSA in PBS for 3 h at 4 °C. Spheroids were then incubated overnight at 4 °C with the primary antibody diluted in PBS with 1 % BSA. Samples were washed 6 x 10 min with 1 % BSA in PBS, prior to incubation with the secondary antibody and Hoechst 33342 (1:100) for nuclear counter stain over night at 4 °C, again diluted in PBS with 1 % BSA. Embedded spheroids were washed 2 x 20 min with 1 % BSA in PBS, once 20 min with PBS and sealed with FluorSave reagent mounting medium. All stainings were performed in hydrophilized 8 well or μ-slides.

3.2.6.3 Fluorescence recovery after photobleaching (FRAP)

HUVECs were transiently transfected with mCitrine-VE-Cadherin-N-10, seeded directly on different substrates (plastic and PDMS) and incubated for 24 h. The FRAP assay was conducted with the Leica TCS SP8 SMD microscope with the HC PL APO CS2 63x/1.4 NA oil objective and the heating and gas incubation system from Okolab ensuring constant 37 °C under 5 % CO_2 and 80 % humidity. Using the LAS X Core Software, the FRAP settings were adjusted to one pre-bleach iteration, 20 bleach iterations, five post-bleach iterations with 30 sec intervals and seven with 60 sec intervals. Images were taken with a pinhole size adjusted to 1.0 airy units and a scanning speed of 400 Hz. The line 488 (argon) and the PMT detector were applied.

3.2.7 Endocytosis assays

3.2.7.1 Trans-endocytosis assay

Cells grown to 80 % confluency (HUVECs or MCEC-WTs) were transiently transfected separately with the plasmids pcDNA3-hN1-citrine and pcDNA5-TO-hDll4-mCherry and incubated on plastic for 24 h. Cells were then washed, detached, and reseeded together in a

co-culture ratio 1:1. Doxycycline was added during reseeding in a concentration of 100 ng/ml for activation of the Dll4-mCherry expression. After 6 h incubation, co-cultures were fixed with 4 % methanol free formaldehyde in PBS for 10 min. Samples were washed twice with PBS and sealed with FluorSave mounting medium. Trans-endocytosis was visualized by confocal microscopy.

3.2.7.2 Transferrin endocytosis assay

Cells grown to 100 % confluency were washed once with PBS^+ and then incubated for 10 min with 5 µg/ml Transferrin, Alexa Flour 488 conjugate at 37 °C under 5 % CO_2. Cells were washed once with acid wash medium (room temperature) and then fixed with 4 % methanol free formaldehyde in PBS for 10 min. Samples were washed twice with PBS and sealed with FluorSave mounting medium. Transferrin uptake was visualized by confocal microscopy.

3.2.8 Angiogenesis assays

3.2.8.1 Tube formation assay

Tube formation assays were performed in µ-slides angiogenesis (ibiTreat) from ibidi. The inner well of the slides was filled with 10 µl Matrigel. After polymerization at 37 °C and 5 % CO_2 for 30 min, 50 µl of cell suspension at a concentration of 200,000 cells/ml was added to the upper well and incubated for 24 h. For treatment with DAPT, it was diluted in the cell suspension to the indicated concentration and seeded onto the Matrigel. Tube formation was visualized using a Leica DMi1 microscope with 4x phase contrast objective.

3.2.8.2 Spheroid sprouting assay

Spheroids were generated using hanging drop cell culture. Cell suspension drops of 1000 cells/drop with 20 % methocel stock solution in the culture medium were pipetted to the lid of 100 mm petri dishes and incubated for 24 h. Spheroids were collected in PBS, centrifuged at room temperature and 1000 rpm for 5 min, and resuspended in a mixture of 80 % methocel stock solution and 20 % FCS. Collagen and spheroid solution were mixed in a ratio of 2:1 and

pipetted as a dome into hydrophilized 8 well slides (untreated). After incubation for 30 min at 37 °C and 5 % CO_2, ECGM + 25 nM VEGF was added to the embedded spheroids and incubated for 24 – 48 h. For the treatment with DAPT, the DAPT was diluted in the collagen spheroid mixture to the appropriate concentration. The embedding of the spheroids was performed similar to the untreated spheroids. Spheroid sprouting was either visualized using a Leica DMi1 microscope with 4x phase contrast objective or stained for tip cell markers by immunofluorescence staining (see 3.2.6.2).

3.2.9 Live cell imaging

Live cell imaging of tube formation was performed with the Leica TCS SP8 microscope equipped with an HC PL APO CS2 10x/0.40 dry or an 63x/1.4 oil objective and PMT or HyD detectors, using the LAS X core software. Slides were placed in the Bold line incubation system from Okolab at 37 °C, 5 % CO_2 atmosphere and 80 % humidity. Tube formation was imaged for 20 h.

3.2.10 Statistical analysis

All images and time lapse sequences were processed and evaluated using ImageJ version 1.53c. Unless stated otherwise, entire images of confluent cells were evaluated. Data was derived from three independent experiments represented as the mean ± SEM. Statistical analysis (mean, standard deviation, unpaired Student's t-test, ordinary one-way ANOVA with Dunnett's multiple comparison test, two-way ANOVA with Tukey's multiple comparison test) were performed using GraphPad Prism 9.2.0. Statistical significances are indicated in the respective figures.

4 Results

4.1 Part I: Effect of matrix stiffness on Notch signaling activation

4.1.1 Decreased substrate stiffness increases Notch signaling activity

To investigate the mechanosensitivity of the Notch signaling pathway, synthetic substrates with defined stiffness in a range from 0.5 to 70 kPa were applied. The stiffness of the PDMS was confirmed by rheological measurements, outlined in Figure 7-1A. Endothelial cells (HUVEC and MCEC-WT cells) were used as prototypic models for Notch signaling. The Notch signaling pathway was first activated via cell seeding onto an rhDll4 coating. Analysis of a Notch reporter gene assay showed a continuous increase in Notch transcriptional activity on softer substrates (Figure 4-1A). These findings were supported by intensity analysis of the nuclear localization of the Notch intracellular domain (NICD) after immunofluorescence staining: the softer the substrate, the higher the NICD intensity in the Notch receiver cells upon stimulation (Figure 4-1B). Thus, mechanosensitivity of the Notch signaling pathway can be assumed. The efficiency and reproducibility of coating of the PDMS substrates with rhDll4 were controlled in an availability assay by immunostaining, which showed that the rhDll4 coating was evenly distributed, and showed a comparable intensity on all substrates (Figure 4-1C).

The behavior of the endothelial cells on the PDMS substrates was verified by morphological analysis. This shows that the cell area remained unchanged, but the cells on the PDMS became slightly narrower and longer (indicated by the reduced aspect ratio), shown in Figure 7-1B and C. However, the effect was observed to the same extent on all stiffnesses, so that no stiffness-dependent morphology changes were present.

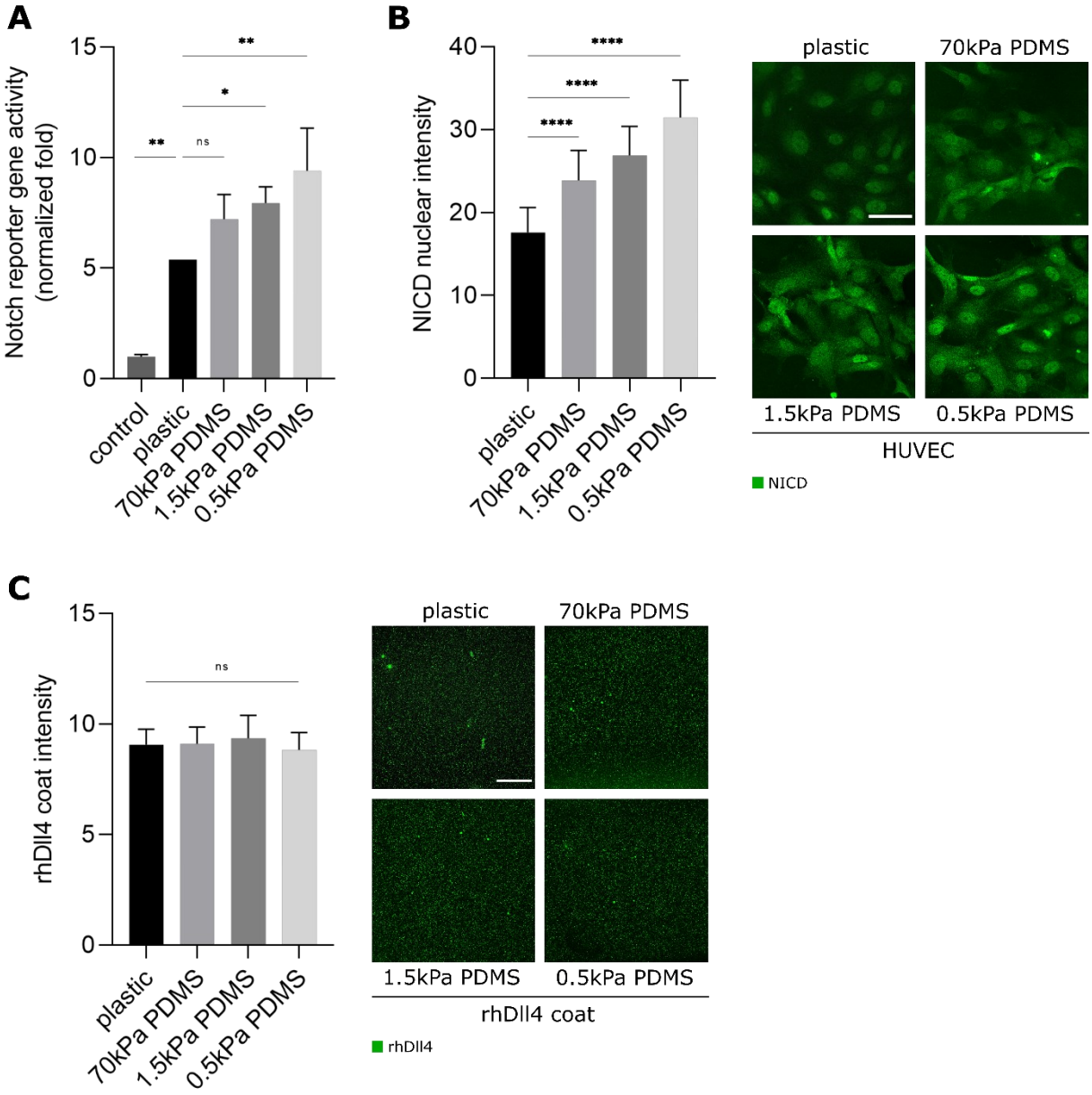

Figure 4-1: Notch activity in endothelial cells increases on soft substrates after pathway activation via rhDll4 coating. (A,B) Induction of Notch activity by coating with rhDll4. **(A)** Normalized fold Notch activity in confluent HUVEC cells on substrates with different stiffnesses, determined by detection of cellular luciferase levels under control of the TP1-luc Notch reporter (mean ± SEM, one-way ANOVA followed by Dunnett's multiple comparison test, *P<0.1, **P<0.01). Control shows the activities of non-transfected cells. **(B)** Nuclear NICD intensities in HUVEC cells seeded onto different plastic and PDMS substrates. Left panel: quantitative evaluation of nuclear fluorescence intensity of NICD (mean ± SEM, Dunnett's corrected one-way ANOVA, ****P<0.0001); right panel: representative images of cells stained for NICD (shown in green, scale bar 50 µm). **(C)** rhDll4 coating efficiency on different substrates. PDMS substrates were coated with rhDll4 and stained for Dll4 (shown in green). rhDll4 distribution was compared by evaluation of intensity, summarized in a bar plot in the left panel (mean ± SEM, two-way ANOVA followed by Tukey's multiple comparison test, ns ≙ not significant). Representative images of the rhDll4 coating are shown on the right panel (scale bar 250 µm).

Further, the Notch signaling pathway was activated by co-culture of wildtype cells (receivers) with Dll4 overexpressing MCECs (MCEC-Dll4-mCherry, senders) in a ratio of 1:1. Due to the dependence of the primary endothelial cells in in vitro culture on a protein coat, the surfaces were coated with collagen G. Again, a Notch reporter gene assay and intensity analysis of the NICD were performed. The results show the same effect as after signal path activation via rhDll4 coating. The softer the substrate, the higher the Notch reporter gene activity and the NICD intensity (Figure 4-2A and B). Activation of the Notch signaling pathway by co-culture of HUVECs as signal receiver cells with MCEC-Dll4s in different ratios receiver cells showed a 1:1 ratio to be optimal. With a higher amount of sender cells overall signal intensity decreased (Figure 4-2C).

MCEC-WT cells were used as an additional endothelial cell model. After co-culture with MCEC-Dll4-mCherrys they showed results comparable to HUVECs and the same mechanosensitivity (Figure 7-2A and B). In contrast to the HUVECs, the signal intensity of the MCEC-WTs as receiver cells increases slightly but non-significant with larger numbers of transmitter cells (Figure 7-2C).

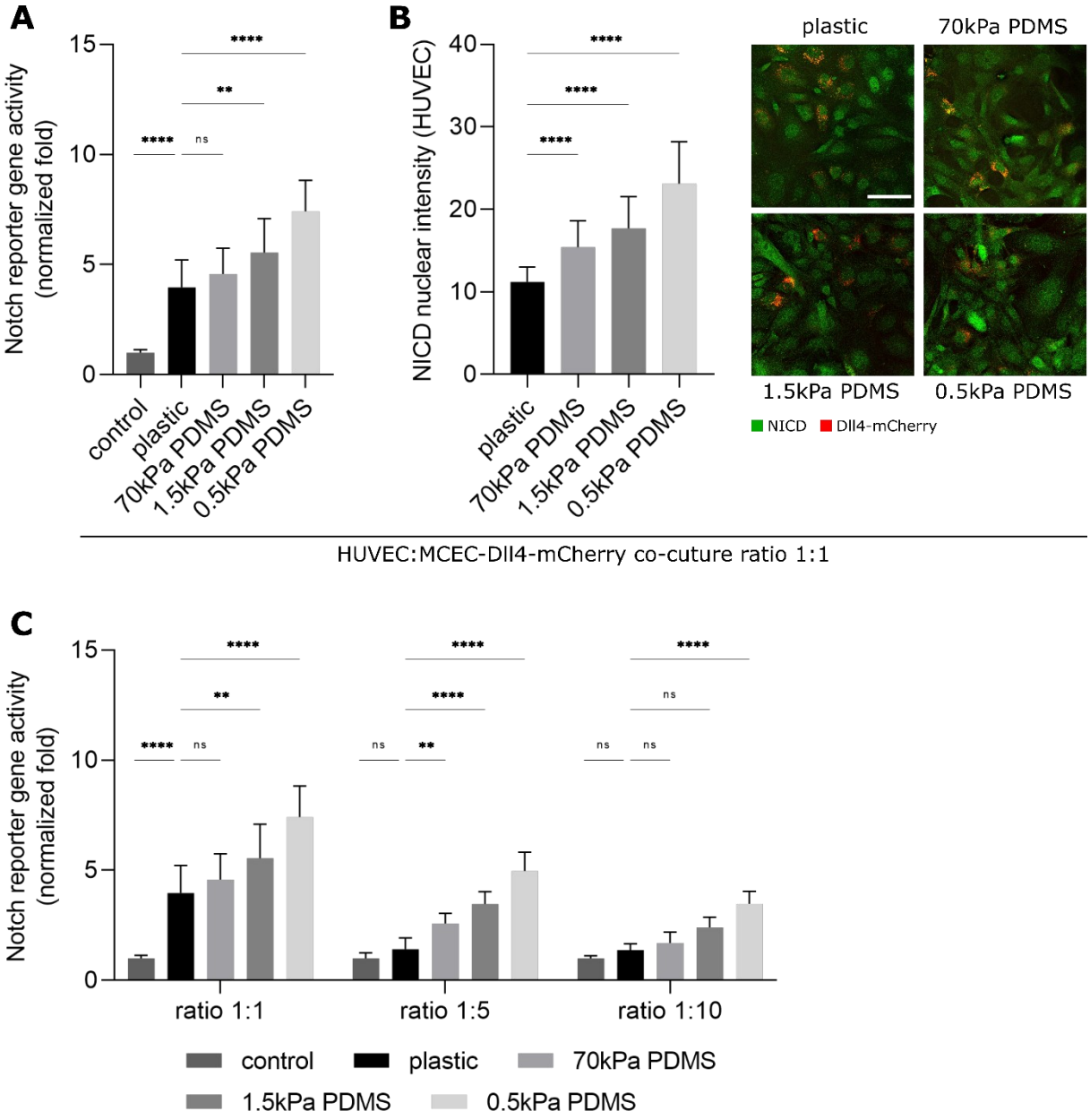

Figure 4-2: Notch activity in endothelial cells also increases on soft substrates after pathway activation by co-culture with Dll4 overexpressing cells but is dependent on the seeding ratio. (A,B) Induction of Notch activity by co-culture with MCEC-Dll4-mCherry cells on a collagen G coat. **(A)** Normalized fold Notch activity in confluent HUVEC/MCEC-Dll4-mCherry co-cultures on substrates with different stiffnesses, determined by detection of cellular luciferase levels under control of the TP1-luc Notch reporter (mean ± SEM, one-way ANOVA followed by Dunnett's multiple comparison test, ns ≙ not significant, **P<0.01, ****P<0.0001). Control shows the activities of non-transfected cells. **(B)** Left panel: nuclear NICD intensities in HUVEC cells seeded in co-culture with MCEC-Dll4-mCherry cells on different plastic and PDMS substrates. Intensities are shown in a bar graph on the left panel (mean ± SEM, Tukey's corrected one-way ANOVA, ****P<0.0001), quantified in ≥300 single cells derived from three independent experiments; right panel: representative images of cells stained for NICD (shown in green, mCherry-Dll4 reporter of MCEC-Dll4-mCherry cells shown in red, scale bar 50 µm). **(C)** Normalized fold Notch activity in endothelial co-cultures of HUVEC/MCEC-Dll4-mCherry cells in seeding ratios of 1:1, 1:5 and 1:10. Bar plots were generated by evaluation of reporter gene assays on substrates with different stiffnesses (two-way ANOVA followed by Tukey's multiple comparison test, ns ≙ not significant, **P<0.01, ****P<0.0001).

4.1.2 Yes-associated protein (YAP) signaling and Notch are inversely mechanoregulated

Next, the principle of the stiffness-dependent activation of the Notch signaling pathway and the link to other pathways was aimed to be investigated. The role of the Yes-associated protein YAP as a mechanotransducer and the related mechanosensitivity of the YAP/TAZ signaling pathway are well known [5, 60]. This and other studies have shown that YAP activity decreases on soft substrates [61]. To assess a possible YAP/Notch crosstalk in this endothelial cell model, immunofluorescence staining in HUVEC cells seeded on plastic and PDMS substrates was performed, with and without addition of the γ-secretase inhibitor DAPT (25 μM, 24 h). As expected, the results show progressively decreased nuclear YAP intensity in HUVEC cells on softer substrates, demonstrating the mechanosensitivity of the YAP/TAZ signaling pathway in these cells (Figure 4-3A). However, inhibition of the Notch signaling pathway has no clear effect on nuclear YAP intensity, only on the softest substrate of 0.5kPa Notch inhibition rescued YAP activation to some degree (Figure 4-3B). Consistent results were obtained with the control cell line MCEC-WT, shown in Figure 7-3A. Since YAP and Notch activity are inversely regulated by substrate stiffness, there seems to be no direct crosstalk between these two signaling pathways in the applied cell model.

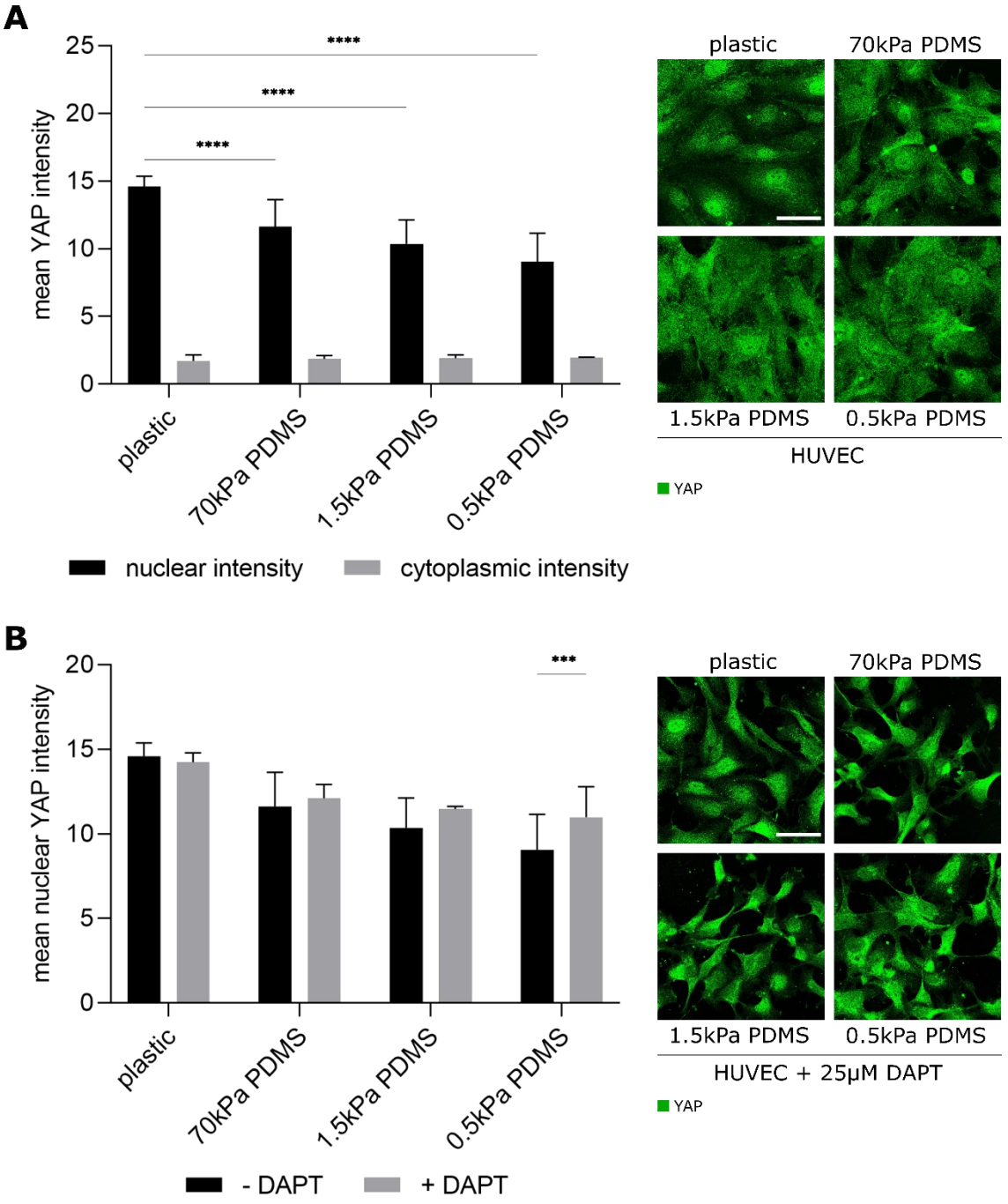

Figure 4-3: Nuclear YAP intensity is reduced on softer substrates but is only marginally affected by Notch inhibition. (A) Nuclear and cytoplasmic YAP intensities. HUVEC cells were seeded on varying substrate stiffness and were stained for YAP. Intensities were analyzed with the Intensity Ratio Nuclei Cytoplasm Tool plugin for ImageJ and are presented in a bar graph on the left panel (mean ± SEM, Sidak's corrected two-way ANOVA, ****P<0.0001). Representative images of immunofluorescence staining are shown on the right panel, with YAP in green (scale bar 50 µm). **(B)** Nuclear YAP intensities with and without Notch inhibition. HUVEC cells were seeded on varying substrate stiffness, treated with 25 µM DAPT for 24 h and stained for YAP. Intensities ± SEM of untreated and treated cells are summarized in a bar graph on the left panel (two-way ANOVA followed by Sidak's multiple comparison test, ***P<0.001). Representative images of immunofluorescent stained HUVEC cells treated with DAPT are shown on the right panel with YAP in green (scale bar 50 µm).

4.1.3 Substrate stiffness has no significant effect on cell-matrix adhesion

To investigate cell adhesion on the PDMS substrates, we performed a cell-matrix adhesion assay. Cells were seeded onto the different substrates and incubated for specific times. The number of adherent cells was quantitatively determined by absorption measurement. The results show that incubations of 45 min and 90 min slightly increased adhesion on softer substrates (Figure 4-4). However, all differences in absorption are non-significant and the influence of substrate stiffness is notably less than that observed for Notch activity.

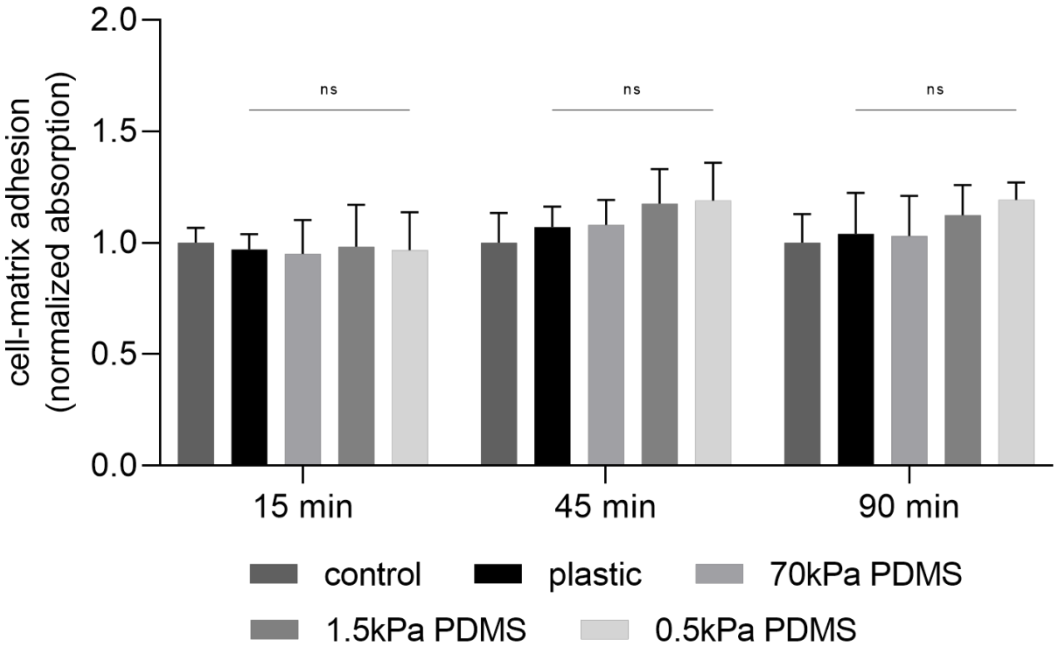

Figure 4-4: Cell-matrix adhesion is non-significantly increased on soft substrates. Normalized absorption of adhered HUVEC cells incubated on substrates with different stiffnesses for 15 min, 45 min or 90 min. Mean ± SEM are presented as bar graphs (two-way ANOVA followed by Dunnett's multiple comparison test, ns ≙ not significant).

4.1.4 Active integrin β1 increases on softer substrates and is influenced by Notch

Since interaction with the ECM is known to be mediated by integrin signaling [12], it should be check if Notch signaling affects or is affected by integrins. Integrin β1 represents the largest subchain of integrins and is involved in several biological processes such as adhesion, migration, and cell cycle regulation [62]. Due to the involvement of β1 subchains in cell-ECM interaction, integrin β1 plays a major role especially in ECs [63]. To determine, whether mechanosensitivity of Notch lies up- or downstream of integrin signaling, total and activated β1 integrin levels with and without pretreatment of cells with the Notch inhibitor DAPT were quantified on the different substrates. Previous studies have already shown that activated but not overall integrin levels are substrate dependent and increased on softer substrates [64]. Accordingly, in the model of this study overall intensity of integrin β1 in HUVEC cells does not change on the different substrates (Figure 4-5A). In contrast, the softer the substrate, the more integrin β1 is activated (Figure 4-5B). Upon blocking of basal Notch1 cleavage and thus downstream of Notch signaling, integrin β1 activation decreases substantially, although the correlation between softer substrates and increased integrin β1 activation remains to a small degree (Figure 4-5B). This effect is also distinctly visible in the representative images (Figure 4-5C). Thus, Notch signaling occurs upstream of integrin activation, as far as mechanosignaling is concerned. This result was confirmed in the second endothelial cell line MCEC-WT (Figure 7-3B).

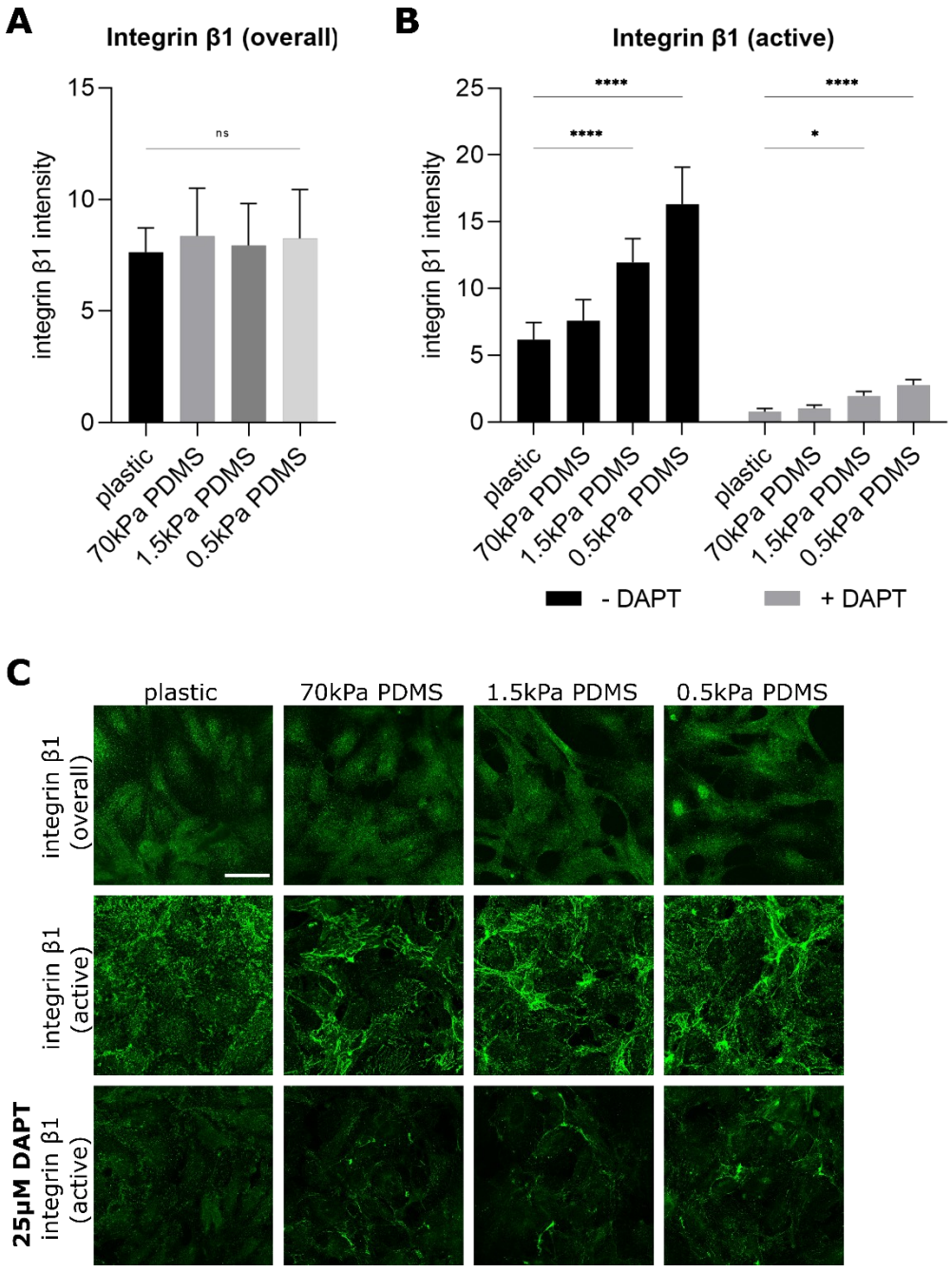

Figure 4-5: Integrin β1 activity relates to substrate stiffness and is influenced by Notch. (A) Integrin β1 intensities in HUVECs. Cells were seeded on varying substrate stiffness and were stained for total integrin β1. Mean intensities ± SEM are depicted in bar graphs (one-way ANOVA followed by Tukey's multiple comparison test, ns ≙ not significant). **(B)** Integrin β1 (active) intensity in HUVECs. Cells were seeded on varying substrate stiffness, treated with 25 µM DAPT for 24 h and stained for the activated form of integrin β1. Data is presented in a bar plot and compared with the integrin β1 intensities without DAPT treatment (mean intensity ± SEM, Tukey's corrected two-way ANOVA, *P<0.1, ****P<0.0001). **(C)** Representative images of HUVEC cells on plastic and PDMS substrates +/- DAPT treatment stained for total or activated integrin β1 (green) are shown (scale bar 50 µm).

4.1.5 VE-cadherin levels and trafficking to cell-cell borders are not affected by substrate stiffness, although the morphology of cell-cell contacts changes

Since the Notch signaling pathway is a contact-dependent pathway, not only the cell-matrix adhesion, but also the influence of substrate stiffness on the major endothelial cohesion molecule VE-cadherin were analyzed. No correlation between VE-cadherin intensity and substrate stiffness was detected. The junction patterns, however, showed stiffness-related changes. The softer the substrate, the less typically branched and interlinked junction pattern is evident at the cell-cell contacts. Instead, a continuous VE-cadherin junction with larger intensity area without branches or comb-like structures is visible, as shown in the representative images (Figure 4-6A and B). Further, the influence of substrate stiffness on VE-cadherin trafficking at cell-cell contacts using a FRAP assay was investigated. HUVEC cells were transiently transfected with a citrine-coupled VE-cadherin plasmid and seeded on PDMS substrate with different stiffness. VE-cadherin recovered to the same extent and with the same kinetics on all substrates and therefore no significant differences in the recovery half time were observed (Figure 4-6C). Thus, the altered junction patterns on the different substrates does not depend on or affect VE-cadherin kinetics.

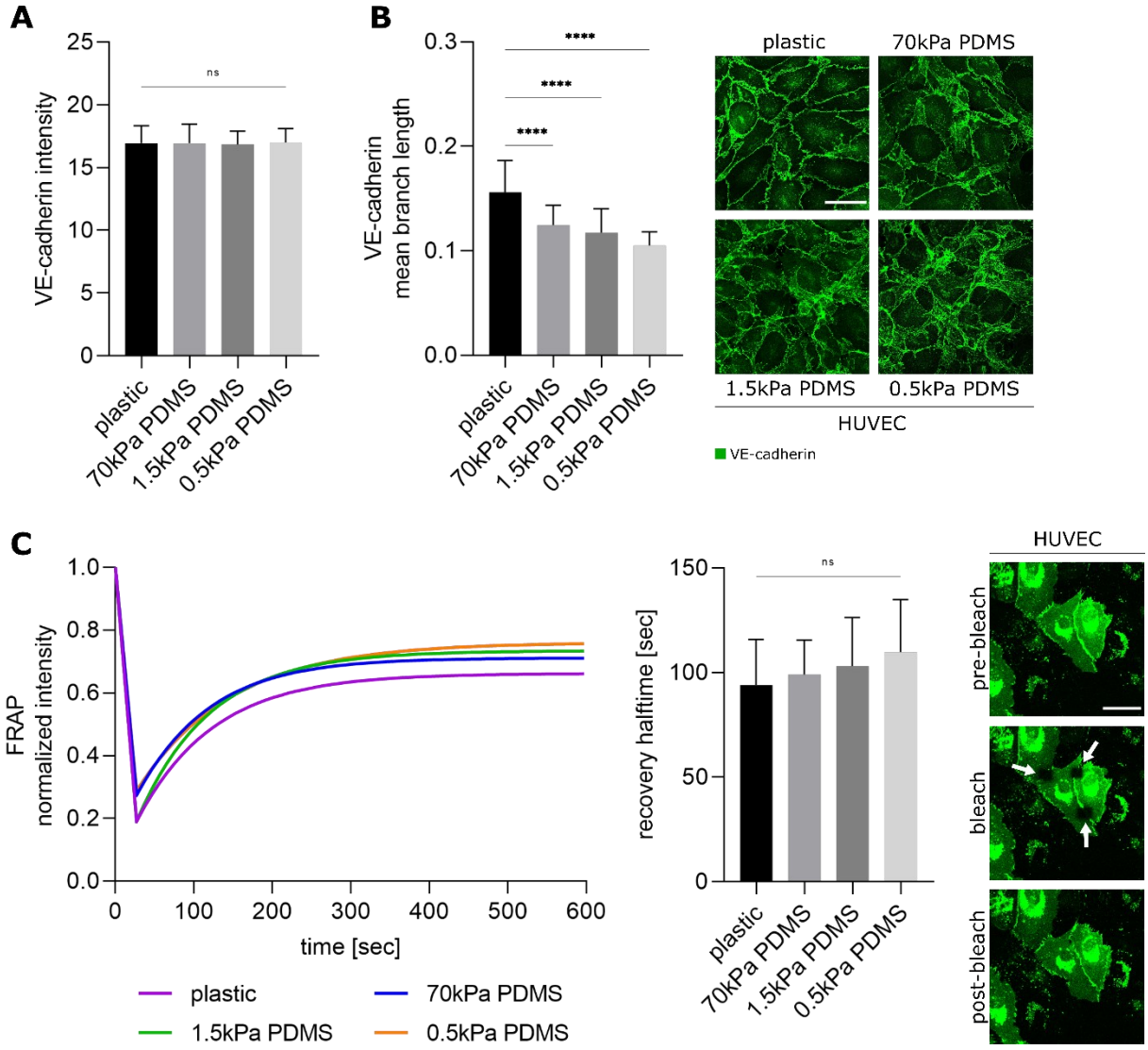

Figure 4-6: Softer substrates change VE-cadherin junction morphology but not VE-cadherin levels or its mobility. (A) VE-cadherin intensity in HUVEC cells, shown in a bar graph (mean ± SEM, Dunnett's corrected one-way ANOVA, ns ≙ not significant). **(B)** VE-cadherin junction analysis in HUVECs, quantified by evaluation of the mean branch length. Cells were seeded on varying substrate stiffness and were stained for VE-cadherin. Intensity and junction analysis are presented in bar graphs on the left panel (mean ± SEM, one-way ANOVA followed by Tukey's multiple comparison test, ****P<0.0001). Representative images of immunofluorescence staining are shown on the right panel, with VE-cadherin in green (scale bar 50 µm). **(C)** Analysis of VE-cadherin mobility at the cell-cell border in HUVEC via a FRAP assay. Cells were transiently transfected with mCitrine-VE-Cadherin-N-10 and seeded on varying substrate stiffness. FRAP was conducted with the Leica photo bleaching module. VE-cadherin recovery is plotted over time (left panel) and quantified as recovery half time (middle panel), shown in a bar graph (mean ± SEM, Tukey's corrected one-way ANOVA, ns ≙ not significant). Representative images of the three FRAP steps, with citrine-coupled VE-cadherin in green are shown on the right panel (scale bar 50 µm).

4.1.6 Endogenous Notch activity is affected by breaking up of cell-cell contacts

To investigate the importance of existing cell-cell contacts for basal Notch activity, HUVEC cells were seeded on substrates of different stiffness, VE-cadherin adhesion molecules were first acutely destabilized by EGTA and then inhibited in a prolonged manner using a VE-cadherin blocking antibody. Treated cells were stained for NICD and its intensity was analyzed in the nuclei as readout for Notch activity. Since studies showed that EGTA can affect the structural integrity of Notch1, leading to receptor cleavage and activation [65, 66], the effect of EGTA on NICD in the cells was checked first. Destabilization of cell-cell contacts leads to a reduction in nuclear NICD levels. Further blocking of VE-cadherin enhances this effect independently of substrate stiffness (Figure 4-7A). The representative images (0.5kPa PDMS) confirm the quantitative analyses and show that the treatment changes the cell morphology and causes the cells to drift apart, leading to diminished cell-cell contacts. Additionally, the effect of Notch on VE-cadherin by treatment of the cells with DAPT (25 μM, 24 h) was investigated. The results show a significant reduction in VE-cadherin intensity after Notch inhibition on all substrates. The junction patterns, however, do not change with the addition of DAPT (Figure 4-7B). Thus, changes in VE-cadherin morphology due to substrate stiffness seem to be independent of Notch signaling, while overall VE-cadherin expression is not.

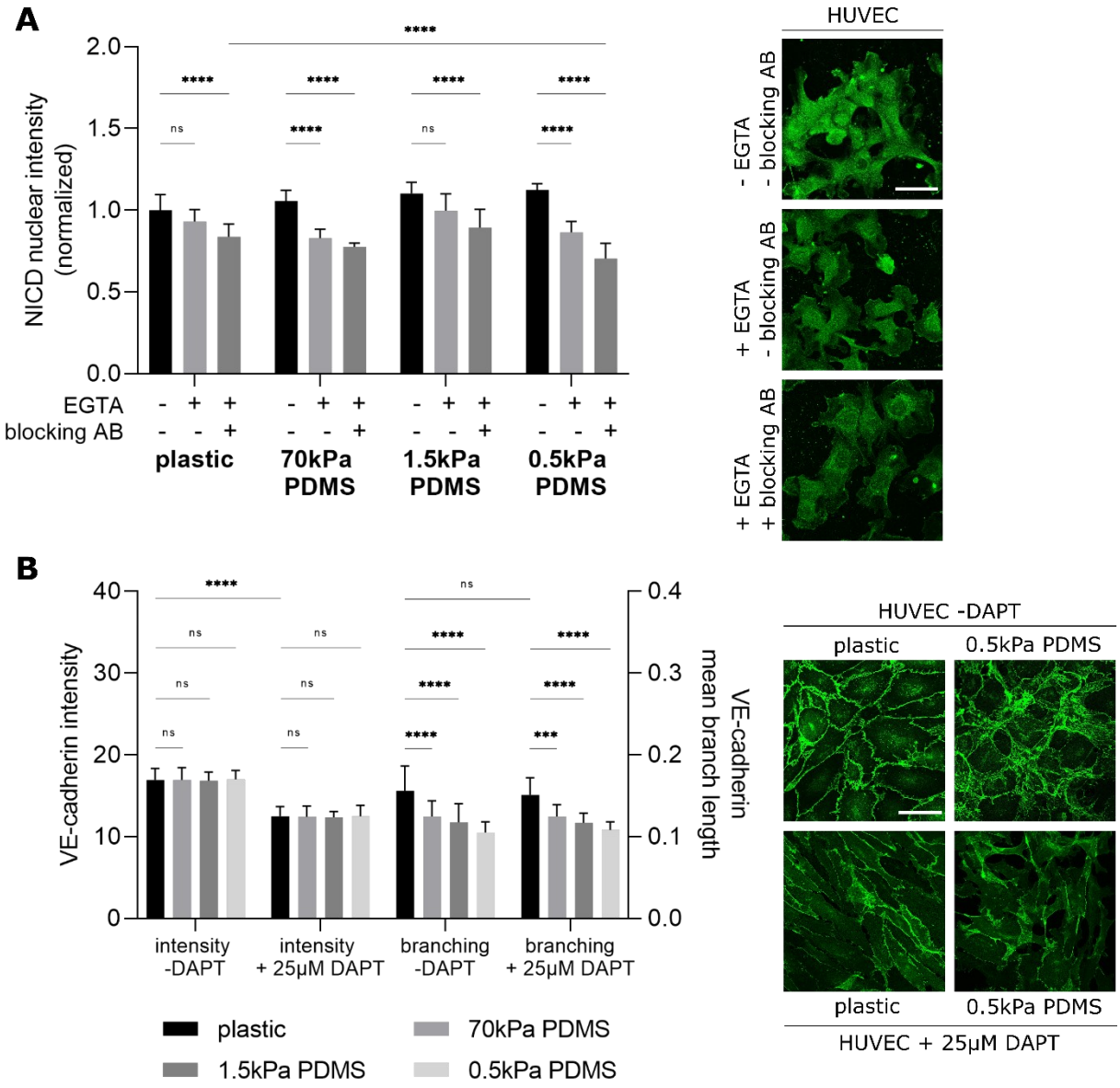

Figure 4-7: Notch and VE-cadherin influence each other: basal Notch activity is reduced by VE-cadherin blocking and VE-cadherin intensity is decreased by Notch inhibition. (A) Nuclear NICD intensity in HUVECs after cell-cell contact inhibition. Cells were seeded on substrates of varying stiffness without activation of the Notch signaling pathway, treated with 5 mM EGTA and VE-cadherin blocking antibody for 30 min each and stained for NICD. Intensities are compared in a bar graph (mean ± SEM, Tukey's corrected two-way ANOVA, ns ≙ not significant, ****P<0.0001) on the left panel. Representative images of HUVEC cells on 0.5kPa PDMS after immunofluorescence staining are shown on the right panel, with NICD in green (scale bar 50 µm). **(B)** VE-cadherin intensity and junction analysis in HUVEC with and without Notch inhibition. Cells were seeded on varying substrate stiffness, treated with 25 µM DAPT for 24 h and stained for VE-cadherin. Bar plots were generated by evaluation of intensity and mean branch length, displayed on the left panel (mean ± SEM, one-way ANOVA followed by Tukey's multiple comparison test, ns ≙ not significant, ***P<0.001, ****P<0.0001). Representative images of HUVECs on plastic and 0.5kPa PDMS +/- addition of DAPT after immunofluorescence staining are displayed on the right panel (VE-cadherin in green, scale bar 50 µm).

4.1.7 Decreased substrate stiffness elevate NECD trans-endocytosis but not general endocytosis

To investigate the role of Notch receptor-ligand binding in increased Notch signaling activity on softer substrates, a trans-endocytosis assay was performed [67]. Separate cell populations were transfected with a Notch1-citrine fusion plasmid, or a doxycycline controlled Dll4-mCherry fusion plasmid. Dll4 expression was induced by adding doxycycline to the co-culture of both transfected cells. Analysis was performed in the areas where the signals of Notch1 receptor and Dll4 ligand overlap at the cell-cell contacts of a signal-sending and a signal-receiving cell using ImageJ. To quantify trans-endocytosis and examine the stiffness effects, the colocalization of Notch receptor and ligand was analyzed both in the form of intensity analysis of the overlay areas and as a correlation analysis using Pearson's *r* coefficient. Trans-endocytosis peaked after 6 h of incubation as described by Shaya et al. [67]. Results show that trans-endocytosis increases on soft substrates, which is reflected in an increased intensity of the interaction area, as well as in a higher colocalization coefficient, the Pearson's r value (Figure 4-8A). A transferrin endocytosis assay was performed on the substrates to exclude a stiffness effect on endocytosis in general. The results indicate that softer substrates do not enhance general endocytosis (Figure 4-8B), so the increased trans-endocytosis cannot be attributed to general increase in endocytosis. Thus, trans-endocytosis seems to selectively exhibit mechanosensitivity in cell-cell contact dependent receptor binding. The same experiments were performed with the endothelial cell line MCEC-WT for comparison, showing similar results and the same effect; the softer the substrate, the more trans-endocytosis occurs upon cell-cell contact (Figure 7-4).

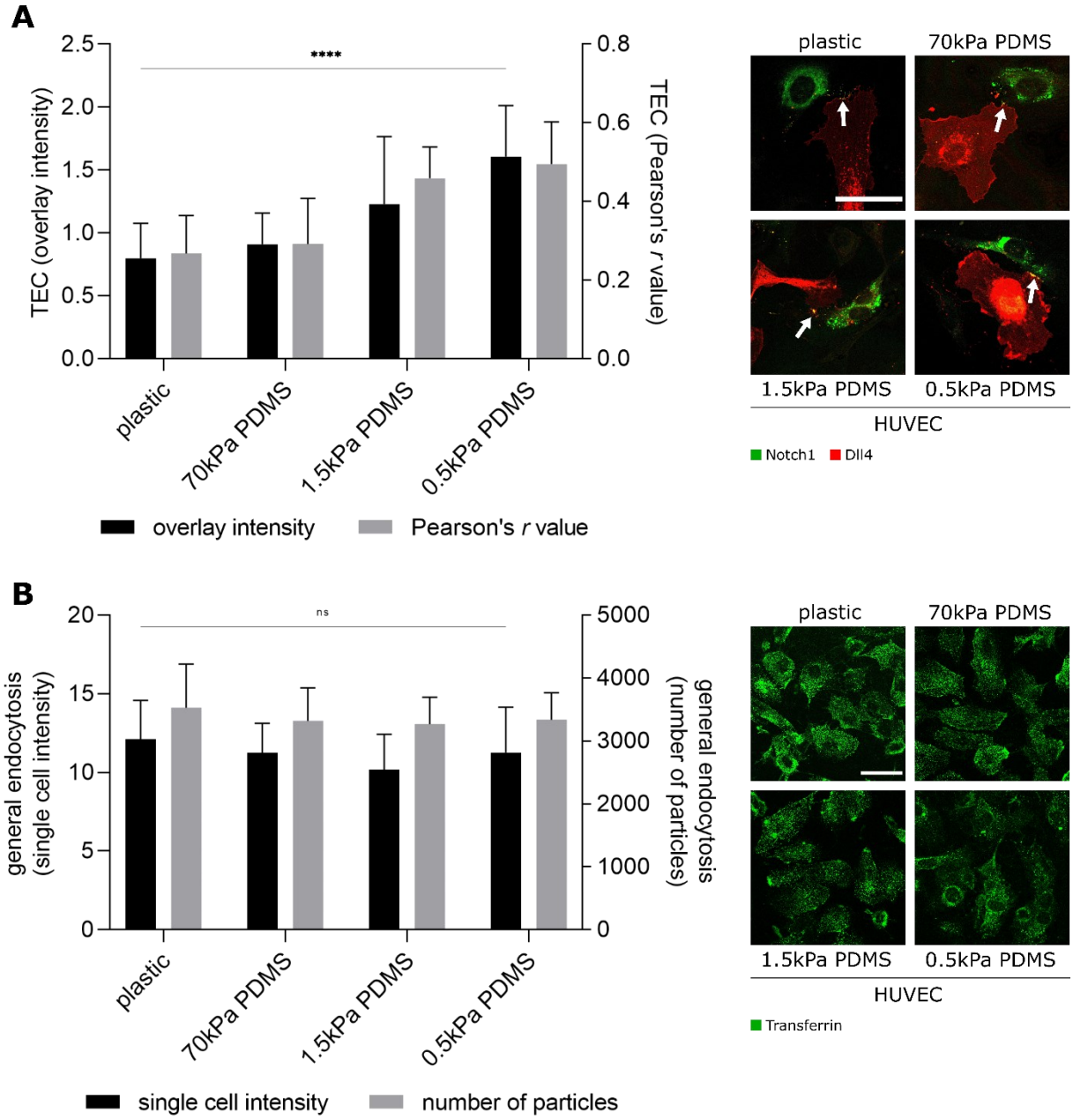

Figure 4-8: Trans-endocytosis is increased on softer substrates. (A) Overlay intensity and Pearson's *r* value in areas of Notch receptor-ligand interactions in the course of trans-endocytosis. Overlay areas are indicated by the white arrows. HUVEC cells were transfected separately with a citrine-coupled Notch1 plasmid and a mCherry-coupled Dll4 plasmid. Trans-endocytosis was quantified at cell-cell contacts in ≥30 cells per substrate condition in three independent experiments. Data is presented as a bar plot on the left panel (mean value ± SEM, two-way ANOVA with Sidak's multiple comparison test, ****P<0.0001). Representative images of TEC are shown on the right panel (Notch1 expression in Notch receiver cells is shown in green, Dll4 expression in Notch sender cells are shown in red, scale bar 50 µm). **(B)** General endocytosis in HUCECs. Cells were seeded on substrates with different stiffness and a transferrin endocytosis assay was conducted. Intensity and number of particles in individual cells are presented in a bar plot as means ± SEM of ≥300 cells per substrate condition conducted in three independent experiments (Sidak's corrected two-way ANOVA, ns ≙ not significant). Representative images of the general endocytosis are shown on the right panel (endocytosed transferrin is shown in green, scale bar 50 µm).

4.1.8 Notch signaling can be activated either by cell-cell contact or by interaction of single cells with exposed Notch ligands

The initial results show that after activation with the rhDll4 coating, Notch receptor cells also display increased signaling activity even without trans-endocytosis taking place. Therefore, to investigate whether the stiffness effect of the Notch signaling pathway is also detectable independently of cell-cell contacts and thus independently of trans-endocytosis only by Notch activation with rhDll4, a reporter gene assay was performed in nonconfluent HUVECs. A significant increase in reporter gene activity after Notch activation by rhDll4 on softer substrates can be observed (Figure 4-9). In contrast, no change in reporter gene activity was evaluated on the substrates without Notch activation (collagen G coat). Thus, cell-cell contacts contribute to Notch activity but are not necessary for a Notch signaling effect in this setting. Although both activation approaches of the Notch signaling pathway show increased Notch signaling activity on softer substrates, little is known about cell contact independent Notch activation. Consequently, activation by rhDll4 and the subsequent pathway may be affected by stiffness changes differently than activation by a neighboring cell.

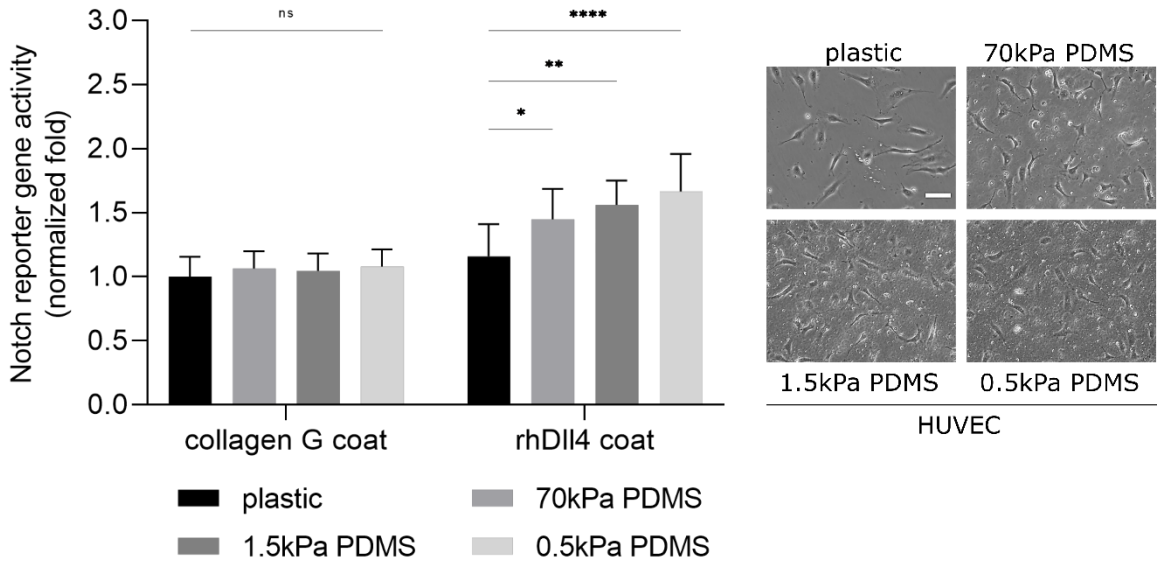

Figure 4-9: Cell-cell contacts are dispensable for Notch activation with rhDll4. Normalized reporter gene activity in nonconfluent HUVEC cells with and without Notch activation via rhDll4 coating, determined by detection of cellular luciferase levels under control of the TP1-luc Notch reporter. Bar plots were generated by evaluation of reporter gene assays on substrates with different stiffness shown on the left panel (one-way ANOVA followed by Tukey's multiple comparison test, ns ≙ not significant, *P<0.1, **P<0.01, ****P<0.0001). Representative images of the cell density are shown on the right panel (scale bar 50 μm).

4.2 Part II: Role of Notch signaling and substrate stiffness in angiogenesis using 2D and 3D models

4.2.1 Tube formation is affected by Dll4 overexpression and Notch inhibition

To investigate the role of the Notch signaling pathway in angiogenesis, tube formation assays on Matrigel were applied as a 2D angiogenesis model. The tube formation was performed with HUVECs, MCEC-WTs and MCEC-Dll4-mCherrys as well as co-cultures of the Notch receiver cells with the Dll4 overexpressing MCEC sender cells in a ratio of 1:1. Evaluation of the nodes and tubes after 24 h incubation shows that HUVECs forms a significantly more complex and branched network than both MCEC cell lines. The co-culture of HUVEC and MCEC-Dll4 cells did not result in an increased tubular network but categorize between the networks of sender and receiver cells (Figure 4-10A). These findings are also confirmed in co-cultures of both MCEC cell lines (Figure 7-5A and C). The representative images in Figure 4-10C support the results and display that the networks of HUVECs consisted of single, elongated cells, whereas MCECs formed tubes of multiple cells. In order to identify the extent to which Notch inhibition influences tube formation, cells were pretreated with DAPT. Results show a significantly reduced network (Figure 4-10B) with interrupted tubes (Figure 4-10C). Thus, the tubular network is reduced by both Notch inhibition and Dll4 overexpression, although the influence of the different endothelial tube structures with varying cell numbers forming the tubes remains to be determined.

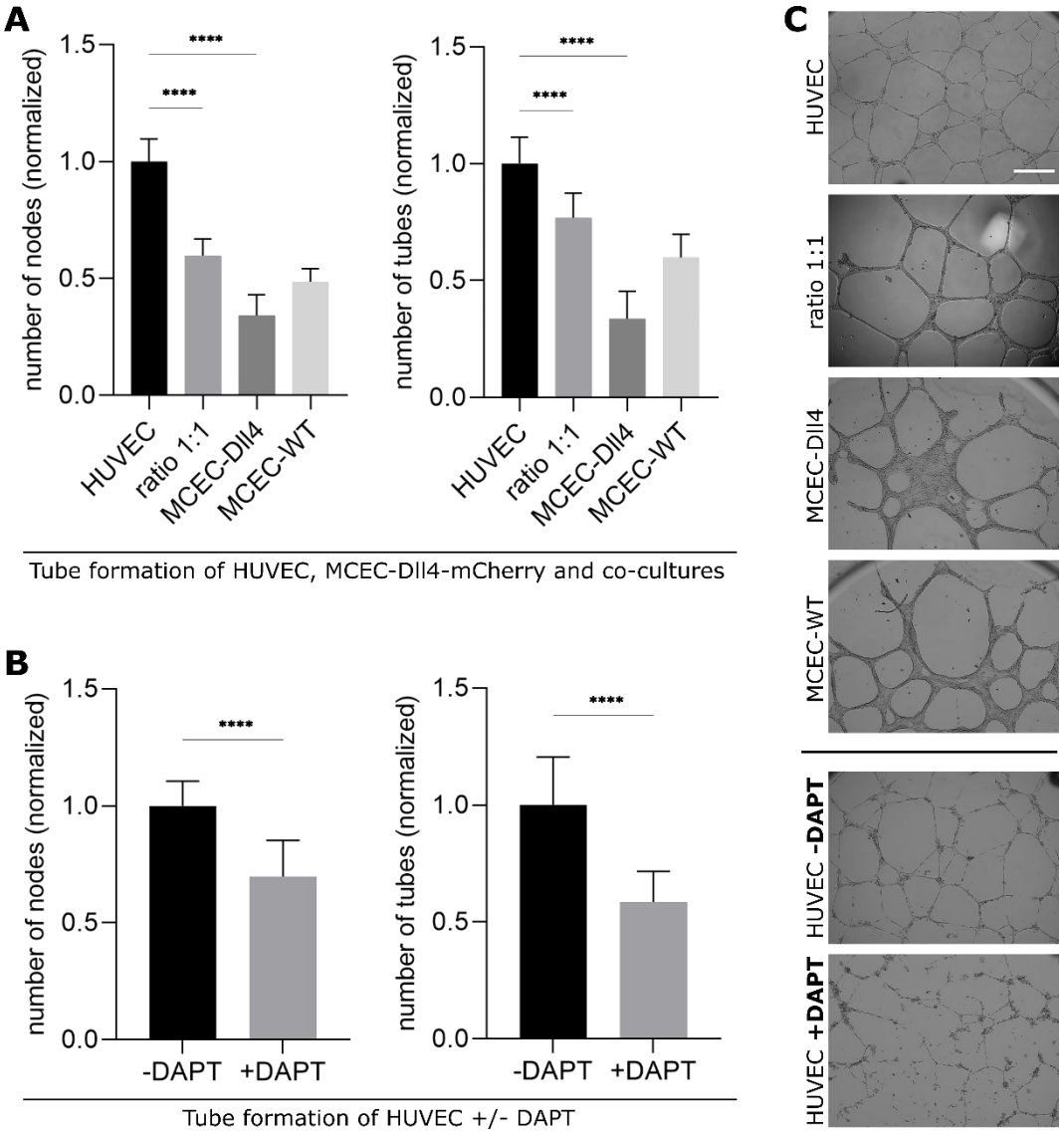

Figure 4-10: Tube Formation is reduced by both: Notch inhibition and Dll4 overexpression. (A) Quantification of the number of nodes and tubes 24 h after cell seeding on Matrigel. Data is normalized to HUVEC tube formation and is presented in bar graphs (mean ± SEM) with significance determined by one-way ANOVA followed by Dunnett's multiple comparison test (****P<0.0001). **(B)** Quantification of the number of nodes and tubes of HUVEC tube formation pretreated with 25 μM DAPT. Tube formation was incubated for 24 h. Data is presented in a bar plot and compared with the tube formation of non-treated HUVECs (mean ± SEM, Dunnett's corrected one-way ANOVA, ****P<0.0001). **(C)** Representative images of tube formations of different endothelial cells and +/- DAPT treatment (scale bar 250 μm).

4.2.2 Dll4 overexpression and Notch inhibition promote spheroid sprouting, although only Notch inhibition causes disrupted sprouts

Further, the influence of Notch signaling on angiogenesis was investigated in a 3D model. Spheroid sprouting assays were again performed with HUVECs, MCEC-WTs and MCEC-Dll4-mCherrys as well as co-cultures of the Notch receiver cells with the Dll4 overexpressing MCEC sender cells in a ratio of 1:1. Spheroids were generated using the hanging drop culture and embedded in collagen I (2 mg/ml). Sprouting was advanced by addition of 25 nM VEGF. Analysis of the number of sprouts and the sprouting length shows that Dll4 overexpression led to more, but shorter sprouts compared to the HUVEC receiver cells. Co-culture of sender and receiver cells increases both the number of sprouts and the sprouting length (Figure 4-11A). A similar response can be observed in co-culture of both MCEC cell lines as shown in Figure 7-5B and C. Again, the effect of Notch inhibition on sprouting behavior was reviewed in HUVEC spheroids. The DAPT was added during the embedding of the spheroids. While the quantitative analysis shows that the number of sprouts as well as the sprouting length increases with Notch inhibition, the images display that all sprouts were disconnected and incomplete. This data suggests that Dll4 overexpression causes excessive but ineffective sprouting, whereas in co-culture with Notch receiver cells, it increases and prolongs sprouting, in contrast to the receiver cells alone. A similar effect can be observed with Notch pathway inhibition.

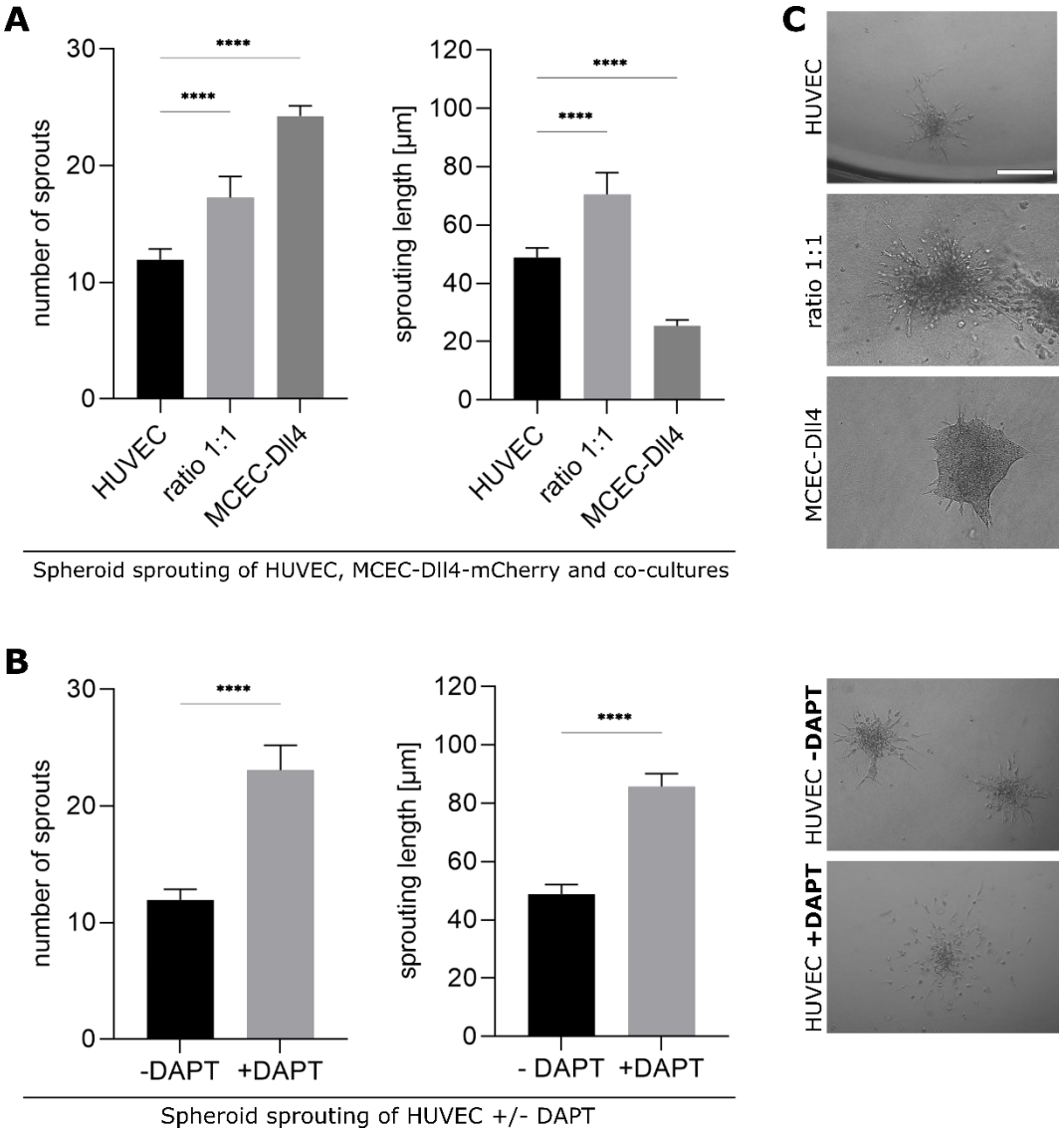

Figure 4-11: Spheroid sprouting increases in co-cultured Notch receiver cells with overexpressing sender cells and at Notch inhibition. (A) Quantification of the number of sprouts and its length in sprouted spheroids. Data is presented in bar graph (mean ± SEM of ≥ 15 spheroids per condition) with significance determined by one-way ANOVA followed by Dunnett's multiple comparison test (****P<0.0001). **(B)** Quantification of the number of sprouts and its total length in HUVEC sprouted spheroids pretreated with 25 µM DAPT. For both conditions, the end points of the sprouts were analyzed, regardless of whether the sprouts were interrupted or continuous. Spheroids were incubated for 24 h. Data is presented in a bar plot and compared with the sprouting behavior of non-treated HUVECs (mean ± SEM of ≥ 15 spheroids per condition, Dunnett's corrected one-way ANOVA, ****P<0.0001). **(C)** Representative images of sprouted spheroids of different endothelial cells and +/- DAPT treatment (scale bar 100 µm).

4.2.3 Dll4 overexpressing cells are distributed randomly in a co-culture with Notch receiver cells during tube formation

The Notch signaling pathway plays an important role during angiogenesis and especially in tip/stalk cell selection [1, 46]. To determine whether Dll4-overexpressing cells behave in the same way as Notch receiving cells during tube formation, the cell velocities and displacements during the process of tube formation were compared. Cell velocities do not change during tube formation and also in the comparison of the different cells. Only the Dll4-overexpressing cells in monoculture move slightly slower, but this is no longer evident in co-culture and overall displacement (Figure 4-12A). Furthermore, the cell distributions and positions at the endpoint of the tube formation were observed. As shown in the representative images, the Dll4 overexpressing cells in co-culture with HUVECs are evenly distributed according to the seeding ratio and do not occupy any particular position (Figure 4-12B). Analysis of the co-culture of the MCEC-WT as a second endothelial cell line with the MCEC-Dll4-mCherry shows the similar outcome (Figure 7-6A and B).

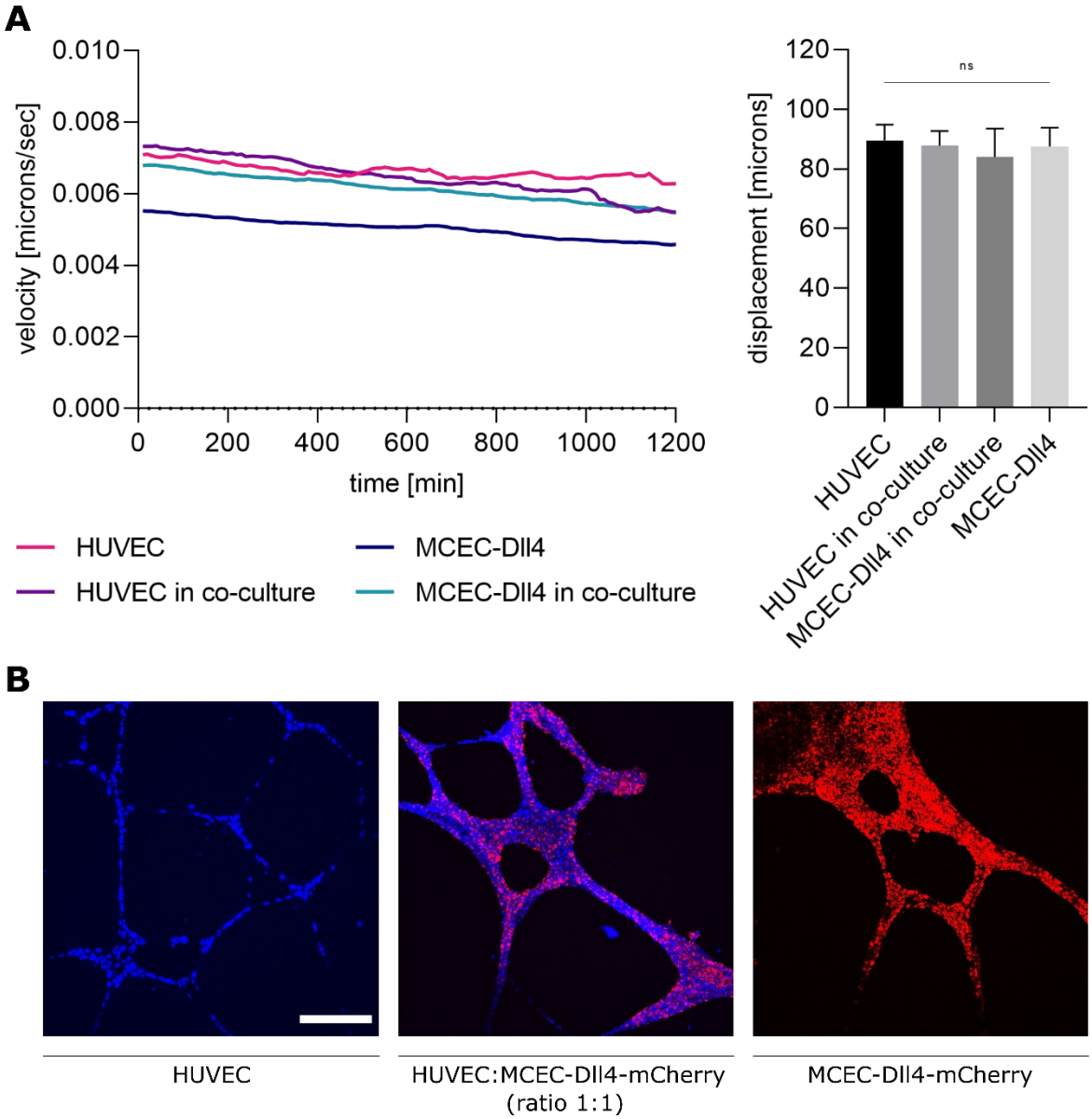

Figure 4-12: Dll4 overexpressing cells do not have any impact in velocity and displacement during tube formation, nor do they occupy particular positions. (A) Velocity and displacement analysis of tube formation live cell imaging. Here, HUVECs and MCEC-Dll4s were evaluated in monoculture, as well as separately in the co-culture ratio 1:1. Changes in velocity are plotted over time (left panel) and the overall displacement (right panel) is shown in a bar graph (mean ± SEM, Dunnett's corrected one-way ANOVA, ns ≙ not significant). **(B)** Representative images of the tube formation endpoint (24 h) with the HUVEC nuclei stained with Hoechst in blue and the mCherry-Dll4 reporter of MCEC-Dll4-mCherry cells in red (scale bar 250 μm).

4.2.4 Dll4 overexpression does not ensure a tip cell position during spheroid sprouting

Expression of the Notch ligand Dll4 in tip cells activates the Notch signaling pathway in subsequent stalk cells, enabling the formation and elongations of vessels during angiogenesis, and thus making Dll4 an important tip cell marker [47, 48]. To investigate whether Dll4 overexpression of MCEC-Dll4-mCherry cells has an effect on cell positions during sprouting, as individual cells migrate directionally from the spheroid during the sprouting assay, the cell positions in the sprouted spheroids, composed of HUVECs and MCEC-Dll4-mcherrys in the ratios 1:1 and 5:1, were analyzed. By immunofluorescence staining of a second tip cell marker, ADAMTS, additionally the leading cells of the spheroids independent of Dll4 overexpression were identified. Results show that ADAMTS intensities are significantly increased at the tip of all sprouts in contrast to the following cells, regardless of which cell is at the tip and in which ratio cells of the spheroid are co-cultured (Figure 4-13A and B, left panel). This data suggests that all the cells leading the different sprouts exhibit tip cell characteristics. However, the distribution of Dll4-overexpressing MCECs and HUVECs shows that the cells are distributed depending on the seeding ratio in the spheroid and sprouts and the MCEC-Dll4-mCherries not always occupy a leading position despite their overexpression (Figure 4-13A and B, middle panel). Accordingly, the results imply that Dll4 expression is not primarily critical for tip cell selection. Analysis of the MCEC-WT/-Dll4-mCherry spheroids results in the same findings (Figure 7-6C).

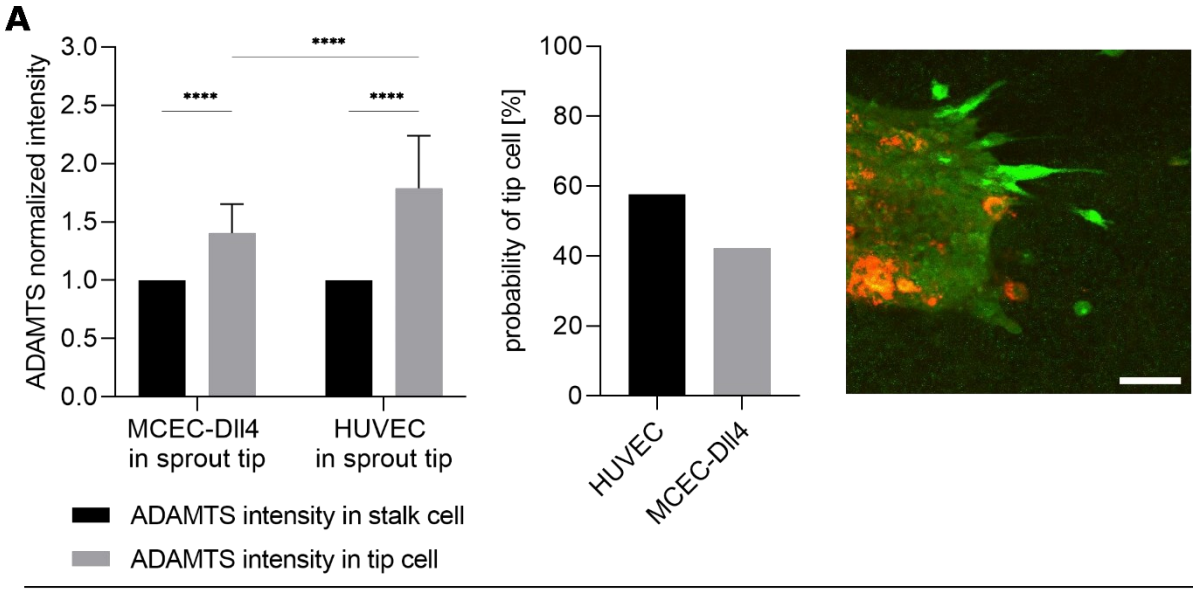

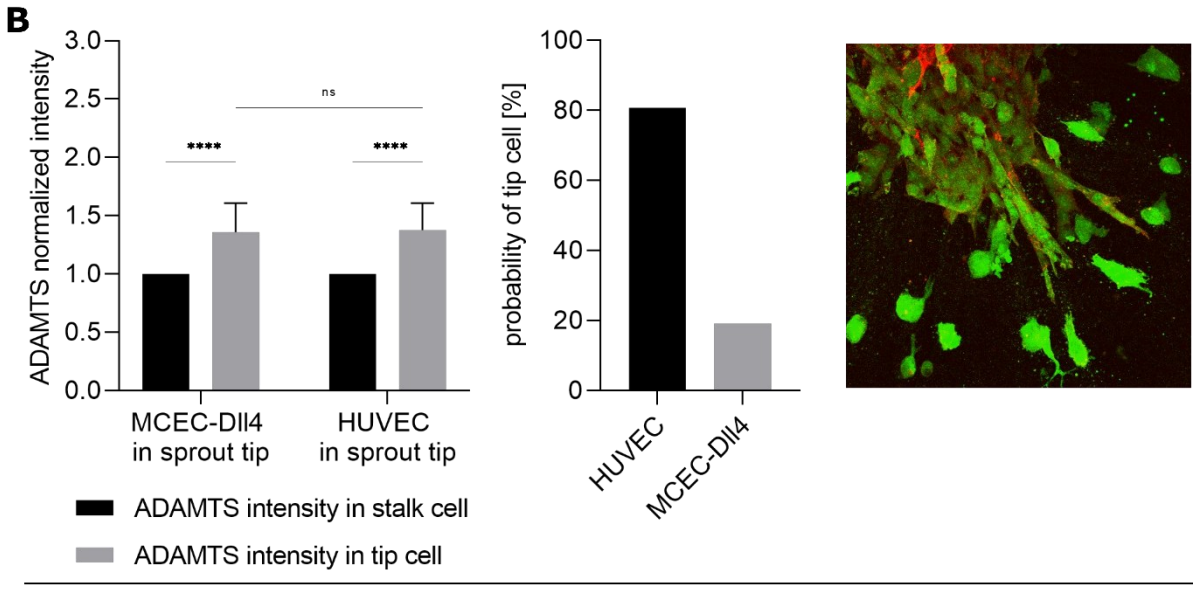

Figure 4-13: Notch receiver and sender cells are distributed depending on the seeding ratio in sprouting spheroids although all cells leading the sprouts show a tip cell characteristic. (A,B) Analysis of tip cell characteristics and cell distribution intensities of HUVEC and MCEC-Dll4-mCherry spheroids in the ratio 1:1 **(A)** and 5:1 **(B)**. ADAMTS normalized intensities in the leading tip cells and following stalk cells were evaluated after immunofluorescence staining and are presented on the left panel. Probability of a HUVEC or MCEC-Dll4-mcherry cell leading a sprout was determined by distribution analysis and is presented on the middle panel. All data is normalized to HUVEC spheroids and is displayed in bar graphs (mean ± SEM of ≥ 15 spheroids per condition, Tukey's corrected one-way ANOVA, ns ≙ not significant, ****P<0.0001). Representative images of the sprouted spheroids, with ADAMTS in green and the mCherry-Dll4 reporter in red are shown on the right panel (scale bar 50 μm).

4.2.5 Decreased substrate stiffnesses enhance spheroid sprouting

Continuing the results of endothelial cell behavior on different substrate stiffnesses, the sprouting behavior of HUVEC spheroids in different collagen matrices was invesigated. Using UV-inducible PhotoCol®, different stiffnesses could be selectively adjusted by different exposure times (Figure 4-14A, Figure 7-7). The stiffness of the previously used collagen I corresponds approximately to that of the PhotoCol® after 30 sec UV illumination. Results show that lower substrate stiffnesses increase sprouting, while high substrate stiffnesses decrease sprouting and also limit the spread of the spheroid core, quantified in Figure 4-14B. In this analysis, the previously used collagen I has a medium stiffness, which ensures an average sprouting behavior, comparable to that of PhotoCol® with the same stiffness, as shown in the evaluations and representative images (Figure 4-14C).

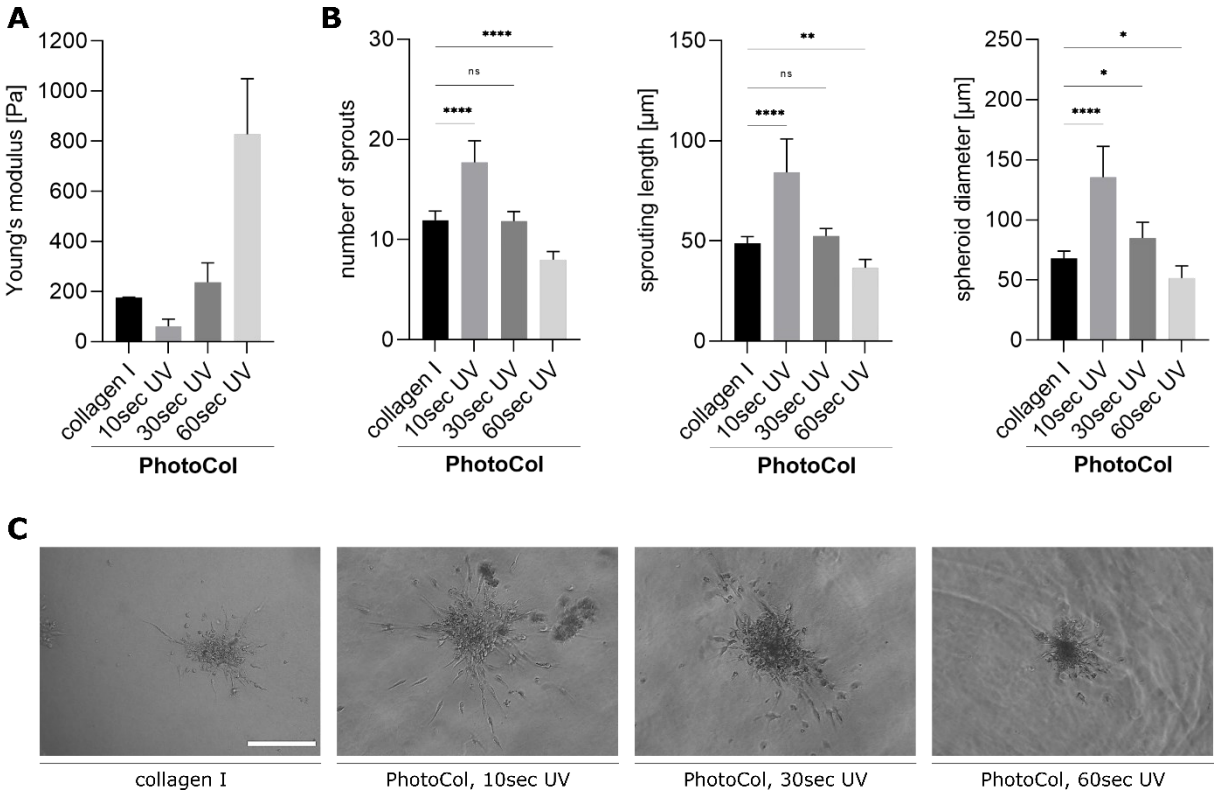

Figure 4-14: Sprouting of HUVEC spheroids increases in softer substrates and decreases in stiffer substrates. (A) Stiffness determination of collagen substrate by atomic force microscopy (AFM) measurements, performed by Daniel Rüdiger. Mean Young's modulus ± SEM is depicted in a bar graph. **(B)** Quantification of the number of sprouts sprouting length and the spheroid diameter of sprouted HUVEC spheroids. Data is presented in bar graphs (mean ± SEM, one-way ANOVA followed by Dunnett's multiple comparison test, ns ≙ not significant, *P<0.1, **P<0.01, ****P<0.0001). **(C)** Representative images of HUVEC spheroids in collagen I and PhotoCol® substrates with different stiffnesses (scale bar 100 µm).

5 Discussion

5.1 Matrix stiffness regulates Notch signaling activity in endothelial cells

The Notch signaling pathway plays multiple and crucial roles in developmental and pathological processes [68-70]. Many of these scenarios are related to changes in the composition and the biomechanical features of the extracellular matrix (ECM). During angiogenesis the Notch signaling pathway regulates cell fate decisions such as migration, proliferation, and differentiation, essential for vascular development and angiogenesis [14, 46]. Endothelial Notch signaling can be activated by VEGF and, at the same time, VEGF controls matrix composition, causing local ECM softening or stiffening [1, 4]. Previous studies on biophysical aspects of Notch signaling focus on a pulling force exerted by the bound receptor [71] that is a prerequisite for Notch receptor cleavage. To date, however, little is known on whether the Notch signaling pathway is modulated by substrate stiffness. To address this question, an endothelial cell model based on synthetic PDMS substrates with tunable stiffnesses was used.

Interestingly, nuclear NICD localization and transcriptional activity of Notch both increase with decreasing substrate stiffness. This phenomenon occurs irrespective of whether Notch activation was achieved by surface bound ligand (rhDll4) or Dll4 overexpressing sender cells (Fig. 4-1, Fig. 4-2).

The role of the Yes-associated protein YAP as a mechanotransducer and the related mechanosensitivity of the YAP/TAZ signaling pathway are well known and studied. Upon YAP activation, for example by higher ECM rigidly or substrate stiffness, YAP/TAZ are not phosphorylated and can thus be relocated from the cytoplasm to the nucleus, where binding to a transcription factor regulates genes necessary for cell migration and proliferation [60, 72]. Accordingly, it was investigated how the YAP/TAZ pathway relates to stiffness modulated Notch signaling. As expected, YAP activity decreased with lower stiffness of the substrate (Fig. 4-3). It has been previously shown that activation of YAP reduces Notch signaling by repression of the ligand Dll4, while knockdown of YAP increases Dll4 [72]. However, this mechanism is not sufficient to explain the correlation between substrate stiffness and Notch activity in the model of this study since the Notch activation after co-culture with a stably

overexpressing cell line was examined. Additionally, increased activity of Notch with lower stiffness was also observed after activation by rhDll4, which is independent of YAP activity. There also seems to be no feedback loop between Notch and YAP translocation, since DAPT treatment did not alter the stiffness dependence of YAP translocation to the nucleus (Fig. 4-3). However, a concomitant activation of YAP and Notch on a transcriptional level, which has been described previously, cannot be excluded [11].

Endothelial cells sense changes of matrix properties via cell-matrix adhesion proteins [8, 44]. To investigate the effect of the synthetic PDMS substrates on cell-matrix binding, the adhesion of endothelial cells to the different substrates was examined. The adhesion assay displays that the general adhesion on the PDMS substrates was not significantly affected and, most importantly, shows no stiffness dependency (Fig. 4-4), suggesting that the previously shown mechanosensitivity of the Notch signaling pathway may not be due to the PDMS but to the lower stiffnesses. Especially integrin β1 plays a crucial role in regulating cellular adhesion to enable migration and proliferation [4, 5]. Since integrins have been previously identified both up- [73] and downstream of Notch in signaling pathways [12], this issue was investigated first. For integrin β1, it has already been shown that the overall levels do not change with different substrate stiffnesses, but that the active state of integrin β1 increases on softer substrates [64]. The data confirms these observations in the applied model. Furthermore, results show that cell-matrix adhesion is directly influenced by the Notch signaling pathway. Notch inhibition by DAPT treatment significantly reduced the integrin β1 intensity of the activated form, although substrate-dependent activation was further observed (Fig. 4-5). These results corroborate the findings of Hodkinson et al., which show that Notch1, through NICD cleavage and subsequent R-ras binding, can induce a conformational change in the membrane-bound integrin from a low affinity state to a high affinity state, promoting the active form [12]. This clearly positions integrins downstream of Notch. Despite Notch inhibition, a continuous increase in integrin β1 levels on softer substrates can be observed, however to a much lower extent. Thus, either pharmacological Notch inhibition was not complete, or integrin activity is additionally influenced by substrate stiffness via an alternative pathway.

In addition to the cell-matrix adhesions, a stiffness effect has already been established for cell-cell contacts. On stiffer substrates, VE-cadherin junctions are wider and discontinuous, whereas on soft substrates they are narrower but continuous [6]. This finding was

corroborated by analyzing VE-cadherin patterns through mean branch length evaluation. The VE-cadherin junctions on plastic show a branched, comb-like structure with larger branch length in contrast to the narrower junctions on softer substrates with smaller branch length, which appear more distinct and continuous (Fig. 4-6). A role for cadherins in the regulation of the Notch signaling pathway was previously described by Kwak et al., who demonstrated that cadherin-based adherens junctions control Notch-γ-secretase interactions [74]. In this context, the changes in VE-cadherin junctions on the soft substrates could be related to the increased Notch activities. However, it should be noted that the VE-cadherin patterns on the changing substrate stiffnesses have no influence on VE-cadherin intensity level or trafficking. Furthermore, Notch signaling is regulated by the cell-cell contact area [11, 67], as signaling is directly linked to the contact area of two interacting cells [67]. By destabilizing and blocking the VE-cadherin cell-cell contacts, results show that, as expected, Notch activity is significantly reduced. This effect is, however, independent of substrate stiffness (Fig. 4-7). With these results, it should be noted that the Notch receptor has a Ca^{2+} dependency, which means that the use of EGTA to destabilize the cell-cell contacts could also destabilize the receptor, leading to Notch cleavage and activation [65, 66]. However, analysis of NICD levels after EGTA treatment shows that in the applied model a reduced NICD nuclear intensity was detected and thus no EGTA-mediated Notch activation occurred, additionally noting that EGTA was dissolved in medium here in contrast to other studies [65]. Blocking the Notch signaling pathway leads to a uniform decline of VE-cadherin on all substrates. The change of junctional patterns due to variation of stiffness is not influenced by DAPT treatment (Fig. 4-7). These findings argue against an upstream role of VE-cadherin in stiffness-dependent Notch signaling.

By endocytosis of the Notch ligand after binding to the receptor into the signal-sending cell, the accumulation of the Notch receptor on the cell surface of the signal-receiving cell can be counteracted on the one hand and serves primarily for receptor activation on the other [47, 75]. During trans-endocytosis, the extracellular part of the Notch receptor bound to the Notch ligand is pulled into the ligand-presenting cell, thus releasing the intracellular part of the receptor (activated form), which can be released from the membrane in a further cleavage event [20]. Data from the TEC assay on the different substrates shows that trans-endocytosis is significantly enhanced on soft substrates, which is consistent with the enhanced Notch

activity on softer substrates (Fig. 4-8). A stiffness effect on the general endocytosis can be excluded. Taken together, the observations demonstrate a mechanosensitivity of the Notch signaling pathway that may in part be due to trans-endocytosis.

5.1.1 Critical view on Notch activation by a surface bound ligand

The initiation of the canonical Notch signaling pathway via Notch activation through binding of the receptor to the ligand is well studied and understood [9, 76]. In this process, the ligand of a neighboring cell binds to the Notch receptor, which is facilitated in vivo by cell-cell contact [13, 19]. In vitro, stimulation of the Notch signaling pathway is also achieved by a surface bound ligand. Among others, You et al. demonstrated that stimulation with the immobilized ligand increased both Notch receptor levels and expression of Notch target genes, comparable to that observed after cell-cell contact-dependent activation [77-79]. Blocked Notch signaling after inhibition of γ-secretase following surface bound ligand activation further demonstrated that the processing of the receptor is also comparable to Notch activation in vivo [80].
As previously described, through nuclear NICD localization and increased Notch activity, activation of the Notch signaling pathway by immobilized rhDll4 can also be demonstrated. The mechanosensitivity of the Notch signaling pathway is further confirmed in this activation approach (Fig. 4-1). Interestingly, by activation of the Notch signaling pathway in a cell-cell contact independent manner using rhDll4 as a stimulus for subconfluent single cells, results indicate that the cell-cell contacts are to a certain degree dispensable in this setting with the stiffness dependence of Notch still shown (Fig. 4-9). However, compared with the results of Notch pathway activation by interaction with a ligand-presenting cell, these data suggest that receptor activation and processing are different in the two ligand presentation models. Notch activation by cell-cell contact-dependent ligand binding shows a mechanical aspect of the pulling movement of the ligand into the sender cells, proposing a link between the trans-endocytosis and the mechanosensitivtiy of the Notch signaling pathway (Fig. 4-8). The absence of trans-endocytosis at Notch activation by a surface bound ligand and a nevertheless existing mechanosensitivity of the Notch pathway, however, indicates a different mechanism and a further mechanical force. The mechanosensitive effects in course of the Notch signaling

pathway for the two different activation approaches are summarized graphically in Figure 5-1.

The role and process of trans-endocytosis in the Notch signaling pathway is highly controversial. The majority of data suggest that during uptake of NECD into the ligand cell, mechanical pulling forces act to expose the S2 cleavage site and thus enable Notch receptor activation [21, 26, 47]. The assumption is supported by further work showing inhibition of Notch signaling after blocking receptor internalization [81, 82] and this mechanism is also considered for the model of this study. Other studies, however, suggest that trans-endocytosis regulates the number of receptors on the surface of signal receiver cells and thus down-regulates Notch [20, 75]. In this context, using a NEXT construct (receptor after S2 cleavage), Sorensen et al. show that S3 receptor processing by γ-secretase can occur even in the absence of endocytosis [83]. Although this again reflects only a small part of the signaling pathway and is a model approach, this type of receptor cleavage could also occur in the experiments after Notch activation by the immobilized ligand.

In summary, a surface bound ligand can be applied to activate the Notch signaling pathway, demonstrating both activation of Notch target genes and mechanosensitivity of Notch. However, the signaling pathway is not completely overlapping with that following cell-cell contact-dependent Notch activation, and the potentially altered effects associated with this should be considered and investigated.

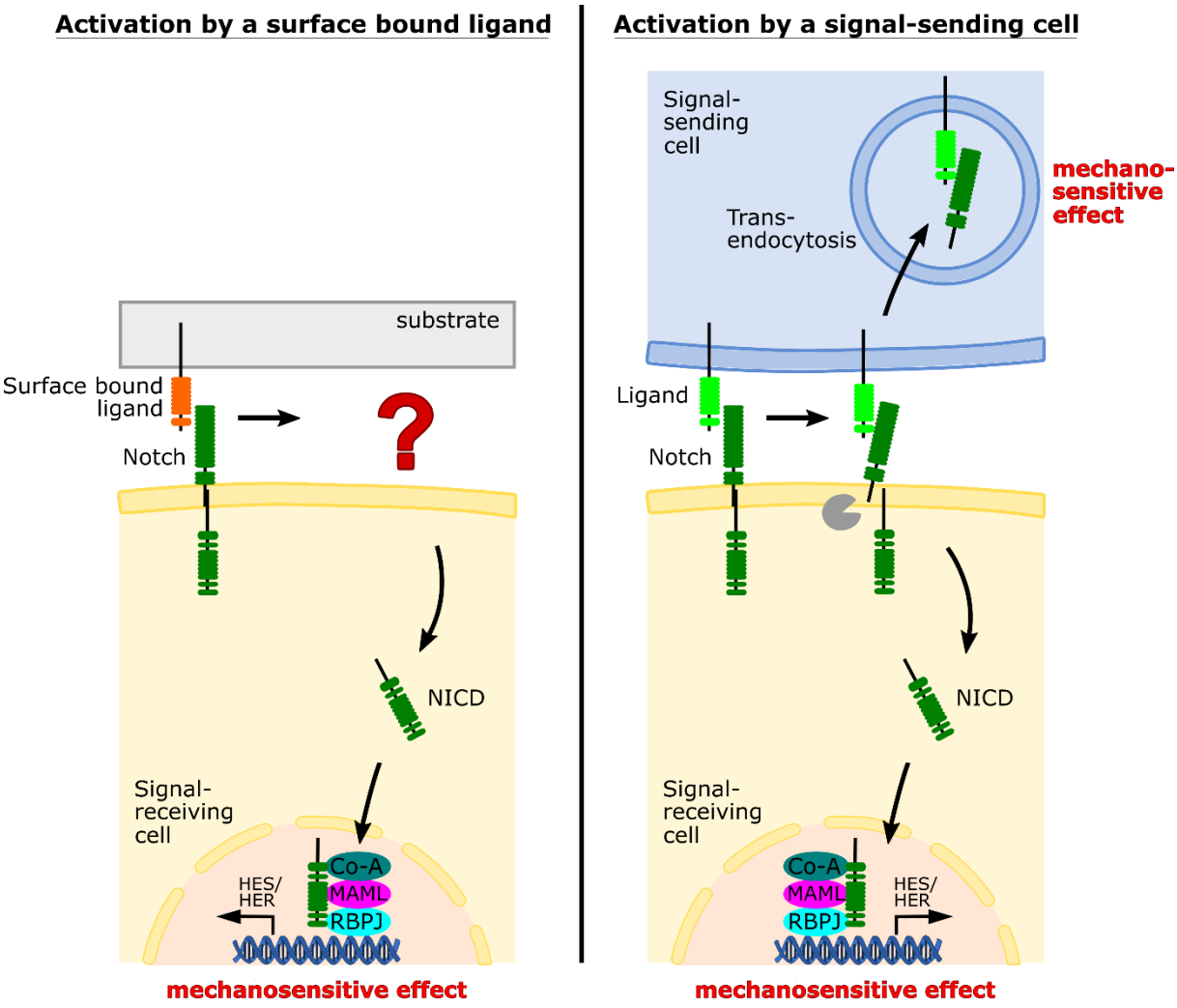

Figure 5-1: Graphical summary of the mechanosensitive effects in the course of the Notch signal pathway with comparison of the two activation approaches. After activation by a surface bound ligand as well as by a signal-sending cell, an increased Notch activity on softer substrates and thus a mechanosensitive effect at Notch transcription complex formation in the nucleus can be shown. At cell-cell contact, this mechanosensitive effect can already be observed during trans-endocytosis (right panel). In contrast, receptor processing after the surface bound ligand activation is unknown due to the absence of trans-endocytosis (left panel).

5.2 A new insight into the role of Notch signaling in angiogenic sprouting and tip/stalk cell selection

The Notch signaling pathway is one of the main mediators of angiogenesis by driving the adaption of a tip or stalk cell phenotype in endothelial cells [1, 46]. In a feedback system together with VEGF, Dll4/Notch regulates the number of tip and stalk cells, enabling sprout formation and elongation [47, 50]. The tip cells are characterized by elevated Dll4 and VEGFR2 expression, whereas stalk cells exhibit high Notch. The Notch signaling in these stalk cells is activated by the tip cells [1, 40]. While it is known that Dll4 expression in the tip cells is initiated by binding of VEGF and VEGFR2 [47], the relationship between the reactivation of quiescent cells in the vessel complex, the escape of a cell by loosening of cell-matrix junctions, and tip cell selection by Notch are poorly understood. To investigate this connection, both a 2D and a 3D angiogenesis model were applied, using wild-type and Dll4-overexpressing endothelial cells.

Tube formation (2D) and sprouting (3D) assays show that overexpression of Dll4 in endothelial cells result in increased sprouting with many short tubes, whereas inhibition of the Notch signaling pathway causes increased but ineffective and incomplete sprouts (Fig. 4-10, Fig. 4-11). This is consistent with the characteristic of Dll4 expression in tip cells leading to vessel sprouting, whereas Notch signaling in stalk cells contributes to vessel elongation and lumen formation [1, 40]. The effects of Dll4 overexpression and Notch inhibition in in vitro angiogenesis assays have also been shown by Williams et al and Caliceti et al., among others, comparable with the results of the model of this study [84-87]. However, interestingly, the applied 3D angiogenesis model also demonstrates that Dll4 overexpression in endothelial cells does not ensure a tip cell position in spheroid sprouts (Fig. 4-13). In sprouting spheroids consisting of co-cultured Dll4-overexpressing Notch sender cells and Notch receiver cells, all tip cells show high intensities of the additional tip cell marker ADAMTS, but the Dll4-overexpressing cells are distributed according to seeding ratio in spheroid and sprouts. This suggests that Dll4 expression and Notch-mediated control of angiogenic sprouting is a consequence of prior tip cell initiation by other biochemical and mechanical signals. Thus, expression of the tip cell phenotype and breakout of this cell from an existing vessel would first be triggered by ECM remodeling [2, 8] and coherently loosened cell-matrix adhesions [8, 35]. Consequently, only afterwards VEGF would drive expression of VEGFR2 and Dll4 [47].

The adaption of the stalk cell phenotype would therefore still be selected by the Notch signaling pathway [1]. This assumed initiation of angiogenesis is also shown schematically in Figure 5-2. Individual factors of the proposed tip cell selection process have already been investigated and confirmed, although the exact timing of tip cell migration from an existing vessel has not yet been conclusively determined.

Thus, the results of this study can help to clarify the process of tip/stalk cell selection and the influence of the Notch signaling pathway during the early stages of angiogenesis, indicating the importance of mechanical cell-matrix interactions and its impact on the signaling pathways involved during angiogenesis.

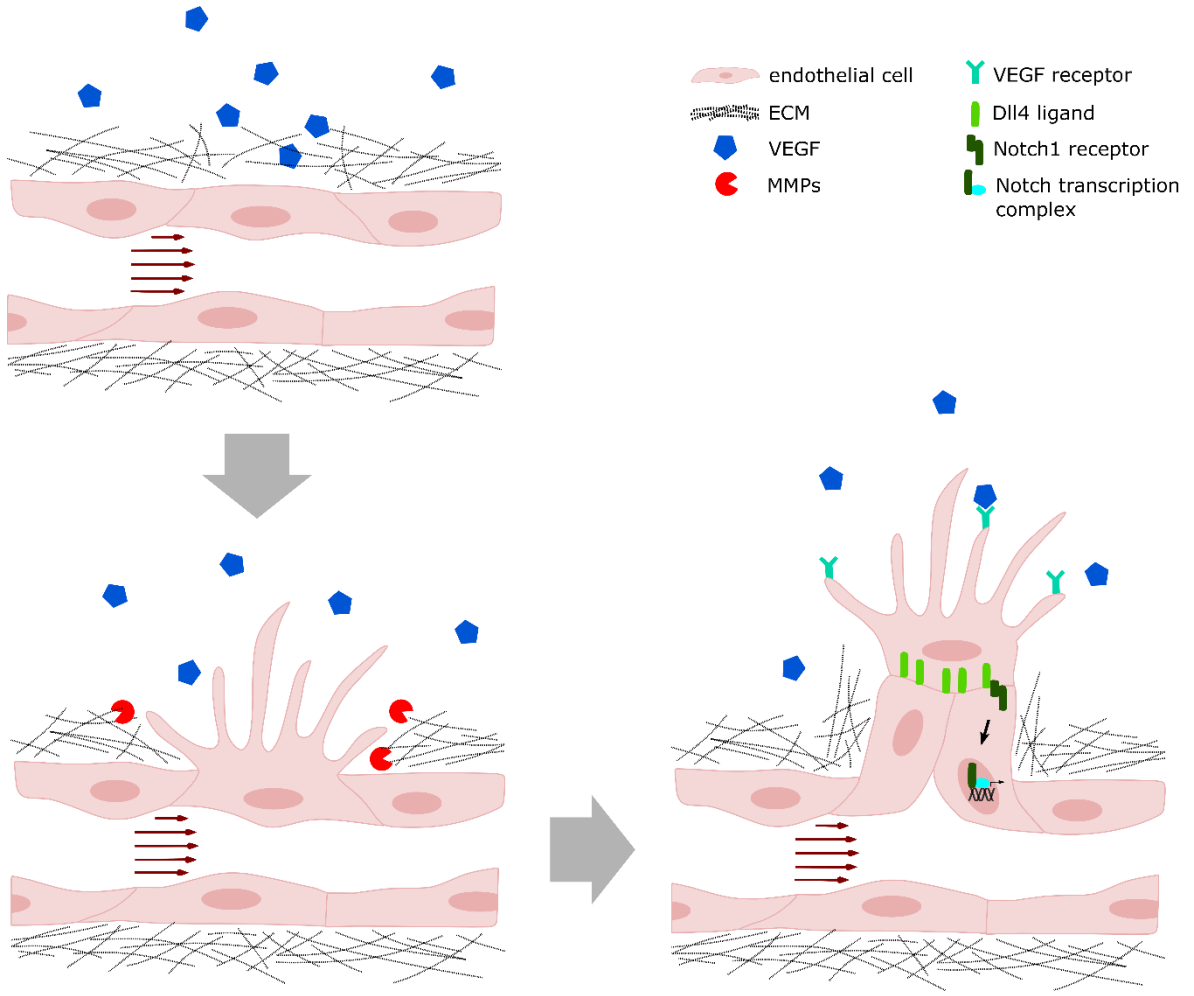

Figure 5-2: Schematic overview of the proposed tip cell selection process. Local release of VEGF initiates angiogenesis and induces matrix remodeling at sites where the new sprout is to be formed. Matrix remodeling and the associated increase in matrix elasticity and loosening of the cell-matrix contacts allow a cell to break out of the existing vessel. The release of MMPs further promotes the migration of the first cell (tip cell). Binding of VEGF to VEGFR in the tip cells leads to increased expression of Dll4 in the tip cells, which activates Notch signaling in the following stalk cells.

5.2.1 Matrix stiffness influences the sprouting behavior of endothelial cells

Initiation of angiogenesis is based on biochemical cues, such as VEGF, which are emitted by the surrounding tissue or transmitted by cell interactions [3, 40]. In addition to biochemical signals, the influence of mechanical cues on the process of angiogenesis, mainly originating from stiffness changes of the extracellular matrix, is receiving more attention [3, 5]. ECM stiffness affects endothelial cell functions, regulating migration and proliferation and thus angiogenic sprouting [5, 88]. To investigate the influence of overall stiffness changes during angiogenesis, the spheroid sprouting model was extended with stiffness tunable collagen matrices. The sprouting behavior of HUVECs shows that the number of sprouts, the sprouting length as well as the spheroid diameter behave in a stiffness-dependent manner (Fig. 4-14). The softer the surrounding matrix, the stronger the sprouting with the opposite behavior at higher stiffnesses. Thus, the results also indicate that the lower matrix stiffness supports migration of the cells, which results in the increased sprouting behavior. In summary, this 3D in vitro angiogenesis model allows the analysis of the influence of Notch and Dll4 expression as well as the impact of stiffness changes of the extracellular matrix during angiogenic sprouting. However, the focus of angiogenesis studies with the applied model is on the onset of sprouting and tip cell differentiation and migration, where only an overall matrix stiffness can be adjusted. During in vivo angiogenesis an ongoing adjustment of ECM stiffness is necessary to regulate migration and proliferation of endothelial cells and thus vessel elongation and lumen formation [2, 88].

5.3 Clinical and pharmacological relevance

While most cell types are surrounded by or even form a tissue with a stiffness of 50 – 15,000 Pa, the behavior of these cells is mostly studied in in vitro approaches on plastic or glass, which have stiffnesses of 2 – 4 GPa, comparable to the stiffness of bone [44, 89]. Studies on plastic facilitate the investigation of cellular structures and functions but may differ from in vivo behavior [44]. Particularly for endothelial cells, a mechanosensitivity has already been demonstrated, whereby these cells adapt their gene expression profiles depending on the stiffness of the surrounding organ tissue [1, 6], demonstrating the need for 2D and 3D cell models with adapted matrices for these cells. In addition to studying general cell behaviors, including migration and proliferation, those cell models can also be used to investigate the regulation of various signaling pathways in endothelial cells, such as the Notch signaling pathway. During angiogenesis, the Notch signaling pathway controls the number of endothelial tip and stalk cells, regulating vessel sprouting and elongation [47, 50]. This process also requires tight regulation of matrix elasticity and stiffness, which enables migration and proliferation through mechanical signaling [2, 88]. Thus, the findings of this study might be of importance to better understand the effect of matrix remodeling on endothelial cell behavior and adjustment of their gene expression. The data of the Notch signaling pathway as a mechanosensor and the interplay with cell-matrix and cell-cell adhesion could further demonstrate the influence of mechanical cues on cellular signaling pathways. This suggests that the changes in matrix stiffness during angiogenesis affect not only migration and proliferation but also angiogenesis-regulating signaling pathways in endothelial cells.

Modifications in the extracellular matrix towards matrix stiffening also play a role in several pathologies, such as fibrosis, diabetes, cardiovascular diseases, and cancer [90, 91]. In particular, the microenvironment of tumors exhibits a marked increase in stiffness due to enhanced collagen deposition on the one hand and cross-linking by cell-secreted enzymes on the other [43]. These changes in the ECM increase the solid stress and mechanical pressure on the tumor tissue, but also affect the tumor microvasculature [92]. Tumor vessels are mostly malformed, permeable, increasingly branched, and tortuous and thus exhibit disturbed blood flow, caused both by the mechanical influences of the ECM and by upregulated VEGF expression [6, 92, 93]. The perturbed structure of the tumor vasculature increases fluid pressure and shear stress on the vessel and tissue and may also affect the surrounding healthy

tissue, promoting tumor invasion [91, 92]. The increased permeability of the tumor vessels limits the perfusion of the tissue, on the one hand further promoting branching and outgrowth, on the other hand also complicating the administration of drugs in cancer therapy [6, 93]. Most approaches to cancer therapy by normalizing the tumor vasculature involve inhibition of pro-angiogenic factors, such as VEGF [93, 94]. Several studies have shown that restriction of VEGF signaling can reduce tumor growth [45, 93, 94]. However, the administration of VEGF inhibitors is not successful in all cancers and, even when initially effective, is often short-lived and subsequently leads to resumption of tumor progression [94, 95]. Due to the significant influence of matrix stiffening and mechanical forces on tumor vasculature and progression, newer treatment strategies are based on therapeutically targeting tumor stiffness, which has already been shown to normalize vasculature [6, 92, 93]. This can reduce pressure on the tissue and improve blood flow through the tumor tissue, also adapting angiogenic key factors, like VEGF binding and Notch signaling [6, 92]. In this context, the results of this study can give a deeper insight into the consequences of normal and pathological matrix changes on endothelial behavior and sprout morphology during angiogenic sprouting in development and maintenance, especially regarding the data showing Notch as a mechanosensor with an upregulation on softer substrates and the role of Dll4 expression and Notch signaling during tip/stalk cell selection. This could help to better understand and predict the consequences of targeting vascular-specific targets in cancer treatment, and will also allow the therapy itself to be adapted according to the type of cancer and the disease pattern, minimizing the risk of metastasis and treatment resistance [6, 45, 96].

5.4 Conclusion and outlook

In conclusion, this study indicates a role of substrate rigidity as a modulator of Notch signaling, in that the Notch signaling pathway can be activated via mechanotransduction in dependence on substrate stiffness. This mechnanosensitivity may likely be associated with trans-endocytosis. Based on two different angiogenesis models, the results of this thesis also confirm the function of Notch during angiogenesis by ligand overexpression and Notch inhibition. However, further investigation of the properties of tip cells implies that Dll4 overexpressing cells do not automatically adopt a tip cell position. Thus, the increased Dll4 expression characteristic of tip cells does not appear to be a selection factor, but rather occurs as a result of tip cell determination by other factors. Together, this study provides a better understanding of the impact of substrate stiffness on the Notch signaling pathway and its influence especially during angiogenic sprouting and tip/stalk cell selection. This may have important implications in pathological situations, such as tumor growth, associated with stiffening of the extracellular matrix.

For further investigation, the two models of cellular Notch investigation on different substrates and angiogenesis analysis should be combined. Using stiffness tunable collagen, such as PhotoCol®, the stiffness-dependent behavior of Notch during angiogenesis can then be determined. The role of Dll4 expression in tip cell selection should also be further investigated. Using Dll4 overexpression at different time points during angiogenic sprouting (e.g., with an inducible plasmid), the effect of Dll4 on sprouting behavior and cell positions in the sprouts can be analyzed. It can be suggested that tip cell selection first proceeds from changes in matrix density that allow mobility and migration of these cells [36]. Inducing a local change in stiffness in a collagen matrix can be a major challenge without affecting or damaging the cells. However, stiffness sensing probes can be used to detect the changes in the matrix in a spheroid sprouting assay [97]; at the same time, the expression of Dll4 or other tip cell markers, for example with SmartFlare reagents [98], can be studied to clarify the processes of tip cell selection.

6 References

1. Stepanova, D., et al., *A multiscale model of complex endothelial cell dynamics in early angiogenesis.* PLoS Comput Biol, 2021. **17**(1): p. e1008055.
2. Shamloo, A., et al., *A Comparative Study of Collagen Matrix Density Effect on Endothelial Sprout Formation Using Experimental and Computational Approaches.* Ann Biomed Eng, 2016. **44**(4): p. 929-41.
3. Mammoto, A., et al., *A mechanosensitive transcriptional mechanism that controls angiogenesis.* Nature, 2009. **457**(7233): p. 1103-8.
4. Estrach, S., et al., *Laminin-binding integrins induce Dll4 expression and Notch signaling in endothelial cells.* Circ Res, 2011. **109**(2): p. 172-82.
5. Matsuo, E., et al., *Substrate stiffness modulates endothelial cell function via the YAP-Dll4-Notch1 pathway.* Exp Cell Res, 2021. **408**(1): p. 112835.
6. Bordeleau, F., et al., *Matrix stiffening promotes a tumor vasculature phenotype.* Proc Natl Acad Sci U S A, 2017. **114**(3): p. 492-497.
7. Rudiger, D., et al., *Cell-Based Strain Remodeling of a Nonfibrous Matrix as an Organizing Principle for Vasculogenesis.* Cell Rep, 2020. **32**(6): p. 108015.
8. Fischer, R.S., et al., *Local cortical tension by myosin II guides 3D endothelial cell branching.* Curr Biol, 2009. **19**(3): p. 260-5.
9. Liu, Z.J., et al., *Regulation of Notch1 and Dll4 by vascular endothelial growth factor in arterial endothelial cells: implications for modulating arteriogenesis and angiogenesis.* Mol Cell Biol, 2003. **23**(1): p. 14-25.
10. Nandagopal, N., et al., *Dynamic Ligand Discrimination in the Notch Signaling Pathway.* Cell, 2018. **172**(4): p. 869-880 e19.
11. Totaro, A., et al., *Crosstalk between YAP/TAZ and Notch Signaling.* Trends Cell Biol, 2018. **28**(7): p. 560-573.
12. Hodkinson, P.S., et al., *Mammalian NOTCH-1 activates beta1 integrins via the small GTPase R-Ras.* J Biol Chem, 2007. **282**(39): p. 28991-29001.
13. Boareto, M., et al., *Jagged-Delta asymmetry in Notch signaling can give rise to a Sender/Receiver hybrid phenotype.* Proc Natl Acad Sci U S A, 2015. **112**(5): p. E402-9.
14. Takeshita, K., et al., *Critical role of endothelial Notch1 signaling in postnatal angiogenesis.* Circ Res, 2007. **100**(1): p. 70-8.
15. Steinbuck, M.P. and S. Winandy, *A Review of Notch Processing With New Insights Into Ligand-Independent Notch Signaling in T-Cells.* Front Immunol, 2018. **9**: p. 1230.
16. van Tetering, G., et al., *Metalloprotease ADAM10 is required for Notch1 site 2 cleavage.* J Biol Chem, 2009. **284**(45): p. 31018-27.

17. Lake, R.J., et al., *In vivo analysis of the Notch receptor S1 cleavage.* PLoS One, 2009. **4**(8): p. e6728.

18. Gordon, W.R., et al., *Effects of S1 cleavage on the structure, surface export, and signaling activity of human Notch1 and Notch2.* PLoS One, 2009. **4**(8): p. e6613.

19. Sprinzak, D., et al., *Cis-interactions between Notch and Delta generate mutually exclusive signalling states.* Nature, 2010. **465**(7294): p. 86-90.

20. Nichols, J.T., et al., *DSL ligand endocytosis physically dissociates Notch1 heterodimers before activating proteolysis can occur.* J Cell Biol, 2007. **176**(4): p. 445-58.

21. Meloty-Kapella, L., et al., *Notch ligand endocytosis generates mechanical pulling force dependent on dynamin, epsins, and actin.* Dev Cell, 2012. **22**(6): p. 1299-312.

22. Jiang, L.Y., et al., *gamma-Secretase Inhibitor, DAPT Inhibits Self-renewal and Stemness Maintenance of Ovarian Cancer Stem-like Cells In Vitro.* Chin J Cancer Res, 2011. **23**(2): p. 140-6.

23. Koon, Y.L., et al., *Enhanced Delta-Notch Lateral Inhibition Model Incorporating Intracellular Notch Heterogeneity and Tension-Dependent Rate of Delta-Notch Binding that Reproduces Sprouting Angiogenesis Patterns.* Sci Rep, 2018. **8**(1): p. 9519.

24. Chillakuri, C.R., et al., *Notch receptor-ligand binding and activation: insights from molecular studies.* Semin Cell Dev Biol, 2012. **23**(4): p. 421-8.

25. Ahimou, F., et al., *The adhesion force of Notch with Delta and the rate of Notch signaling.* J Cell Biol, 2004. **167**(6): p. 1217-29.

26. Riahi, R., et al., *Notch1-Dll4 signalling and mechanical force regulate leader cell formation during collective cell migration.* Nat Commun, 2015. **6**: p. 6556.

27. Gordon, W.R., et al., *Mechanical Allostery: Evidence for a Force Requirement in the Proteolytic Activation of Notch.* Dev Cell, 2015. **33**(6): p. 729-36.

28. Du, Y., et al., *Three-Dimensional Characterization of Mechanical Interactions between Endothelial Cells and Extracellular Matrix during Angiogenic Sprouting.* Sci Rep, 2016. **6**: p. 21362.

29. Potente, M., H. Gerhardt, and P. Carmeliet, *Basic and therapeutic aspects of angiogenesis.* Cell, 2011. **146**(6): p. 873-87.

30. Apte, R.S., D.S. Chen, and N. Ferrara, *VEGF in Signaling and Disease: Beyond Discovery and Development.* Cell, 2019. **176**(6): p. 1248-1264.

31. Blanco, R. and H. Gerhardt, *VEGF and Notch in tip and stalk cell selection.* Cold Spring Harb Perspect Med, 2013. **3**(1): p. a006569.

32. Hanahan, D. and R.A. Weinberg, *The hallmarks of cancer.* Cell, 2000. **100**(1): p. 57-70.

33. Kretschmer, M., D. Rudiger, and S. Zahler, *Mechanical Aspects of Angiogenesis.* Cancers (Basel), 2021. **13**(19).

34. Santos-Oliveira, P., et al., *The Force at the Tip--Modelling Tension and Proliferation in Sprouting Angiogenesis.* PLoS Comput Biol, 2015. **11**(8): p. e1004436.

35. Shen, C.J., et al., *Decreased cell adhesion promotes angiogenesis in a Pyk2-dependent manner.* Exp Cell Res, 2011. **317**(13): p. 1860-71.

36. Perfahl, H., et al., *3D hybrid modelling of vascular network formation.* J Theor Biol, 2017. **414**: p. 254-268.

37. Ribatti, D. and E. Crivellato, *"Sprouting angiogenesis", a reappraisal.* Dev Biol, 2012. **372**(2): p. 157-65.

38. Kiran, M.S., et al., *Changes in expression of VE-cadherin and MMPs in endothelial cells: Implications for angiogenesis.* Vasc Cell, 2011. **3**(1): p. 6.

39. van Duinen, V., et al., *Perfused 3D angiogenic sprouting in a high-throughput in vitro platform.* Angiogenesis, 2019. **22**(1): p. 157-165.

40. Pauty, J., et al., *A Vascular Endothelial Growth Factor-Dependent Sprouting Angiogenesis Assay Based on an In Vitro Human Blood Vessel Model for the Study of Anti-Angiogenic Drugs.* EBioMedicine, 2018. **27**: p. 225-236.

41. Davidson, C.D., et al., *Cell force-mediated matrix reorganization underlies multicellular network assembly.* Sci Rep, 2019. **9**(1): p. 12.

42. Landau, S., S. Ben-Shaul, and S. Levenberg, *Oscillatory Strain Promotes Vessel Stabilization and Alignment through Fibroblast YAP-Mediated Mechanosensitivity.* Adv Sci (Weinh), 2018. **5**(9): p. 1800506.

43. Bordeleau, F., et al., *Tissue stiffness regulates serine/arginine-rich protein-mediated splicing of the extra domain B-fibronectin isoform in tumors.* Proc Natl Acad Sci U S A, 2015. **112**(27): p. 8314-9.

44. Yeung, T., et al., *Effects of substrate stiffness on cell morphology, cytoskeletal structure, and adhesion.* Cell Motil Cytoskeleton, 2005. **60**(1): p. 24-34.

45. Jain, R.K., *Normalizing tumor microenvironment to treat cancer: bench to bedside to biomarkers.* J Clin Oncol, 2013. **31**(17): p. 2205-18.

46. Merk, H., et al., *Inhibition of endothelial Cdk5 reduces tumor growth by promoting non-productive angiogenesis.* Oncotarget, 2016. **7**(5): p. 6088-104.

47. Antfolk, D., et al., *Selective regulation of Notch ligands during angiogenesis is mediated by vimentin.* Proc Natl Acad Sci U S A, 2017. **114**(23): p. E4574-E4581.

48. Pitulescu, M.E., et al., *Dll4 and Notch signalling couples sprouting angiogenesis and artery formation.* Nat Cell Biol, 2017. **19**(8): p. 915-927.

49. Andrawes, M.B., et al., *Intrinsic selectivity of Notch 1 for Delta-like 4 over Delta-like 1.* J Biol Chem, 2013. **288**(35): p. 25477-25489.

50. Ubezio, B., et al., *Synchronization of endothelial Dll4-Notch dynamics switch blood vessels from branching to expansion.* Elife, 2016. **5**.

51. Badenes, M., et al., *Delta-like 4/Notch signaling promotes Apc (Min/+) tumor initiation through angiogenic and non-angiogenic related mechanisms.* BMC Cancer, 2017. **17**(1): p. 50.

52. Rehman, A.O. and C.Y. Wang, *Notch signaling in the regulation of tumor angiogenesis.* Trends Cell Biol, 2006. **16**(6): p. 293-300.

53. Kofler, N.M., et al., *Notch signaling in developmental and tumor angiogenesis.* Genes Cancer, 2011. **2**(12): p. 1106-16.

54. Akil, A., et al., *Notch Signaling in Vascular Endothelial Cells, Angiogenesis, and Tumor Progression: An Update and Prospective.* Front Cell Dev Biol, 2021. **9**: p. 642352.

55. Dufraine, J., Y. Funahashi, and J. Kitajewski, *Notch signaling regulates tumor angiogenesis by diverse mechanisms.* Oncogene, 2008. **27**(38): p. 5132-7.

56. Wieland, E., et al., *Endothelial Notch1 Activity Facilitates Metastasis.* Cancer Cell, 2017. **31**(3): p. 355-367.

57. Arganda-Carreras, I., et al., *3D reconstruction of histological sections: Application to mammary gland tissue.* Microsc Res Tech, 2010. **73**(11): p. 1019-29.

58. Tinevez, J.Y., et al., *TrackMate: An open and extensible platform for single-particle tracking.* Methods, 2017. **115**: p. 80-90.

59. Arganda-Carreras, I., et al., *Trainable Weka Segmentation: a machine learning tool for microscopy pixel classification.* Bioinformatics, 2017. **33**(15): p. 2424-2426.

60. Nukuda, A., et al., *Stiff substrates increase YAP-signaling-mediated matrix metalloproteinase-7 expression.* Oncogenesis, 2015. **4**: p. e165.

61. Gegenfurtner, F.A., et al., *Micropatterning as a tool to identify regulatory triggers and kinetics of actin-mediated endothelial mechanosensing.* J Cell Sci, 2018. **131**(10).

62. Lei, L., et al., *Endothelial expression of beta1 integrin is required for embryonic vascular patterning and postnatal vascular remodeling.* Mol Cell Biol, 2008. **28**(2): p. 794-802.

63. Howe, G.A. and C.L. Addison, *beta1 integrin: an emerging player in the modulation of tumorigenesis and response to therapy.* Cell Adh Migr, 2012. **6**(2): p. 71-7.

64. Du, J., et al., *Integrin activation and internalization on soft ECM as a mechanism of induction of stem cell differentiation by ECM elasticity.* Proc Natl Acad Sci U S A, 2011. **108**(23): p. 9466-71.

65. Rand, M.D., et al., *Calcium depletion dissociates and activates heterodimeric notch receptors.* Mol Cell Biol, 2000. **20**(5): p. 1825-35.

66. Tremblay, I., et al., *The MEK/ERK pathway promotes NOTCH signalling in pancreatic cancer cells.* PLoS One, 2013. **8**(12): p. e85502.

67. Shaya, O., et al., *Cell-Cell Contact Area Affects Notch Signaling and Notch-Dependent Patterning.* Dev Cell, 2017. **40**(5): p. 505-511 e6.

68. Artavanis-Tsakonas, S., M.D. Rand, and R.J. Lake, *Notch signaling: cell fate control and signal integration in development.* Science, 1999. **284**(5415): p. 770-6.

69. Aster, J.C., W.S. Pear, and S.C. Blacklow, *The Varied Roles of Notch in Cancer.* Annu Rev Pathol, 2017. **12**: p. 245-275.

70. Bray, S.J., *Notch signalling in context.* Nat Rev Mol Cell Biol, 2016. **17**(11): p. 722-735.

71. Sprinzak, D. and S.C. Blacklow, *Biophysics of Notch Signaling.* Annu Rev Biophys, 2021. **50**: p. 157-189.

72. Das, A., et al., *YAP Nuclear Localization in the Absence of Cell-Cell Contact Is Mediated by a Filamentous Actin-dependent, Myosin II- and Phospho-YAP-independent Pathway during Extracellular Matrix Mechanosensing.* J Biol Chem, 2016. **291**(12): p. 6096-110.

73. Rallis, C., S.M. Pinchin, and D. Ish-Horowicz, *Cell-autonomous integrin control of Wnt and Notch signalling during somitogenesis.* Development, 2010. **137**(21): p. 3591-601.

74. Kwak, M., et al., *Size-dependent protein segregation creates a spatial switch for Notch signaling and function.* bioRxiv, 2021: p. 2020.06.28.176560.

75. Shergill, B., et al., *Optical tweezers studies on Notch: single-molecule interaction strength is independent of ligand endocytosis.* Dev Cell, 2012. **22**(6): p. 1313-20.

76. Sprinzak, D., et al., *Mutual inactivation of Notch receptors and ligands facilitates developmental patterning.* PLoS Comput Biol, 2011. **7**(6): p. e1002069.

77. You, C., et al., *Loss of CCM3 impairs DLL4-Notch signalling: implication in endothelial angiogenesis and in inherited cerebral cavernous malformations.* J Cell Mol Med, 2013. **17**(3): p. 407-18.

78. You, C., et al., *EphB4 forward signalling mediates angiogenesis caused by CCM3/PDCD10-ablation.* J Cell Mol Med, 2017. **21**(9): p. 1848-1858.

79. Venkatesh, D., et al., *RhoA-mediated signaling in Notch-induced senescence-like growth arrest and endothelial barrier dysfunction.* Arterioscler Thromb Vasc Biol, 2011. **31**(4): p. 876-82.

80. Bridges, E., et al., *RHOQ is induced by DLL4 and regulates angiogenesis by determining the intracellular route of the Notch intracellular domain.* Angiogenesis, 2020. **23**(3): p. 493-513.

81. Seugnet, L., P. Simpson, and M. Haenlin, *Requirement for dynamin during Notch signaling in Drosophila neurogenesis.* Dev Biol, 1997. **192**(2): p. 585-98.

82. Parks, A.L., et al., *Ligand endocytosis drives receptor dissociation and activation in the Notch pathway.* Development, 2000. **127**(7): p. 1373-85.

83. Sorensen, E.B. and S.D. Conner, *gamma-secretase-dependent cleavage initiates notch signaling from the plasma membrane.* Traffic, 2010. **11**(9): p. 1234-45.

84. Williams, C.K., et al., *Up-regulation of the Notch ligand Delta-like 4 inhibits VEGF-induced endothelial cell function.* Blood, 2006. **107**(3): p. 931-9.

85. Caliceti, C., et al., *17beta-estradiol enhances signalling mediated by VEGF-A-delta-like ligand 4-notch1 axis in human endothelial cells.* PLoS One, 2013. **8**(8): p. e71440.

86. Wei, Y., et al., *Nrf2 acts cell-autonomously in endothelium to regulate tip cell formation and vascular branching.* Proc Natl Acad Sci U S A, 2013. **110**(41): p. E3910-8.

87. Zheng, W., et al., *Notch restricts lymphatic vessel sprouting induced by vascular endothelial growth factor.* Blood, 2011. **118**(4): p. 1154-62.

88. Wang, W.Y., et al., *Functional angiogenesis requires microenvironmental cues balancing endothelial cell migration and proliferation.* Lab Chip, 2020. **20**(6): p. 1153-1166.

89. Cox, T.R. and J.T. Erler, *Remodeling and homeostasis of the extracellular matrix: implications for fibrotic diseases and cancer.* Dis Model Mech, 2011. **4**(2): p. 165-78.

90. Korn, C. and H.G. Augustin, *Mechanisms of Vessel Pruning and Regression.* Dev Cell, 2015. **34**(1): p. 5-17.

91. Lampi, M.C. and C.A. Reinhart-King, *Targeting extracellular matrix stiffness to attenuate disease: From molecular mechanisms to clinical trials.* Sci Transl Med, 2018. **10**(422).

92. Zanotelli, M.R. and C.A. Reinhart-King, *Mechanical Forces in Tumor Angiogenesis.* Adv Exp Med Biol, 2018. **1092**: p. 91-112.

93. Ghosh, K., et al., *Tumor-derived endothelial cells exhibit aberrant Rho-mediated mechanosensing and abnormal angiogenesis in vitro.* Proc Natl Acad Sci U S A, 2008. **105**(32): p. 11305-10.

94. Zirlik, K. and J. Duyster, *Anti-Angiogenics: Current Situation and Future Perspectives.* Oncol Res Treat, 2018. **41**(4): p. 166-171.

95. Chekhonin, V.P., et al., *VEGF in tumor progression and targeted therapy.* Curr Cancer Drug Targets, 2013. **13**(4): p. 423-43.

96. Augustin, H.G. and G.Y. Koh, *Organotypic vasculature: From descriptive heterogeneity to functional pathophysiology.* Science, 2017. **357**(6353).

97. Li, J., et al., *A stiffness probe based on force and vision sensing for soft tissue diagnosis.* Annu Int Conf IEEE Eng Med Biol Soc, 2012. **2012**: p. 944-7.

98. McClellan, S., et al., *mRNA detection in living cells: A next generation cancer stem cell identification technique.* Methods, 2015. **82**: p. 47-54.

7 Appendix

7.1 Supplementary figures

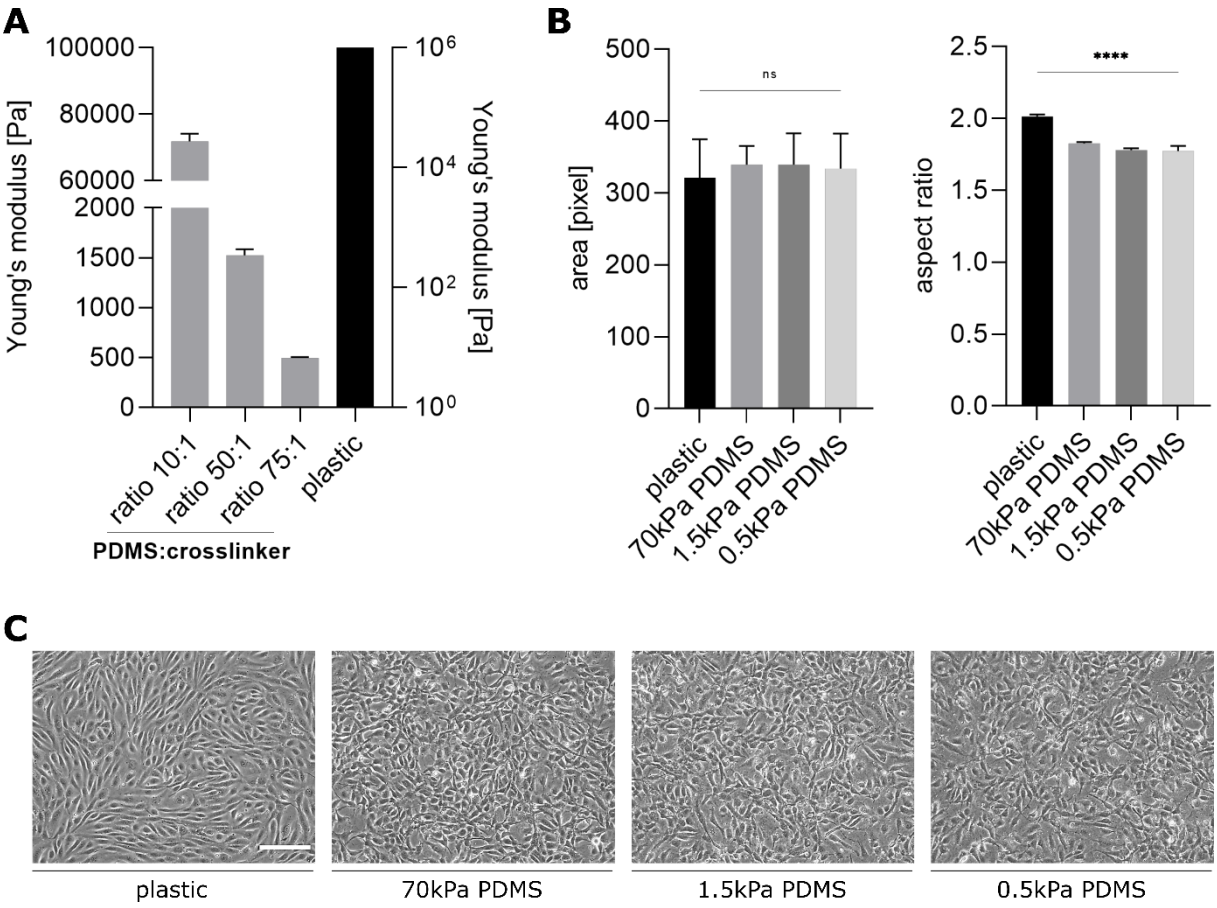

Figure 7-1: Cell morphologies change slightly on all PDMS substrates but independent of substrate stiffness. (A) Stiffness determination of PDMS substrates by rheometric measurements. Mean Young's modulus ± SEM are depicted in a bar graph and compared to the stiffness of plastic. **(B)** Mean cell areas and aspect ratios ± SEM of HUVECs seeded on collagen G coated plastic and PDMS substrates with different stiffness are summarized in bar graphs (Dunnett's corrected one-way ANOVA, ns ≙ not significant, ****P<0.0001). **(C)** Representative images of HUVECs seeded on plastic and PDMS (scale bar 100 μm).

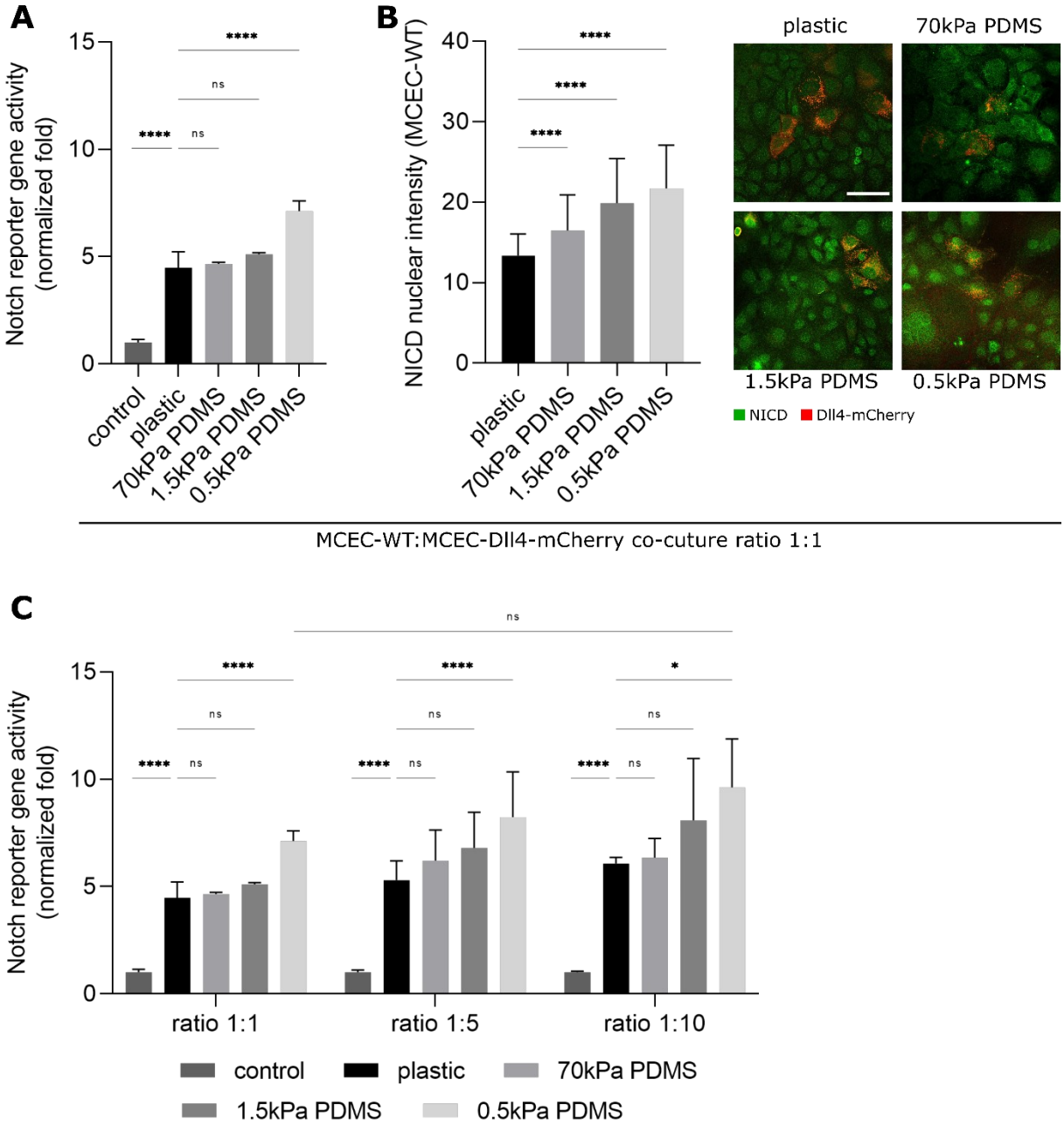

Figure 7-2: Notch activation by co-culture of Notch sender and receiver cells increases on soft substrates in MCEC-WT receiver cells but is dependent on the seeding ratio. (A,B) Induction of Notch activity by co-culture with MCEC-Dll4-mCherry cells with collagen G coating. **(A)** Normalized fold Notch activity in confluent MCEC-WT/MCEC-Dll4-mCherry co-cultures on substrates with different stiffnesses, determined by detection of cellular luciferase levels under control of the TP1-luc Notch reporter (mean ± SEM, one-way ANOVA followed by Dunnett's multiple comparison test, ns ≙ not significant, ****P<0.0001). **(B)** Left panel: nuclear NICD intensities in MCEC-WT cells seeded in co-culture with MCEC-Dll4-mCherry cells on different plastic and PDMS substrates. Intensities are shown in a bar graph on the left panel, quantified in ≥300 single cells derived from 3 independent experiments (Tukey's corrected one-way ANOVA, ****P<0.0001); right panel: representative images of cells stained for NICD (shown in green, mCherry-Dll4 reporter of MCEC-Dll4-mCherry cells shown in red, scale bar 50 µm). **(C)** Normalized fold Notch activity in endothelial co-cultures of MCEC-WT/MCEC-Dll4-mCherry cells in seeding ratios of 1:1, 1:5 and 1:10, determined by detection of cellular luciferase levels under control of the TP1-luc Notch reporter. Bar plots were generated by evaluation of reporter gene assays on substrates with different stiffnesses (two-way ANOVA followed by Tukey's multiple comparison test, ns ≙ not significant, *P<0.1, ****P<0.0001).

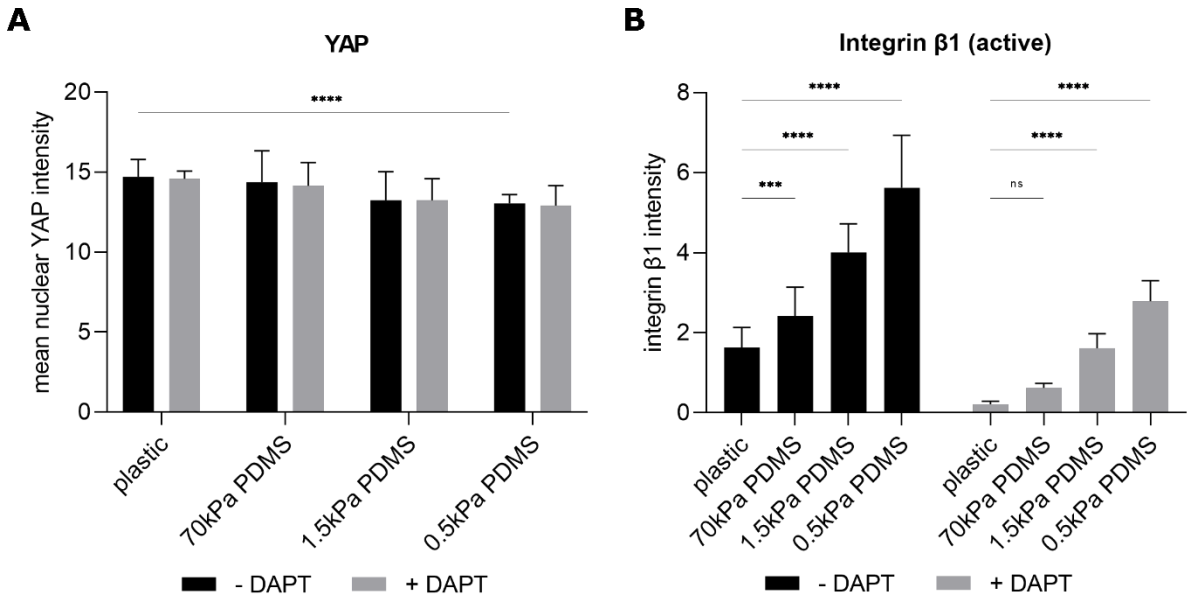

Figure 7-3: YAP and integrin β1 intensity in MCEC-WT cells are dependent on substrate stiffness as well as the Notch signaling pathway, whereas the integrin β1 intensity is also influenced by the Notch signaling pathway but the nuclear intensity of YAP does not change after Notch inhibition. (A,B) MCEC-WT cells were seeded on varying substrate stiffness, treated with 25 µM DAPT for 24 h and stained for either the activated form of YAP or integrin β1. The nuclear intensities for YAP and the mean overall intensity for integrin β1 ± SEM of untreated and treated cells are summarized in bar graphs (Tukey's/Sidak's corrected two-way ANOVA, ns ≙ not significant, ***P<0.001, ****P<0.0001).

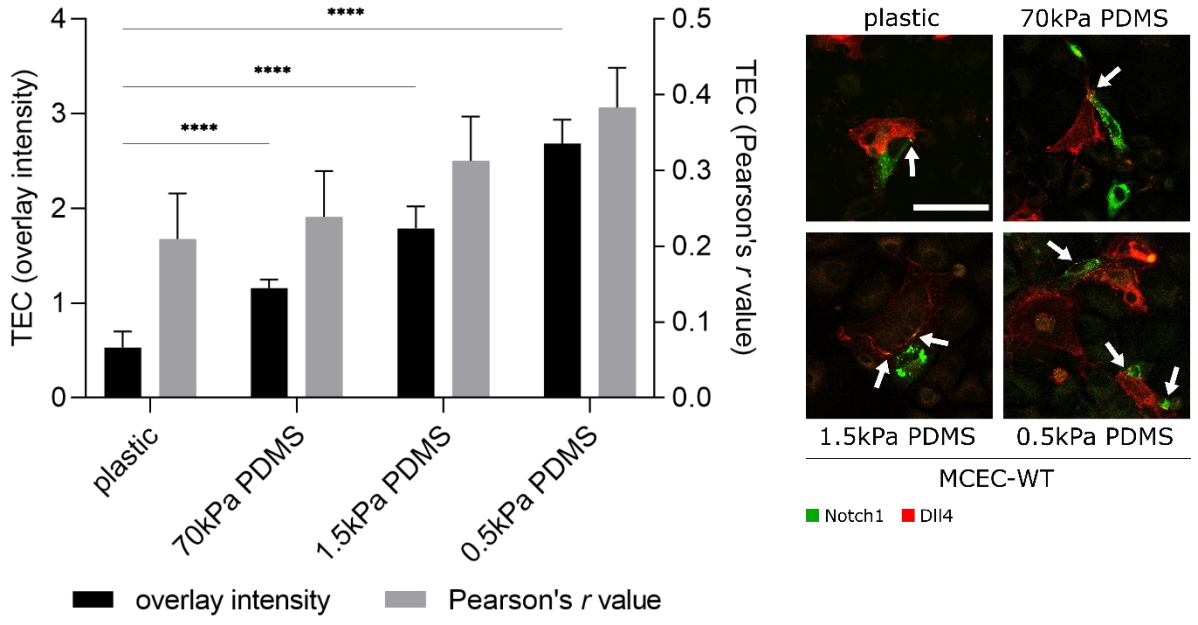

Figure 7-4: Trans-endocytosis is increased in MCEC-WT cells on softer substrates. Overlay intensity and Pearson's r value in areas of Notch receptor-ligand interactions in the course of trans-endocytosis. Overlay areas are indicated by the white arrows. MCEC-WT cells were transfected separately with a citrine-coupled Notch1 plasmid and a mCherry-coupled Dll4 plasmid. Notch1 expressing Notch receiver cells are shown in green, Dll4 expressing Notch sender cells are shown in red. Trans-endocytosis was quantified at cell-cell contacts in ≥30 cells per substrate condition in three independent experiments. Data is presented as a bar plot (mean value ± SEM, two-way ANOVA with Sidak's multiple comparison test, ****P<0.0001).

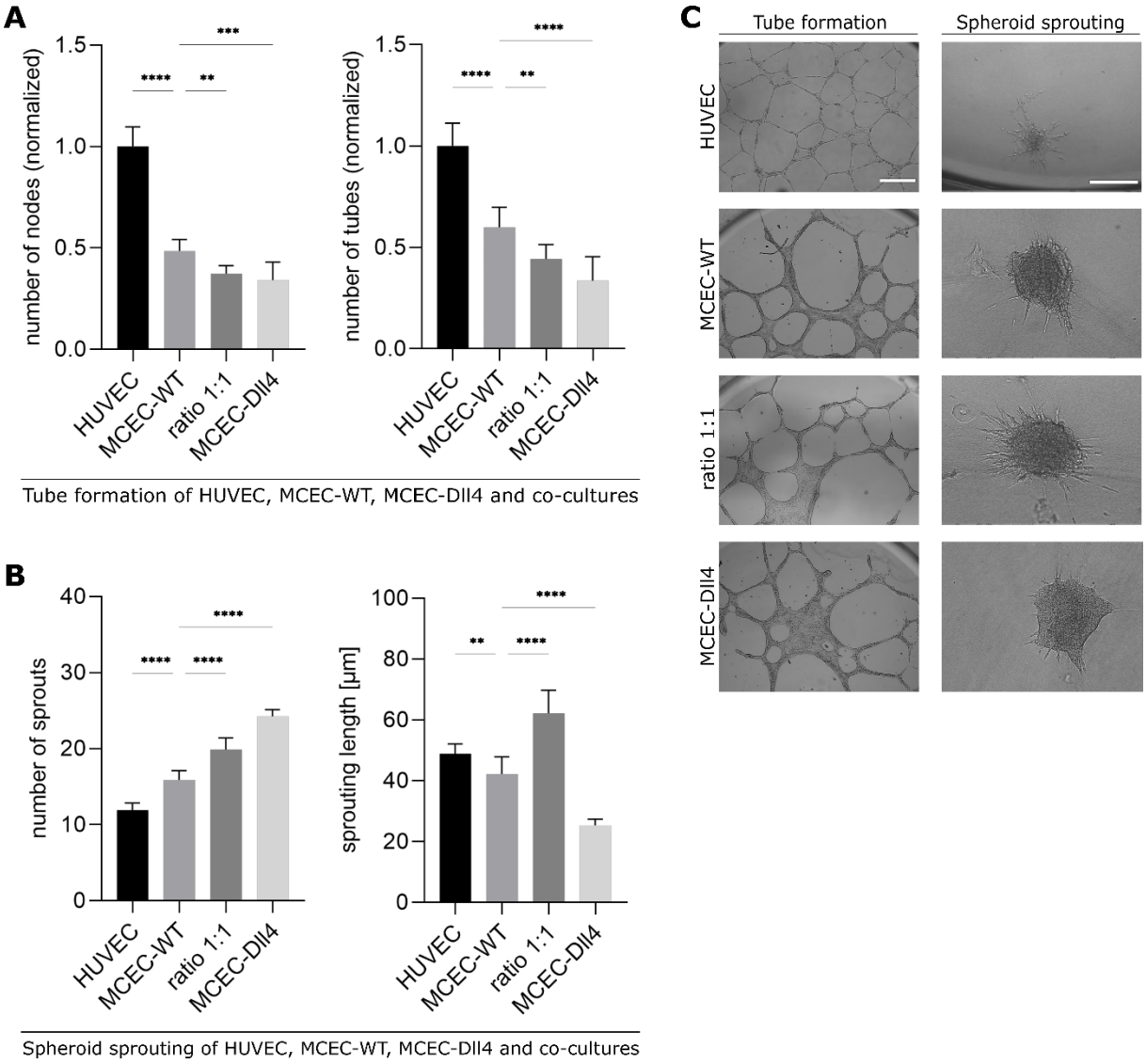

Figure 7-5: Dll4 overexpressing cells reduce tube formation but enhance sprouting in co-culture with MCEC-WT Notch receiver cells. (A) Quantification of the number of nodes and tubes 24 h after cell seeding on Matrigel. Data is normalized to HUVEC tube formation and is presented in bar graph (mean ± SEM) with significance determined by one-way ANOVA followed by Dunnett's multiple comparison test (**P<0.01, ***P<0.001, ****P<0.0001). **(B)** Quantification of the number of sprouts and its length in sprouted spheroids. Data is normalized to HUVEC spheroids and is presented in bar graph (mean ± SEM of ≥ 15 spheroids per condition) with significance determined by one-way ANOVA followed by Dunnett's multiple comparison test (**P<0.01, ****P<0.0001). **(C)** Representative images of tube formations of different endothelial cells (left panel, scale bar 250 µm) and sprouted spheroids of different endothelial cells (right panel, scale bar 100 µm).

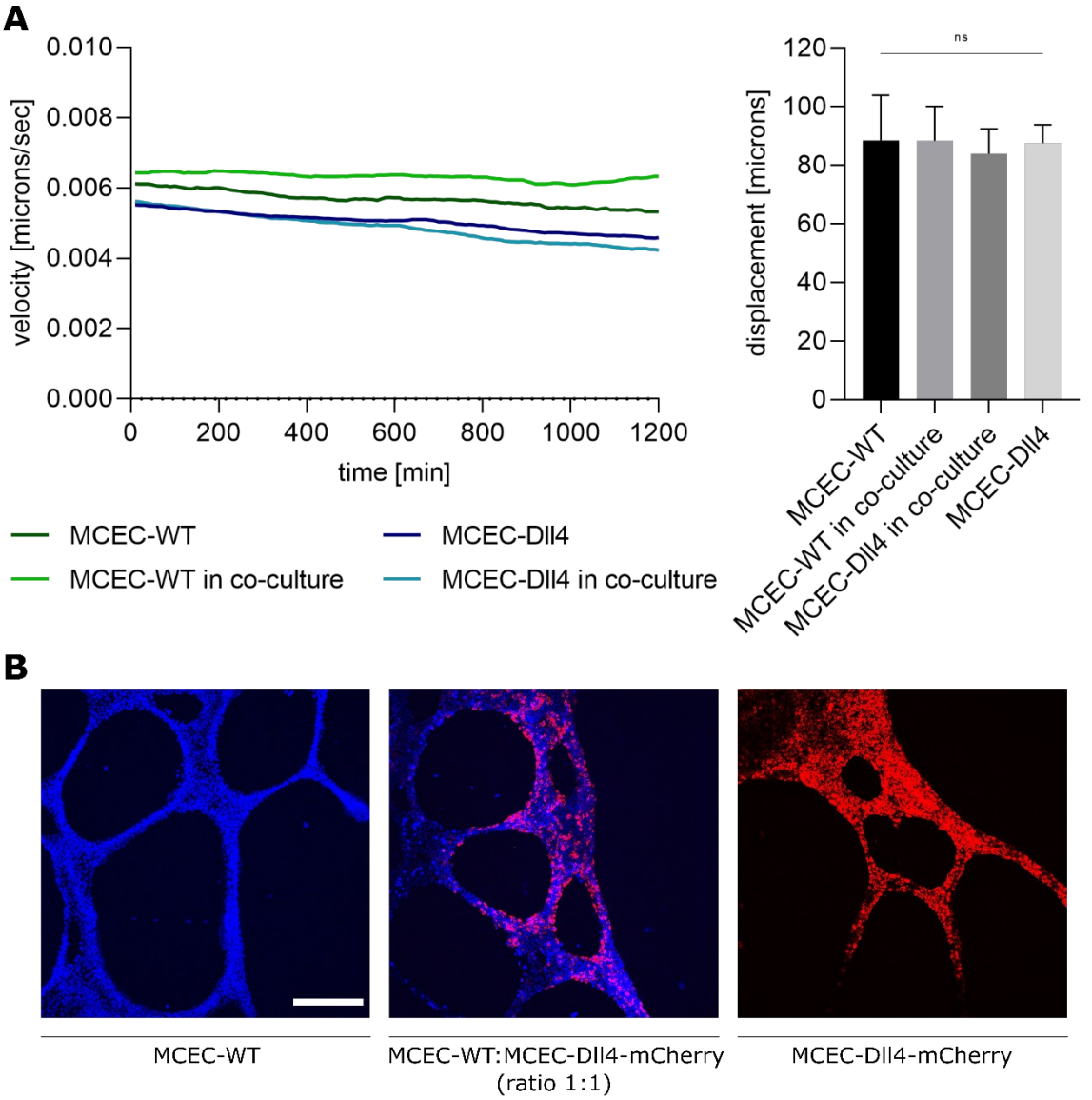
A
velocity [microns/sec]
0.010
0.008
0.006
0.004
0.002
0.000
0
200
400
600
800
1000
1200
time [min]
MCEC-WT
MCEC-WT in co-culture
MCEC-Dll4
MCEC-Dll4 in co-culture
displacement [microns]
ns
120
100
80
60
40
20
0
MCEC-WT
MCEC-WT in co-culture
MCEC-Dll4 in co-culture
MCEC-Dll4
B
MCEC-WT
MCEC-WT:MCEC-Dll4-mCherry
(ratio 1:1)
MCEC-Dll4-mCherry
C
ADAMTS normalized intensity
3.0
2.5
2.0
1.5
1.0
0.5
0.0
ns
ns
****
****
**
****
MCEC-Dll4 in tip
MCEC-WT in tip
MCEC-Dll4 in tip
MCEC-WT in tip
ratio 1:1
ratio 5:1
ADAMTS intensity in stalk cell
ADAMTS intensity in tip cell
probability of tip cell [%]
100
80
60
40
20
0
MCEC-WT
MCEC-Dll4
MCEC-WT
MCEC-Dll4
ratio 1:1
ratio 5:1
ratio 1:1
ratio 5:1

Figure 7-6: Dll4 overexpressing cells do not influence cell migration during tube formation and are evenly distributed in co-cultures with MCEC-WTs depending on the seeding ratio in 2D and 3D angiogenesis. (A) Velocity and displacement analysis of tube formation live cell imaging. Changes in velocity are plotted over time (left panel) and the overall displacement (right panel) is shown in a bar graph (mean ± SEM, Dunnett's corrected one-way ANOVA, ns ≙ not significant). **(B)** Representative images of the tube formation endpoint (24 h) with the MCEC-WT nuclei stained with Hoechst in blue and the mCherry-Dll4 reporter of MCEC-Dll4-mCherry cells in red (scale bar 250 μm). **(C)** Analysis of tip cell characteristics and cell distribution intensities of MCEC-WT and MCEC-Dll4-mCherry spheroids in the ratio 1:1 and 5:1. ADAMTS normalized intensities in the leading tip cells and following stalk cells were evaluated after immunofluorescence staining and are presented on the left panel. Probability of a MCEC-WT or MCEC-Dll4-mCherry cell leading a sprout was determined by distribution analysis and is presented on the middle panel. All data is displayed in bar graphs (mean ± SEM of ≥ 15 spheroids per condition, Tukey's corrected one-way ANOVA, ns ≙ not significant, **P<0.01, ****P<0.0001). Representative images of the sprouted spheroids, with ADAMTS in green and the mCherry-Dll4 reporter in red are shown on the right panel (scale bar 50 μm).

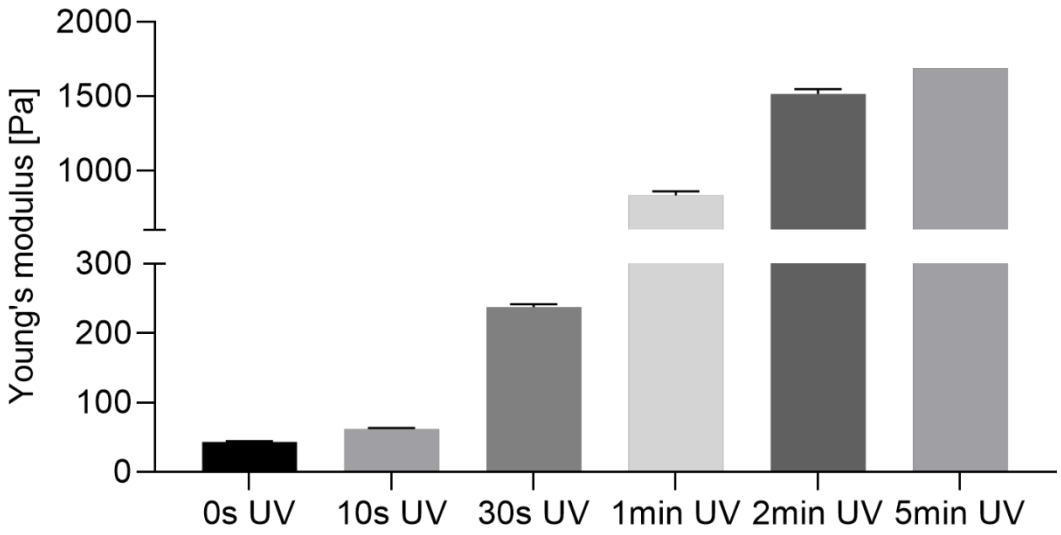

Figure 7-7: PhotoCol® stiffens with increased UV illumination. Stiffness determination of PhotoCol® substrate by atomic force microscopy (AFM) measurements, performed by Daniel Rüdiger. Mean Young's modulus ± SEM are depicted in a bar graph. Stiffness data of 5 min UV illumination were taken from the manufacturer's information and functioned as a comparative value.

7.2 List of publications

First authorship:

I. *Matrix stiffness regulates Notch signaling activity in endothelial cells*

Maibritt Kretschmer, Rose Mamistvalov, David Sprinzak, Angelika M. Vollmar, Stefan Zahler

bioRxiv, 2022: p. 2022.04.20.488899

II. *Zikavirus pr ME Envelope Pseudotyped Human Immunodeficiency Virus Type-1 as a Novel Tool for Glioblastoma-Directed Virotherapy*

Maibritt Kretschmer, Patrycja Kadlubowska, Daniel Hoffmann, Birco Schwalbe, Heidi Auerswald, Michael Schreiber

Cancers, 2020, 12(4)

Co-authorship:

III. *Using the yeast three-hybrid system for the identification of small molecule-protein interactions with the example of ethinylestradiol*

Pengyu Wang, Thomas Klassmüller, Cornelia A Karg, Maibritt Kretschmer, Stefan Zahler, Simone Braig, Franz Bracher, Angelika M Vollmar, Simone Moser

Biol Chem., 2022, 403(4)

IV. *Mechanical Aspects of Angiogenesis*

Maibritt Kretschmer, Daniel Rüdiger and Stefan Zahler

Cancers, 2021, 13(19)

V. *Tetrapyrrolic Pigments from Heme- and Chlorophyll Breakdown are Actin-Targeting Compounds*

Cornelia A. Karg, Dr. Shuaijun Wang, Nader Al Danaf, Dr. Ryan P. Pemberton, Dr. Denzil Bernard, Maibritt Kretschmer, Dr. Sabine Schneider, Dr. Themistoklis Zisis, Prof. Dr. Angelika M. Vollmar, Prof. Dr. Don C. Lamb, Prof. Dr. Stefan Zahler, Dr. Simone Moser

Angew Chem Int Ed Engl., 2021, 60(41)

VI. *Sequential and Switchable Patterning for Studying Cellular Processes under Spatiotemporal Control*

Themistoklis Zisis, Jan Schwarz, Miriam Balles, Maibritt Kretschmer, Maria Nemethova, Remy Chait, Robert Hauschild, Janina Lange, Calin Guet, Michael Sixt, Stefan Zahler

ACS Appl Mater Interfaces, 2021, 13(30)

7.3 Research stay

George S. Wise Faculty of Life Sciences, Tel Aviv University – group of Prof. David Sprinzak

In connection with the DFG-supported project "*The effect of substrate stiffness on Notch signaling in endothelial cells"*

Tel Aviv, Israel, 2019

7.4 Associated bachelor and master theses

Master thesis:

Investigation of the effect of matrix stiffness on the Piezo1 ion channel in endothelial cells and its role in angiogenesis

Pauline Sigge, 2022

Bachelor theses:

Influence of angiogenesis and substrate stiffness on VE-cadherin expression and dynamics in endothelial cells

Simon Traut, 2021

Organization of the Notch1 receptor on the endothelial cell surface and Notch receptor-ligand interactions during angiogenesis

Pauline Sigge, 2020

7.5 Acknowledgements

My sincere thanks go to Prof. Dr. Angelika Vollmar and Prof. Dr. Stefan Zahler for giving me the opportunity to do my PhD in the department of Pharmaceutical Biology. By working in the field of basic research, I was able to broaden my scientific knowledge and experience and to develop myself significantly. Furthermore, I very much appreciate the attentive and supportive supervision as well as the possibilities of independence and freedom in advancing the project. The regular exchange in the form of the team and achievement meetings helped me a lot to keep track of the data I was working on, to solve problems and to make progress.

I would like to express my genuine thanks to the examination committee consisting of Prof. Dr. Stefan Zahler, Prof. Dr. Angelika Vollmar, Prof. Dr. Olivia Merkel, Prof. Dr. Susanne Koch, Prof. Dr. Martin Biel, and Prof. Dr. Ernst Wagner for their willingness to evaluate my work and the time they spent on it.

Special thanks go to Prof. Dr. David Sprinzak for initiating the project together with Prof. Dr. Zahler as well as for the positive cooperation and the helpful answers to all questions and problems. The provision of plasmids and cell lines contributed significantly to the success of this dissertation. A big thank you also goes to Rose Mamistvalov for the successful teamwork on the project and for the production of the stable cell lines. Furthermore, I enjoyed the stay and hospitality at Tel Aviv University very much and am grateful for the methods learned.

I would like to thank my master's student Pauline Sigge, whose bachelor's thesis I also supervised, for her committed participation in the project and her hard work on successful results, as well as for the lively exchange of ideas about our projects, which helped us both. I would also like to thank my bachelor student Simon Traut for his work on the project.

A big thank you also goes to the entire Vollmar working group. Thanks to you, I really enjoyed the time of my promotion and made the move to Munich very worthwhile. I also received a lot of work-related and emotional support through the numerous conversations. In this context, special thanks go to the technical assistants who were a great help with various methodological problems due to their experience. Above all, I would like to emphasize Jana, especially you always had an open ear for all my questions and never hesitated to address all my concerns as quickly as possible. Thank you so much for that.

I would like to thank the numerous current and former doctoral students, especially Daniel, Adrian and the other Zahler group members for the great time and cooperation in the lab. To all involved in the weekly frisbee and basketball events, I very much enjoy the great times together and the friendship that extends beyond the lab.

I dedicate my deepest gratitude to my family, especially my mother, sister, and partner. You are the most important people in my life, and I could not have done it without you. You have always believed in me, supported me in everything and reaffirmed me in various doubts. You are my counterbalance to the work and the stress and for that I thank you from the bottom of my heart.